Rehashing the Bit-Interleaved Coded Modulation

by

Alireabout:za Kenarsari Anhari

B.Sc., The University of Tehran, 2007

A THESIS SUBMITTED IN PARTIAL FULFILLMENT OF
THE REQUIREMENTS FOR THE DEGREE OF

MASTER OF APPLIED SCIENCE

in

The Faculty of Graduate Studies

(Electrical and Computer Engineering)

THE UNIVERSITY OF BRITISH COLUMBIA

(Vancouver)

August 2009

Abstract

Bit-interleaved coded modulation (BICM) is a pragmatic yet powerful approach for spectrally efficient coded transmission. BICM was originally designed as a superior alternative to the conventional trellis coded modulation in fading channels. However, its flexibility and ease of implementation also make BICM an attractive scheme for transmission over unfaded channels. In fact, a noticeable advantage of BICM is its simplicity and flexibility. Notably, most of today's communication systems that achieve high spectral efficiency such as ADSL, Wireless LANs, and WiMax feature BICM. Perceptibly, the design of efficient BICM-based transmission strategies relies on the existence of a general analytical framework for evaluating its performance. Therefore, alongside its vast popularity and deployment, performance evaluation of BICM has attracted considerable attention. Developing such a performance evaluation framework is one of the main contributions of this thesis. In addition to conventional additive white Gaussian noise model, the practically important case of transmission over fading channels impaired by Gaussian mixture noise has also been studied. Different from previously proposed methods, our scheme results in closed-form expressions and is valid for arbitrary mapping rules and fading distributions. Furthermore, making use of the newly developed framework, we propose two novel transmission strategies. First, we consider the problem of optimal power allocation for a BICM system employing orthogonal frequency division multiplexing. In particular, we show that this problem translates into a linear program in the high signal-to-noise ratio regime. This reformulation extends the applicability and delivers considerable complexity reduction in comparison to existing algorithms. Finally, we propose novel detector architectures for a BICM system employing iterative decoding using hard-decision feedback at the receiver. We show that, taking the feedback error into account results in considerable performance improvement while retains decoding complexity.

Table of Contents

List of Tables

List of Figures

Abbreviations

APSK	Amplitude Phase-Shift Keying
AWGN	Additive White Gaussian Noise
BER	Bit-Error Rate
BICM	Bit-Interleaved Coded Modulation
BICM-EB	BICM Expurgated Bound
BICM-HID	BICM with Hard-Feedback Iterative Decoding
BICM-ID	BICM with Iterative Decoding
BICM-SID	BICM with Soft-Feedback Iterative Decoding
BIOS	Binary-Input Output-Symmetric
BPSK	Binary Phase-Shift Keying
CDF	Cumulative Density Function
FEC	Forward Error Correction
FER	Frame-Error Rate
GL	Gray Labeling
i.i.d	Independent and Identically Distributed
LLR	Log-Likelihood Ratio
MBIOS	Memoryless Binary-Input Output Symmetric
MGF	Moment Generating Function
ML	Mixed Labeling

MSPL	Modified Set-Partitioning Labeling
OFDM	Orthogonal Frequency-Division Multiplexing
PA	Power Allocation
PDF	Probability Density Function
PEP	Pairwise Error Probability
PSK	Phase Shift Keying
QAM	Quadrature Amplitude Modulation
QPSK	Quadrature Phase-Shift Keying
SIHO	Soft-Input Hard-Output
SISO	Soft-Input Soft-Output
SNR	Signal-to-Noise Ratio
SPL	Set-Partitioning Labeling
SSPL	Semi Set-Partitioning Labeling
TCM	Trellis Coded Modulation
MLC	Multi-Level Coded Modulation
UPA	Uniform Power Allocation

Acknowledgements

First, I would like to convey my sincere gratitude to my supervisor, Professor Lutz Lampe, for his insightful guidance. I also would like to thank Professors Robert Schober, Vikram Krishnamurthy, and Joel Friedman for their support. Furthermore, I am especially grateful to Mrs. Zahra Ahmadian for her continuous support and encouragement. Finally, I would like to extend my many thanks to my dear colleagues at the University of British Columbia.

Dedication

to my parents

Statement of Co-Authorship

Alireza Kenarsari Anhari is the primary author of all the papers presented in this work. For all these papers, Mr. Kenarsari Anhari identified and proposed the research topic, performed the literature survey and research, analyzed the data, performed the simulations and prepared the manuscripts under the supervision and direction of Professor Lutz Lampe. All this work has been done completely during Mr. Kenrsari Anhari's M.A.Sc. program. None of the papers presented in this work have been received credit or presented in any other thesis work.

Chapter 1

Introduction

1.1 Background

The early designs of communication systems focused separately on modulation and channel coding. The correct perspective of signal space coding, also known as coded modulation, was brought into the focus of communication engineers by Ungerboeck's pioneering work on trellis coded modulation (TCM) [1, 2]. TCM combines trellis codes with (non-binary) modulations through the concept of set partitioning labeling aiming to maximize the minimum Euclidean distance of the code [1]. An alternative coded modulation scheme which has been proposed by Imai and Hirakawa, is multi-level coding (MLC) [3]. MLC uses several binary codes, each protecting a single coded bit in the binary label of the transmitted constellation. At the receiver, instead of optimal joint decoding of all the component binary codes, a suboptimal multi-stage decoding is used. It is known that this decoding scheme achieves good performance with limited complexity [2, 3].

The increasing interest for wireless communications has led to the consideration of coded modulation for fading channels. First, it seemed quite natural to apply the Ungerboeck's paradigm of "keeping coding combined with modulation" even in a situation where the code performance depends strongly, rather than the minimum Euclidian distance of the code, on its minimum Hamming distance (i.e. diversity order of the code) [2]. A notable departure from Ungerboek's paradigm was the core idea of [4]. In [4], Zehavi recognized that code diversity and hence the reliability of coded modulation over fading channels[1] could be further improved via decoupling of channel encoder and modulator. Zehavi's idea was to make the code diversity equal to the smallest number of distinct bits along any error event. This is achieved by bit-wise interleaving at the encoder output. This coded modulation scheme is known as bit-interleaved coded modulation (BICM). Although first introduced by Zehavi's landmark paper, BICM subsequently has been widely generalized by Caire et. al. in [5].

BICM is known as a pragmatic yet powerful approach for coded modulation. Notably, most of today's communication systems that achieve high spectral efficiency such as ADSL, Wireless LANs, and WiMax feature the combination of BICM with orthogonal frequency division multiplexing (OFDM), also known as bit-interleaved coded OFDM (BIC-OFDM) [2, 6]. The most noticeable advantage of BICM is its simplicity and flexibility, as the only provision it takes to combat the multi-path fading is a random bit-wise interleaver. Therefore, a single binary code can be used along with several modulations without the need for further adaptations and vice versa. In particular, BICM separates (binary) channel encoder from the (non-binary) modulator using a bit-wise interleaver. At the receiving side, in order to alleviate the loss of information imposed by this sub-optimal approach, soft information about the coded bits is fed from the demodulator

[1] In his paper, [4], Zehavi considered Rayleigh fading channels.

to the decoder in the form of bit-wise reliability metrics or log-likelihood ratios (LLRs) [2, 5]. [5] illustrated the performance advantages of BICM. It also has provided a comprehensive analysis of BICM in terms of achievable capacity and error probability, showing that in fact the loss incurred by the BICM may be very small. Furthermore, this loss can be recovered by using iterative decoding [2, 7, 8]. Building upon this principle, Li and Ritcey [7, 8] proposed iterative demodulation and decoding for BICM, also known as BICM-ID, and illustrated significant performance gains with respect to classical non-iterative BICM decoding. However, BICM designs based on iterative decoding cannot approach the capacity, unless the number of transmitted bits grows large [2, 7, 8].

1.2 Objectives and Related Previous Work

The first goal of this thesis is to develop a general analytical framework for performance evaluation of BICM transmission over additive white Gaussian noise (AWGN) fading channels. Furthermore, we note that the study of communication systems in non-Gaussian environments has become very popular due to its practical relevance. In many practical cases such as indoor radio communication, partial-time jamming, ultra-wideband communication, and power line communication, this interference is well modeled as a Gaussian mixture noise (GMN) [9–15]. Therefore, we also study the BICM transmission over fading channels impaired by GMN. Finally, we focus on a few applications of the developed analysis in improving the performance of BICM-based transmission systems. In particular, first we focus on the problem of optimal power allocation for a BIC-OFDM transmission system, when the channel information is available at the transmitter. Then, we turn our attention to improving the performance of BICM-ID with hard-decision feedback.

In the following, a brief review of previous work related to each of the objectives is given. The detailed review of previous research on each topic can be found in the "Introduction" section of corresponding chapter(s).

1.2.1 Performance Evaluation of BICM Transmission

Different bounds for the bit error-rate (BER) of BICM have been derived in previous works. A popular technique, which was developed in [5] and referred to as BICM Expurgated bound (BICM-EB), provides tight results but is complex to compute and limited to the Gray labeling. Also, [16] pointed out that the BICM-EB is not an upper bound but rather an error-rate approximation. A generalized version of the BICM-EB has been proposed in [17] which considers finite-length interleaving, but again is limited to the Gray labeling and numerically more complex to compute than the bounds given in [5]. The authors of [18] presented two new approximations, namely, the Gaussian and saddlepoint approximations. Both approximations are applicable to arbitrary labeling rules but rely on numerical integration. Recently, [19] devised an algorithmic approach to compute the probability density function (PDF) of LLRs for the unfaded AWGN channel applicable to arbitrary labeling rules. However, this method results in PDF expressions which are not simple and thus, evaluation of performance expressions, as for example BER, based on these PDF expressions again invokes numerical techniques. These problems have been overcome in the follow-up work [20], where a closed-form expression for the PDF for square quadrature amplitude modulation (QAM) with Gray labeling is obtained, and then further simplified using a Gaussian approximation. In [21] (cf. also [22]), closed-form PDF expressions are derived for BICM transmission over Nakagami-m fading channels with integer m, which are applied for BER approximation using the saddlepoint technique. Again, the approach is restricted to QAM with Gray labeling.

Finally, we note that while performance evaluation of BICM transmission over AWGN channels has been of interest since its invention, the analysis of BICM transmission impaired by non-Gaussian noise has received relatively little attention, cf. e.g. [23, 24]. The authors of [24] has presented a framework that modifies the BICM-EB to encompass non-Gaussian noise. Since the analysis relies on the expurgated bound, it is limited to the case of Gray labeling and does not result in closed-form expressions for BER. Furthermore, the asymptotic performance analysis in [24] is valid only when the diversity order of the system is an integer.

1.2.2 Power Allocation for BIC-OFDM

OFDM enables transmitter side adaptation according to the present channel conditions, assuming that the channel remains unchanged over a sufficiently long interval. In particular, numerous algorithms for bit-loading and power allocation per OFDM sub-carrier have been developed, cf. e.g. [25–27]. Recently, [28] has studied the problem of power allocation for BIC-OFDM aiming at the minimization of BER under a power budget constraint. Using the BER union bound approach to approximate the bit-error probability, it was shown [28] that the problem is a convex optimization problem. However, the solution presented in [28] is limited to (complex) binary transmission, i.e., binary and quadrature phase-shift keying, since linearity of coding and modulation was required. Notably, to the best of our knowledge [28] is the only work which takes the interplay of interleaving, coding and modulation into account for defining the optimization problem.

1.2.3 BICM-ID with Hard Decision Feedback

BICM structure can also be looked at as a concatenated coding system, with the forward error correction (FEC) encoder and the multilevel modulator as outer and inner encoder, respectively. BICM considered as concatenated code is commonly decoded in an iterative fashion, in which the demapper and a SISO channel decoder for the outer FEC code exchange extrinsic information. This decoding scheme is known as BICM with sof-feedback iterative decoding (BICM-SID). An alternative decoder proposed in [29] uses a soft-input hard-output (SIHO) outer decoder, like the Viterbi decoder for convolutional codes. This decoding method is known as BICM with hard-feedback iterative decoding (BICM-HID). BICM-HID has two complexity advantages over BICM-SID. First, the outer SIHO decoder is less complex than its SISO counterpart, and second, the demapper using hard-decision feedback needs to consider only two instead of all constellation points for each labeling bit [7]. On the downside, BICM-HID is considerably outperformed by BICM-SID due to the effect of erroneous feedback. Recently, [23] proposed an alternative detector architecture for BICM-HID which improves its performance. The key idea is that the demapper makes use of the error rate of the hard-decision feedback after each iteration. Notably, [23] requires a SISO decoder for extracting the error-rate estimation and furthermore the detector needs to consider all the signal points in order to recompute the LLRs. The main difference in terms of computational complexity is that, different from BICM-SID, [23] does not require any multiplication operation.

1.3 Summary of Thesis and Contributions

This thesis addresses several topics in performance evaluation and design of BICM-based transmission systems. The main results are divided into four chapters[2]. Furthermore, in Chapter 6, the summary of contributions, concluding remarks, and proposals for further research are offered. In what follows, a brief introduction to the topic covered in each chapter and a summary of contributions made in is given.

In chapter 2, we present an analytical approach to evaluate the performance of BICM transmission over frequency-flat fading AWGN channels. The statistic of the fading envelope is modeled as Nakagami-m distributed, which spans a wide range of practical multi-path fading scenarios through adjustment of the m-parameter. For this setup, we derive approximations for the BER and cutoff rate of BICM. Different from previously proposed methods, our analysis is valid for general QAM and phase shift keying signal constellations and arbitrary bit-to-symbol mapping rules, and it results in

[2]Each of the four chapters in this thesis is self-contained and included in a separate journal article. The notations are also separately defined for each chapter, but has been tried to be consistent throughout the thesis for the ease of understanding.

simple closed-form expressions. The key idea is to use well-chosen subsets of signal points to approximate the PDF of reliability metrics used for decoding. This approximation is accurate for signal-to-noise (SNR) regions of interest for BICM systems with moderate coding complexity such as, e.g., convolutional coded BICM systems. Based on this approximation we also derive an asymptotic BER expression, which reveals the diversity order and coding gain of BICM. The usefulness of the proposed analytical approach is validated through numerical and simulation results for a number of BICM transmission examples.

Furthermore, in chapter 3, we derive BER approximations for BICM transmission over general fading channels impaired by GMN. To this end, we build upon the saddlepoint approximation of the pairwise error probability (PEP) and the approximation developed in chapter 2 for the PDF of bit-wise reliability metrics for AWGN channels. We extend this PDF approximation to the case of GMN, and obtain closed-form expressions for its Laplace transform for fading GMN channels. The latter allows us to express the PEP and thus BER via the saddlepoint approximation. For the special case of fading AWGN channels the presented approximations are closed form, since the saddlepoint is known to be $1/2$. Furthermore, we derive closed-form PEP expressions also for GMN channels in the high SNR regime and establish the diversity and coding gain for BICM transmission over fading GMN channels. Selected numerical results for BER of convolutional coded BICM highlight the usefulness of the proposed approximations and the differences between AWGN and GMN channels.

Then, making use of the performance approximations developed in Chapter 2 and Chapter 3, in the next two chapters we focus of designing transmission strategies for BICM-based communication systems. In particular, Chapter 4 considers the problem of power allocation for a system utilizing the combination of BICM with OFDM. The combination of BICM with OFDM forms a powerful coded modulation scheme for transmission over wideband channels. Recently, Moon and Cox [28] presented a new power allocation method to minimize the BER of BIC-OFDM. Different from many previous related works, the method proposed in [28] considers the interplay of interleaving, coding, and modulation but is limited to (complex) binary modulation as the linearity of coding and modulation was required. Furthermore, it translates into a fairy computationally intense convex optimization problem [28] . Motivated by their work, in this chapter we present an alternative power allocation method, which has the advantages of being a linear program and applicable to arbitrary signal constellations. Our approach relies on using the PDF approximation presented in Chapter 2 and a further simplification of it for asymptotically large SNRs. Simulative evidence shows that the proposed power allocation method achieves a performance very close to that from [28] for the case of binary modulation.

Finally, Chapter 5 considers the iterative decoding of BICM transmission. In particular, if relatively simple FEC codes such as convolutional codes are employed, iterative decoding between demapper and FEC decoder can provide significant performance improvements over non-iterative decoding. In practice, to keep the complexity of iterative decoding low, the use of hard-decision feedback from FEC decoder to demapper is appealing. However, the price to be paid is a performance degradation due to feedback errors. In this chapter, two new demapper designs are developed which are able to strongly mitigate the effect of erroneous feedback. The key ideas are (a) the use of the error rate estimation developed in Chapter 2 for the average error rate in the hard-decision feedback and (b) the interpretation of feedback errors as additive impulsive noise. Simulation results show that the proposed designs achieve error rates close to those for iterative decoding with soft feedback, while they maintain the complexity advantage of using hard-decision feedback.

Bibliography

[1] G. Ungerboeck, "Channel coding with multilevel/phase signals," *IEEE Trans. Inform. Theory*, vol. 28, pp. 55–67, Jan. 1982.

[2] A. Guillén i Fàbregas, A. Martinez, and G. Caire, "Bit-interleaved coded modulation," *Foundations and Trends in Communications and Information Theory*, vol. 5, no. 1-2, pp. 1–153, 2008.

[3] H. Imai and S. Hirakawa, "A new multilevel coding method using error-correcting codes," *Information Theory, IEEE Transactions on*, vol. 23, no. 3, pp. 371–377, May 1977.

[4] E. Zehavi, "8-PSK trellis codes for a Rayleigh channel," *IEEE Trans. Commun.*, vol. 40, no. 5, pp. 873–884, May 1992.

[5] G. Caire, G. Taricco, and E. Biglieri, "Bit-interleaved coded modulation," *IEEE Trans. Inform. Theory*, vol. 44, no. 3, pp. 927–946, May 1998.

[6] K.-B. Song, A. Ekbal, S. T. Chung, and J. Cioffi, "Adaptive modulation and coding (AMC) for bit-interleaved coded OFDM (BIC-OFDM)," vol. 6, June 2004, pp. 3197–3201 Vol.6.

[7] A. Chindapol and J. Ritcey, "Design, analysis, and performance evaluation for BICM-ID with square QAM constellations in Rayleigh fading channels," *"IEEE J. Select. Areas Commun."*, vol. 19, no. 5, pp. 944–957, May 2001.

[8] X. Li, A. Chindapol, and J. Ritcey, "Bit-interleaved coded modulation with iterative decoding and 8PSK signaling," *IEEE Trans. Commun.*, vol. 50, no. 8, pp. 1250–1257, Aug 2002.

[9] D. Middleton, "Statistical-physical models of man-made radio noise-parts I and II," *U.S. Dept. Commerece Office Telecommun.*, April 1974 and 1976.

[10] D. Stein, "Detection of Random Signals in Gaussian Mixture Noise," *IEEE Trans. Inform. Theory*, vol. 41, no. 6, pp. 1788–1801, Nov. 1995.

[11] X. Wang and V. Poor, "Robust Multiuser Detection in Non-Gaussian Channels," *IEEE Trans. Signal Processing*, vol. 47, no. 2, pp. 289–305, Feb. 1999.

[12] J.-W. Moon, T. Wong, and J. Shea, "Pilot-assisted and Blind Joint Data Detection and Channel Estimation in Partial-time Jamming," *IEEE Trans. Commun.*, vol. 54, no. 11, pp. 2092–2102, Nov. 2006.

[13] M. Flury and J.-Y. Le Boudec, "Interference Mitigation by Statistical Interference Modeling in an Impulse Radio UWB Receiver," in *IEEE Intl. Conf. on Ultra-Wideband (ICUWB)*, Waltham, MA, Sept. 2006, pp. 393–398.

[14] M. Zimmermann and K. Dostert, "Analysis and Modeling of Impulsive Noise in Broadband Powerline Communications," *IEEE Trans. Electromagn. Compat.*, vol. 44, no. 1, pp. 249–258, Feb. 2002.

[15] J. Häring and A. Vinck, "Performance Bounds for Optimum and Suboptimum Reception under Class-A Impulsive Noise," *IEEE Trans. Commun.*, vol. 50, no. 7, pp. 1130–1136, July 2002.

[16] V. Sethuraman and B. Hajek, "Comments on "Bit-interleaved coded modulation"," *IEEE Trans. Inform. Theory*, vol. 52, no. 4, pp. 1795–1797, Apr. 2006.

[17] P.-C. Yeh, S. Zummo, and W. Stark, "Error probability of bit-interleaved coded modulation in wireless environments," *IEEE Trans. Veh. Technol.*, vol. 55, no. 2, pp. 722–728, March 2006.

[18] A. Martinez, A. Guillen i Fabregas, and G. Caire, "Error probability analysis of bit-interleaved coded modulation," *IEEE Trans. Inform. Theory*, vol. 52, no. 1, pp. 262–271, Jan. 2006.

[19] L. Szczecinski, R. Bettancourt, and R. Feick, "Probability density function of reliability metrics in BICM with arbitrary modulation: Closed-form through algorithmic approach," *IEEE Trans. Commun.*, vol. 56, no. 5, pp. 736–742, May 2008.

[20] A. Alvarado, L. Szczecinski, R. Feick, and L. Ahumada, "Distribution of L-values in Gray-mapped M^2-QAM: Closed-form approximations and applications," *to appear in the IEEE Trans. Commun., available online at http://externe.emt.inrs.ca/users/leszek/Publications.html.*

[21] L. Szczecinski, A. Alvarado, and R. Feick, "Distribution of max-log metrics for QAM-based BICM in fading channels,"

to appear in the IEEE Trans. Commun., available online at http://externe.emt.inrs.ca/users/leszek/Publications.html.

[22] ——, "Closed-form approximation of coded BER in QAM-based BICM faded transmission," *IEEE Sarnoff Symposium*, pp. 1–5, Apr. 2008.

[23] T. Li, W. Mow, and M. Siu, "Bit-interleaved coded modulation in the presence of unknown impulsive noise," in *IEEE International Conference on Communications (ICC)*, Istanbul, Turkey, June 2006, pp. 3014 – 3019.

[24] A. Nasri and R. Schober, "Performance of BICM-SC and BICM-OFDM systems with diversity reception in non-Gaussian noise and interference," *to appear in the IEEE Trans. Commun., available online at www.ece.ubc.ca/~amirn/TCOM-08-0180.pdf.*

[25] P. Chow, J. Cioffi, and J. Bingham, "A practical discrete multitone transceiver loading algorithm for data transmission over spectrally shaped channels," *IEEE Trans. Commun.*, vol. 43, no. 234, pp. 773–775, Feb/Mar/Apr 1995.

[26] R. Fischer and J. Huber, "A new loading algorithm for discrete multitone transmission," vol. 1, Nov 1996, pp. 724–728 vol.1.

[27] L. Goldfeld, V. Lyandres, and D. Wulich, "Minimum BER power loading for OFDM in fading channel," *IEEE Trans. Commun.*, vol. 50, no. 11, pp. 1729 – 1733, 2002.

[28] H. Moon and D. Cox, "Efficient power allocation for coded OFDM systems," *IEEE Trans. Commun.*, vol. 57, no. 4, pp. 943–947, April 2009.

[29] X. Li and J. Ritcey, "Bit-interleaved coded modulation with iterative decoding," in *IEEE International Conference on Communications (ICC)*, vol. 2, Vancouver, BC, Canada, june 1999, pp. 858–863.

Chapter 2

An Analytical Approach for Performance Evaluation of BICM Transmission over Nakagami-m Fading Channels[3]

2.1 Introduction

Bit-interleaved coded modulation (BICM) introduced in [1] and further generalized in [2] has established itself as the most popular scheme for spectrally efficient coded transmission. BICM connects a binary encoder to a non-binary modulator and achieves nearly optimal performance in terms of, e.g., constellation-constrained channel capacity [2]. The most noticeable advan-

[3]A version of this chapter has been accepted for publication with minor revisions. A. Kenarsari Anhari and L. Lampe, "An Analytical Approach for Performance Evaluation of BICM Transmission over Nakagami-m Fading Channels," *accepted for publication (with minor revisions) in IEEE Transactions on Communications*, August 2009.

tage of BICM is its simplicity and flexibility, as a single binary code can be used along with several modulations without further adaptations. BICM was originally designed as a superior alternative to trellis coded modulation (TCM) [3] in fading channels [1]. However, its flexibility and ease of implementation also make BICM an attractive scheme for transmission over nonfading channels [2].

Different bounds for the bit error-rate (BER) of BICM have been derived in literature, all of which require numerical integration or computer simulation [2, 4–6]. The Bhattacharyya union bound was found to be quite loose but a true upper bound for arbitrary mapping rules [2]. A refined technique, which was also developed in [2] and referred to as BICM Expurgated bound (BICM-EB), provides tighter results but is more complex to compute and limited to the Gray labeling. Also, [5] pointed out that the BICM-EB is not an upper bound but rather an error-rate approximation. A generalized version of the BICM-EB has been proposed in [4] which considers finite-length interleaving, but again is limited to the Gray labeling and numerically more complex to compute than the bounds given in [2]. Recently, [6] presented two new approximations, namely, the Gaussian and saddlepoint approximations. The former is based on the Gaussian approximation of the tail of the probability density function (PDF) of the bitwise log-likelihood ratio (LLR) while the latter is an application of the saddlepoint approximation technique known from statistics [7]. Both approximations are applicable to arbitrary mapping rules but rely on numerical integration using various Gauss quadrature rules for computing the cumulant generating function of the LLRs [6].

The need for numerical integration renders the aforementioned approximations complex to compute and rather hard to use as a design tool. Recently, [8] devised an algorithmic approach to compute the PDF of LLRs for the nonfading additive white Gaussian noise (AWGN) channel applicable to arbitrary mapping rules. However, this method results in PDF expressions which are not simple and thus, evaluation of performance expressions, as for example BER, based on these PDF expressions again invokes numerical techniques. Also the intricacy of the algorithm itself affects its suitability for evaluation and design of BICM-based systems. Furthermore, as stated in [8], the closed-form expressions are achievable only for the case of transmission over nonfading channels.

In this chapter we present a novel approach for performance evaluation of BICM transmission over frequency-flat fading AWGN channels. More specifically, we consider fading according to the Nakagami-m distribution, which often provides the best fit to land-mobile and indoor-mobile multipath propagation channels. Through adjustment of the m parameter, it spans the widest range of "fading figure" among the well-known fading distributions [9], and includes the popular Rayleigh fading and nonfading channels as special cases. The main contributions of this work can be summarized as follows. (i) A closed-form approximation for the PDF of bitwise reliability metrics when transmitting over the nonfading AWGN channel is derived. The resulting PDF expression is valid for arbitrary modulation and mapping rules. Different from [8], the simplicity of our novel PDF approximation enables the expression of pertinent BICM performance parameters in closed form. (ii) Towards this end, we derive the Laplace transform of the newly found PDF expression for general Nakagami-m fading AWGN channels. Using this result together with the saddlepoint approximation, closed-form expressions for the pairwise error probability (PEP) between codewords are obtained. The BER for BICM with linear codes is then easily upper bounded in terms of these PEP expressions. (iii) In addition to BER, also the generalized cutoff for BICM is written in terms of the mentioned Laplace transform and thus can be expressed in closed form. We note that the cutoff rate has widely been used as a parameter to predict the performance of BICM with moderate-complexity coding schemes [2]. (iv) Based on the new PDF approximation we also derive asymptotic BER expressions as the signal-to-noise power ratio (SNR) goes to infinity. It is shown that for the nonfading channel the BER is closely approximated by the BER expression for an equivalent binary transmission scaled by a constant which is a function of the minimum Hamming distance d_{free} of the code and the mapping rule. For the case of Nakagami-m fading it is shown that the diversity order is the product of m and d_{free}. Furthermore, the asymptotic coding gain is shown to depend on a parameter which is a generalization of the harmonic mean presented in [2] for Rayleigh fading (i.e., $m = 1$). (v) A set of numerical and simulation results for BICM with convolutional codes is presented, which provides evidence of the tightness of the proposed approximations, including the asymptotic BER expressions.

The remainder of this chapter is organized as follows. In Section 2.2 the BICM transmission model is introduced. Then, the formulation of BER union bound, saddlepoint approximation for PEP, and cutoff rate for BICM is briefly reviewed, which shows that evaluation of these performance param-

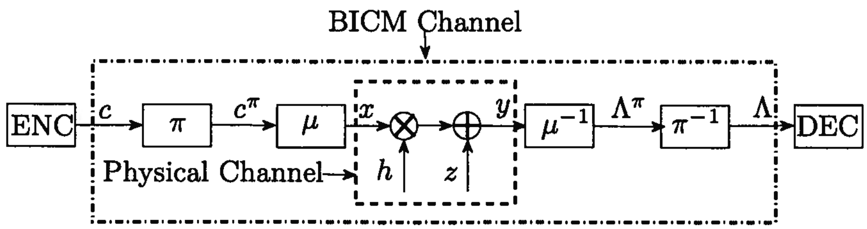

Figure 2.1: Block diagram of BICM transmission over a fading AWGN channel. Also indicated is the binary-input continuous-output equivalent BICM channel.

eters requires knowledge of the Laplace transform of the PDF of LLRs. The novel closed-form approximation for this PDF and its Laplace transform are derived in Section 2.3. The detailed solutions of a number of integrals encountered during the derivations are relegated to the appendix. The asymptotic BER analysis for large SNR is provided in Section 2.4. Comparisons between the proposed analytical approximations and simulation results are given in Section 2.5. Finally, conclusions are offered in Section 2.6.

2.2 Preliminaries

In this section, we first introduce the BICM transmission model. Then, we briefly review error-rate approximations for such systems using union bounding and saddlepoint approximation techniques. Furthermore, we present an expression for the BICM cutoff rate.

2.2.1 System Model

Figure 2.1 shows the block diagram of the equivalent baseband BICM transmission system.

Transmitter

The BICM codeword $\boldsymbol{x} = [x_1, x_2, ..., x_L] \in \mathbb{C}$ comprises L complex valued symbols and is obtained by first interleaving (π) the output of a binary encoder $\boldsymbol{c} = [c_1, c_2, ..., c_N] \in \mathbb{F}_2^N$ into $\boldsymbol{c}^\pi = [c_1^\pi, c_2^\pi, ..., c_N^\pi] \in \mathbb{F}_2^N$ and a subsequent mapping $\mu : \{0,1\}^r \rightarrow \mathcal{X}$ of each $r \triangleq \log_2(M)$ bits such that $x_i = \mu\left(\left[c^\pi_{(i-1)r+1}, c^\pi_{(i-1)r+2}, ..., c^\pi_{ir}\right]\right)$. $\mathcal{X}$ is an M-ary quadrature amplitude modulation (QAM) or phase-shift keying (PSK) constellation with unit symbol energy and we assume that coding and mapping results in a uniform distribution of signal points.

Channel

We consider BICM transmission over AWGN channels. Making the usual assumptions about synchronization, filtering, sampling, and channel-phase compensation in a coherent receiver, the equivalent baseband discrete-time transmission model can be written as

$$y_i = \sqrt{\bar{\gamma}}\, h_i\, x_i + z_i\ , \tag{2.1}$$

where $y_i \in \mathbb{C}$ is the received sample, $h_i \in \mathbb{R}$ denotes the fading gain, $z_i \in \mathbb{C}$ is the additive noise sample at discrete-time i. The noise samples are assumed to be independent and identically distributed (i.i.d.) according to a zero-mean complex Gaussian distribution. We further assume that interleaving effectively renders the fading coefficients h_i i.i.d. random variables. Applying normalization such that h_i and z_i have average power one, $\bar{\gamma}$ represents the average SNR. The instantaneous SNR is given by

$$\gamma_i = \bar{\gamma}\, h_i^2 \,. \tag{2.2}$$

To make matters concrete we consider the widely used Nakagami-m distribution to model multipath fading. Adjustment of the fading parameter $m \geq 1/2$ renders this distribution very flexible. It includes Rayleigh fading ($m = 1$) and nonfading AWGN ($m \to \infty$) channels as special cases and closely approximates Nakagami-n (Rice) and Nakagami-q (Hoyt) distributions [9, Ch. 2.2.14]. The corresponding distribution of the SNR (2.2) reads [9] ($\Gamma(\cdot)$ denotes the Gamma function)

$$f_{\gamma|\bar{\gamma},m}(\gamma) = \frac{m^m\,\gamma^{m-1}}{\bar{\gamma}^m\,\Gamma(m)} \exp\left(-\frac{m\,\gamma}{\bar{\gamma}}\right) \,. \tag{2.3}$$

Receiver

At the receiver, the demapper (μ^{-1} in Figure 2.1) produces r bitwise reliability metrics per symbol in the form of

$$\Lambda^{\pi}_{(i-1)r+j} = -\min_{a\in\mathcal{X}_{j,1}} \left(\|y_i - \sqrt{\bar{\gamma}}\,h_i\,a\|^2\right) + \min_{a\in\mathcal{X}_{j,0}} \left(\|y_i - \sqrt{\bar{\gamma}}\,h_i\,a\|^2\right) , \tag{2.4}$$

where $\mathcal{X}_{j,b}$ is the set of symbols with jth bit in the binary label fixed to b. The metrics Λ^{π} are deinterleaved into Λ, which are then input to the decoder for the binary code. We note that Λ^{π} is the so-called max-log simplification of the LLR, which is known to provide practically maximum-likelihood (ML) decoding performance [1,2]. Therefore we adopt this simple metric expression (cf. also [8, 10]). In slight abuse of terminology, we will refer to Λ from Λ^{π} of (2.4) as LLR in the following.

2.2.2 Error-Rate Approximation Using Union Bounding and Saddlepoint Approximation

The transmission channel between encoder output c and decoder input Λ can be considered as an equivalent binary-input output-symmetric (BIOS) channel [6], which is known as equivalent BICM channel.[4] Assuming ML decoding, the error-rate of linear codes transmitted over BIOS channels is well approximated by the union bound in the region above the cutoff rate [11]. For example, the BER union bound for a convolutional code of rate k_c/n_c is given by

$$P_b \leq \frac{1}{k_c} \sum_{d_{\mathrm{H}}=d_{\mathrm{free}}}^{\infty} w_{d_{\mathrm{H}}} \, \mathrm{PEP}(d_{\mathrm{H}}|\bar{\gamma}, m) \, , \tag{2.5}$$

where $w_{d_{\mathrm{H}}}$ denotes total input weight of error events at Hamming distance d_{H}, d_{free} denotes the free distance of the convolutional code, and $\mathrm{PEP}(d_{\mathrm{H}}|\bar{\gamma}, m)$ is the PEP corresponding to an error event with Hamming weight d_{H}. For clarity, we made the dependency of $\mathrm{PEP}(d_{\mathrm{H}}|\bar{\gamma}, m)$ on average SNR $\bar{\gamma}$ and fading parameter m explicit.

For BIOS channels, the PEP can be considered as the tail probability of a random variable generated by summing d_{H} i.i.d. LLRs. More specifically,

[4] In [2], it has been shown that for BICM systems with signal constellation $\mathcal{X}$ and/or labeling μ which do not preserve the symmetry of the output an equivalent BIOS channel could be considered by switching between the labeling μ and its complement $\bar{\mu}$ with probability of 1/2. This equivalence is valid due to the common hypothesis of uniform encoder outputs.

choosing the all-one codeword as reference codeword,

$$\mathrm{PEP}(d_{\mathrm{H}}|\bar{\gamma}, m) = \Pr\left(\Delta_{d_{\mathrm{H}}} \triangleq \sum_{i=1}^{d_{\mathrm{H}}} \Lambda_i < 0 \middle| \bar{\gamma}, m\right) . \tag{2.6}$$

A common approach for computing such a probability is through the use of the Laplace transform $\Phi_{\Lambda|\bar{\gamma},m}(s)$ of the PDF of Λ. That is [12]

$$\Pr\left(\Delta_{d_{\mathrm{H}}} < 0 | \bar{\gamma}, m\right) = \frac{1}{2\pi \mathrm{j}} \int_{\alpha-\mathrm{j}\infty}^{\alpha+\mathrm{j}\infty} \left[\Phi_{\Lambda|\bar{\gamma},m}(s)\right]^{d_{\mathrm{H}}} \frac{ds}{s} , \tag{2.7}$$

where $\mathrm{j} \triangleq \sqrt{-1}$ and $\alpha \in \mathbb{R}$, $0 < \alpha < \alpha_{\max}$, is chosen in the region of convergence of the integral. The computation of (2.7) itself is often not straightforward and invokes the use of numerical methods [12]. For this reason [12] has proposed a few bounds and estimations, among which the saddlepoint approximation has recently attracted considerable interest due to its simple form and accuracy [6]. Approximation of (2.7) using the saddlepoint technique results in [12] [6]

$$\Pr\left(\Delta_{d_{\mathrm{H}}} < 0 | \bar{\gamma}, m\right) \approx \frac{1}{\hat{\alpha}\sqrt{2\pi\, d_{\mathrm{H}}\, \Phi''_{\Lambda|\bar{\gamma},m}(\hat{\alpha})}} \left(\Phi_{\Lambda|\bar{\gamma},m}(\hat{\alpha})\right)^{(d_{\mathrm{H}}+0.5)} , \tag{2.8}$$

where $\Phi''_{\Lambda|\bar{\gamma},m}(\alpha)$ denotes the second-order derivative of $\Phi_{\Lambda|\bar{\gamma},m}(\alpha)$ and $\hat{\alpha}$ is the saddlepoint defined as

$$\left.\frac{\mathrm{d}\Phi_{\Lambda|\bar{\gamma},m}(\alpha)}{\mathrm{d}\alpha}\right|_{\alpha=\hat{\alpha}} = 0 . \tag{2.9}$$

While $\hat{\alpha} = 1/2$ for BIOS channels with ML decoding, a slightly different saddlepoint may be found for the max-log approximated LLR in (2.4) [10].

2.2.3 Cutoff Rate

From (2.7) we can write the Chernoff bound for the PEP between two codewords $\boldsymbol{c}$ and $\boldsymbol{c}'$ as ($\oplus$ denotes addition in $\mathbb{F}_2$)

$$\Pr(\boldsymbol{c} \to \boldsymbol{c}') \leq \min_{0<\alpha<\alpha_{\max}} \left(\prod_{i=1}^{N} \left(\Phi_{\Lambda|\bar{\gamma},m}(\alpha) \right)^{c_i \oplus c_i'} \right) , \tag{2.10}$$

and thus express the cutoff rate as [13]

$$R_0 = -m \log_2 \left[\min_{0<\alpha<\alpha_{\max}} \left(\sum_{c\in\{0,1\}} \sum_{c'\in\{0,1\}} \Pr(c) \Pr(c') \left(\Phi_{\Lambda|\bar{\gamma},m}(\alpha) \right)^{c \oplus c'} \right) \right] . \tag{2.11}$$

The factor m in (2.11) renders the unit of R_0 bit per transmission symbol. With the assumption of uniformly distributed coded bits, (2.11) can be rewritten as

$$R_0 = m \left(1 - \log_2 \left[1 + \Phi_{\Lambda|\bar{\gamma},m}(\hat{\alpha}) \right] \right) , \tag{2.12}$$

with $\hat{\alpha}$ from (2.9).

We observe that the evaluation of the error-rate approximation via (2.8) and the cutoff rate (2.12) hinge on expressions for the Laplace transform $\Phi_{\Lambda|\bar{\gamma},m}(s)$ for $s \in \mathbb{R}^+$. The derivation of these expressions in closed form is considered in the next section.

2.3 Approximation for the PDF of LLRs and its Laplace Transform

In this section, we first derive an approximation for the PDF of the LLRs defined in (2.4) assuming transmission over the nonfading AWGN channel (i.e., $m \to \infty$). Using this approximation, we then derive closed-form expressions for $\Phi_{\Lambda|\bar{\gamma},m}(s)$ for $s \in \mathbb{R}^{+}$ and arbitrary m.

2.3.1 Approximation for the PDF of LLRs

We denote the PDF of LLRs (2.4) for the nonfading channel with $c = b$ being transmitted by $f_{\Lambda|c=b,\gamma}(\lambda)$ and the complement of b by $\bar{b} = b \oplus 1$. Since the channel is BIOS, the symmetry property

$$f_{\Lambda|c=b,\gamma}(\lambda) = f_{\Lambda|c=\bar{b},\gamma}(-\lambda) \,, \tag{2.13}$$

holds, and thus we consider the transmission of $c = 1$ without loss of generality.

The PDF of LLRs can be considered as a weighted sum of PDFs $f_{\Lambda|j,x,\gamma}(\lambda)$ conditioned on the bit position $1 \le j \le r$ and the transmitted symbol $x \in \mathcal{X}_{j,1}$:

$$\begin{aligned} f_{\Lambda|c=1,\gamma}(\lambda) =& \frac{1}{r}\sum_{j=1}^{r}\sum_{x\in\mathcal{X}_{j,1}} \Pr(x\,|c=1,j)\, f_{\Lambda|j,x,\gamma}(\lambda) \,, \\ =& \frac{2}{rM}\sum_{j=1}^{r}\sum_{x\in\mathcal{X}_{j,1}} f_{\Lambda|j,x,\gamma}(\lambda) \,, \end{aligned} \tag{2.14}$$

where the second step follows from the assumption of equiprobable modulator inputs. Hence, the task is to find expressions for $f_{\Lambda|j,x,\gamma}(\lambda)$ for every $1 \leq j \leq r$ and $x \in \mathcal{X}_{j,1}$. This requires consideration of all signal points in the constellation and, depending on the type of modulation and labeling, may not lead to a closed-form result.

To motivate our approach, consider a transmitted codeword $\boldsymbol{c}$ and a given competitive codeword $\boldsymbol{c}'$ with Hamming distance of d_{H} from $\boldsymbol{c}$. Assuming that the d_{H} distinct bits of $\boldsymbol{c}$ are transmitted using d_{H} symbols and label positions $\boldsymbol{j_c} = [j_1, j_2, ..., j_{d_{\mathrm{H}}}]$, the corresponding bits of $\boldsymbol{c}'$ could be transmitted using any sequence of the signal points in

$$\mathcal{X}_{\boldsymbol{c}'} \triangleq \left\{ \mathcal{X}_{j_1,c'_1} \times \mathcal{X}_{j_2,c'_2} \times \; ... \; \times \mathcal{X}_{j_{d_{\mathrm{H}}-1},c'_{d_{\mathrm{H}}-1}} \times \mathcal{X}_{j_{d_{\mathrm{H}}},c'_{d_{\mathrm{H}}}} \right\} .$$

Using the union upper bound over $\mathcal{X}_{\boldsymbol{c}'}$ results in the BICM Union Bound (BICM-UB) [2, Section IV.B]. In this case, $f_{\Lambda|j,x,\gamma}(\lambda)$ is approximated by considering all signal points in $\mathcal{X}_{j,\bar{b}}$ for $x \in \mathcal{X}_{j,b}$. Replacing $\mathcal{X}_{j,c'}$ with a single, nearest-neighbor signal point leads to the BICM-EB [2, Section IV.C]. That is, the BICM-EB estimates $f_{\Lambda|j,x,\gamma}(\lambda)$ by considering only one member of $\mathcal{X}_{j,\bar{b}}$, which is not a valid simplification for non-Gray labeling rules due to the presence of multiple nearest neighbors [2,4,6]. Instead of these two extreme approaches, we propose to use the set of all nearest signal points in $\mathcal{X}_{j,\bar{b}}$ for a given $x \in \mathcal{X}_{j,b}$. That is, we define the set of nearest competitive signal points of x,

$$\mathcal{A}_{j,x} \triangleq \left\{ a \;\middle|\; a \in \mathcal{X}_{j,\bar{b}},\; \|a - x\| = \min_{z \in \mathcal{X}_{j,\bar{b}}} \|z - x\| \triangleq d_{j,x} \right\} , \tag{2.15}$$

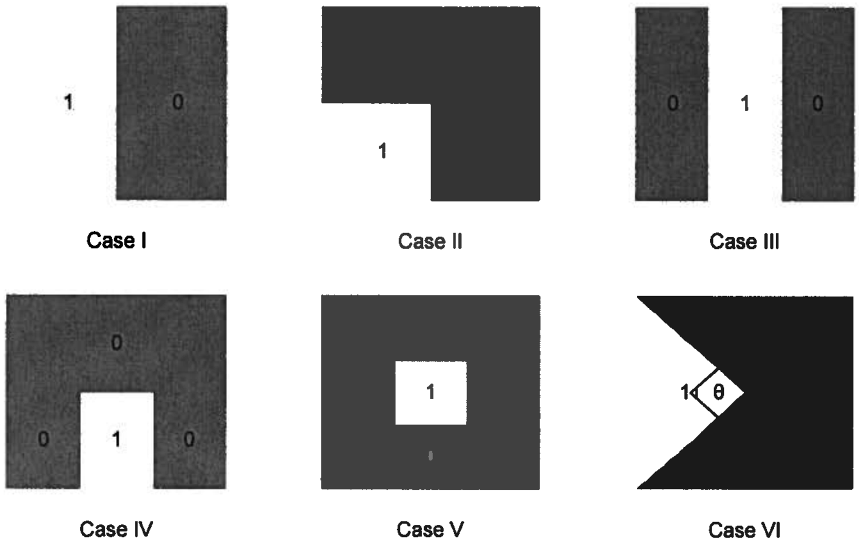

Figure 2.2: Illustration for possible sets of nearest competitive signal points $\mathcal{A}_{j,x}$ for general QAM and PSK constellations. The "1" represents the transmitted signal point x, and the "0" show the elements of $\mathcal{A}_{j,x}$. The shaded areas indicates $\mathbb{D}(\lambda|j,x,\gamma)$ for $\lambda = 0$. For $\lambda > 0$ the boundaries move towards x, for $\lambda < 0$ the boundaries move towards the competitive signal points.

to approximate $f_{\Lambda|j,x,\gamma}(\lambda)$. We note that this corresponds to the approximation

$$\Lambda^{\pi}_{(i-1)r+j} \approx -\left(\|y_i - \sqrt{\gamma}\, h_i\, x_i\|^2\right) + \min_{a \in \mathcal{A}_{j,x_i}} \left(\|y_i - \sqrt{\gamma}\, h_i\, a\|^2\right) , \qquad (2.16)$$

for the LLR in (2.4), which is expected to be tight in the SNR range in which the BER union bound converges to the true error rate.

There are six non-equivalent formations for the sets of nearest competitive signal points $\mathcal{A}_{j,x}$ for QAM and PSK constellations. These are illustrated in Figure 2.2. For each formation we determine the PDF $f_{\Lambda|j,x,\gamma}(\lambda)$ from the corresponding cumulative density function

$$F_{\Lambda|j,x,\gamma}(\lambda) = \Pr\left(z \in \mathbb{D}\left(\lambda|j,x,\gamma\right)\right) \;, \tag{2.17}$$

where $\mathbb{D}(\lambda|j,x,\gamma)$ is the part of complex plane in which the LLR according to (2.16) is less than λ (see Figure 2.2 for $\lambda = 0$). Thus, the PDF is expressed by

$$f_{\Lambda|j,x,\gamma}(\lambda) = \frac{\mathrm{d}}{\mathrm{d}\lambda} \int\limits_{\mathbb{D}(\lambda|j,x,\gamma)} \frac{1}{\pi} \exp\left(-\|z\|^2\right) dz \;, \tag{2.18}$$

whose closed-form solution for the kth configuration from Figure 2.2 is specified as $f_{\Lambda,k|\cdot,\gamma}(\lambda)$ in Table 2.1. For the expressions in Table 2.1 we used the notations

$$\begin{aligned}
\mathcal{N}_{\mu,\sigma^2}(x) &\triangleq \frac{1}{\sqrt{2\pi\sigma^2}} \exp\left(-\frac{(x-\mu)^2}{2\sigma^2}\right) \;, \\
\mathrm{erf}(x) &\triangleq \frac{2}{\sqrt{\pi}} \int\limits_0^x \exp\left(-t^2\right) dt \;, \\
u(x) &\triangleq \begin{cases} 1, & x \geq 0 \\ 0, & x < 0 \end{cases} \;.
\end{aligned}$$

Substituting $f_{\Lambda|j,x,\gamma}(\lambda)$ in (2.14) with the corresponding $f_{\Lambda,k|\cdot,\gamma}(\lambda)$ from Table 2.1 gives us the desired closed-form expression for $f_{\Lambda|c=1,\gamma}(\lambda)$. For a general M-ary QAM constellation we obtain

$$f^{\mathrm{QAM}}_{\Lambda|c=1,\gamma}(\lambda) = \frac{2}{rM} \sum_{k=1}^{5} \sum_{l=1}^{q_{\max}} n_{k,l}\, f_{\Lambda,k|d_l,\gamma}(\lambda) \;, \quad d_l = l\, d_{\min} \;, \tag{2.19}$$

where $n_{k,l}$ denotes the number of nearest competitive signal sets of type k with Euclidean distance d_l, $d_{\min}$ is the minimum Euclidean distance of the constellation, and

$$q_{\max} \triangleq \max_{1\le j\le r}\left\{\max_{a\in\mathcal{X}_{j,1}}\left\{\max_{a'\in\mathcal{A}_{j,a}}\left\{\frac{\|a-a'\|}{d_{\min}}\right\}\right\}\right\} .$$

Similarly, for an M-ary PSK constellation we find

$$\begin{aligned} f^{\text{PSK}}_{\Lambda|c=1,\gamma}(\lambda) =& \frac{2}{rM}\sum_{l=1}^{\frac{M}{2}}\left[n_{1,l}f_{\Lambda,1|d_l,\gamma}(\lambda)+n_{6,l}f_{\Lambda,6|d_l,\theta_l,\gamma}(\lambda)\right] , \\ &\begin{cases} d_l &= \frac{\sin(\frac{\pi l}{M})}{\sin(\frac{\pi}{M})}d_{\min}, \\ \theta_l &= \pi-\frac{2\pi l}{M}. \end{cases} \end{aligned} \tag{2.20}$$

Numerical values for $n_{k,l}$ are summarized for some popular signal constellations and labelings in Table 2.2. It should be noted that the expressions in (2.19) and (2.20) are much easier to evaluate than the PDF approximations in [8]. In particular, their computation does not require any numerical integration.

Figure 2.3 shows a comparison of PDF histograms, obtained through Monte Carlo simulation, and the approximations (2.19) and (2.20) for different constellations, labelings, and SNRs. In addition to popular Gray labeling (GL) [14], two non-Gray labeling, namely modified set partitioning labeling (MSPL) and semi set partitioning labeling (SSPL) (cf. [2,15,16]) are also included. These non-Gray labeling bear significance for BICM transmission with iterative decoding (BICM-ID) [15,16]. From Figure 2.3 we observe that the proposed approximation is very accurate regardless of the type of

Table 2.1: Probability density function of LLRs $f_{\Lambda,k|\cdot,\gamma}(\lambda)$ for transmission over nonfading AWGN channel for the six different sets of competitive signal points $\mathcal{A}_{j,x}$ shown in Figure 2.2.

$f_{\Lambda,1\|d,\gamma}(\lambda)$	$\mathcal{N}_{d^2\gamma,2d^2\gamma}(\lambda)$
$f_{\Lambda,2\|d,\gamma}(\lambda)$	$\mathcal{N}_{d^2\gamma,2d^2\gamma}(\lambda)\left(1-\operatorname{erf}\left(\frac{\lambda-d^2\gamma}{2d\sqrt{\gamma}}\right)\right)$
$f_{\Lambda,3\|d,\gamma}(\lambda)$	$2\mathcal{N}_{d^2\gamma,2d^2\gamma}(\lambda)u\left(d^2\gamma-\lambda\right)$
$f_{\Lambda,4\|d,\gamma}(\lambda)$	$\mathcal{N}_{d^2\gamma,2d^2\gamma}(\lambda)\left(1-2\operatorname{erf}\left(\frac{\lambda-d^2\gamma}{2d\sqrt{\gamma}}\right)\right)u\left(d^2\gamma-\lambda\right)$
$f_{\Lambda,5\|d,\gamma}(\lambda)$	$-4\mathcal{N}_{d^2\gamma,2d^2\gamma}(\lambda)\operatorname{erf}\left(\frac{\lambda-d^2\gamma}{2d\sqrt{\gamma}}\right)u\left(d^2\gamma-\lambda\right)$
$f_{\Lambda,6\|d,\theta,\gamma}(\lambda)$	$\mathcal{N}_{d^2\gamma,2d^2\gamma}(\lambda)\left(1-\operatorname{erf}\left(\tan\left(\frac{\theta}{2}\right)\frac{\lambda-d^2\gamma}{2d\sqrt{\gamma}}\right)\right)$

Table 2.2: Numbers $n_{k,l}$, $1 \leq l \leq \{q_{\max}, M/2\}$, of nearest competitive signal sets of type k, $1 \leq k \leq 6$ (Cases shown in Figure 2.2) for different constellations and labelings used for numerical results in Section 2.5. Only non-zero coefficients $n_{k,l}$ are shown. Gray labeling (GL), set partitioning labeling (SPL), modified set partitioning labeling (MSPL), semi set partitioning labeling (SSPL), and mixed labeling (ML).

4QAM	GL	$n_{1,1}=4$
	SPL	$n_{1,1}=2, n_{2,1}=2$
16QAM	GL	$n_{1,1}=24, n_{1,2}=8$
	SPL	$n_{1,1}=8, n_{1,2}=4, n_{2,1}=10, n_{3,1}=4, n_{4,1}=4, n_{5,1}=2$
	MSPL	$n_{1,1}=16, n_{2,1}=4, n_{2,2}=2, n_{3,1}=4, n_{4,1}=4, n_{5,1}=2$
	ML	$n_{1,1}=24, n_{3,1}=8$
64QAM	GL	$n_{1,1}=112, n_{1,2}=48, n_{1,3}=16, n_{1,4}=16$
8PSK	GL	$n_{1,1}=8, n_{1,2}=4$
	SPL	$n_{1,1}=6, n_{1,2}=2, n_{2,1}=4$
	SSPL	$n_{1,1}=6, n_{2,1}=6$

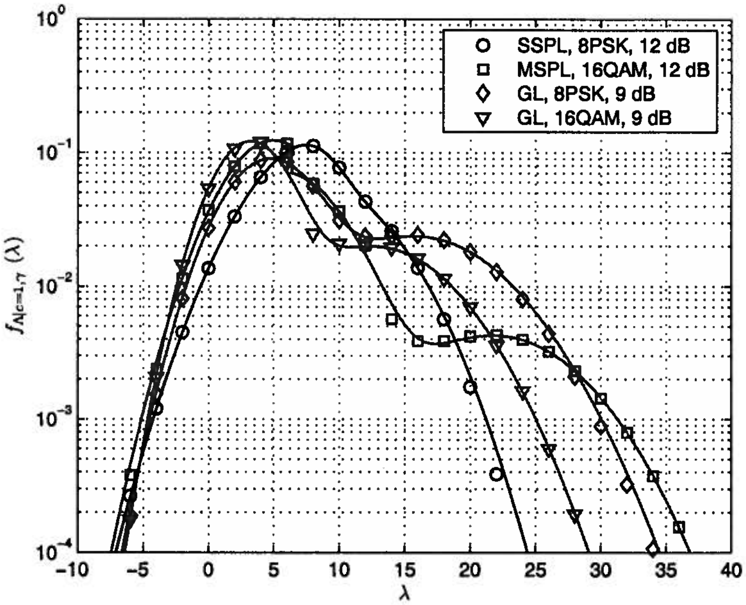

Figure 2.3: Probability density functions of reliability metrics for BICM transmission over the nonfading AWGN channel for different constellations and labeling. Lines represent the PDF approximation given in (2.19) and (2.20) while markers represent the estimated histograms through simulative measurement.

labeling. Especially the negative tail of the PDF is represented faithfully, which is important when evaluating performance parameters.

2.3.2 Laplace Transform of the PDF Approximation

We now apply (2.19) and (2.20) to obtain expressions for the Laplace transform $\Phi_{\Lambda|\bar{\gamma},m}(s)$ which become closed form for $s \in \mathbb{R}^+$.

Table 2.3: Laplace transform of the probability density function of LLRs for transmission over nonfading AWGN channel $\Phi_{\Lambda,k|\cdot,\gamma}(s)$ for the six different sets of competitive signal points $\mathcal{A}_{j,x}$ shown in Figure 2.2.

$\Phi_{\Lambda,1\|d,\gamma}(s)$	$\exp\left(d^2\gamma\left(s^2-s\right)\right)$
$\Phi_{\Lambda,2\|d,\gamma}(s)$	$\exp\left(d^2\gamma\left(s^2-s\right)\right)\left(1+\operatorname{erf}\left(d\sqrt{\frac{\gamma}{2}}\,s\right)\right)$
$\Phi_{\Lambda,3\|d,\gamma}(s)$	$\exp\left(d^2\gamma\left(s^2-s\right)\right)\left(1+\operatorname{erf}\left(d\sqrt{\gamma}\,s\right)\right)$
$\Phi_{\Lambda,4\|d,\gamma}(s)$	$\frac{1}{2}\exp\left(d^2\gamma\left(s^2-s\right)\right)\left(1+\operatorname{erf}\left(d\sqrt{\gamma}\,s\right)+\left(1+\operatorname{erf}\left(d\sqrt{\frac{\gamma}{2}}\,s\right)\right)^2\right)$
$\Phi_{\Lambda,5\|d,\gamma}(s)$	$\exp\left(d^2\gamma\left(s^2-s\right)\right)\left(1+\operatorname{erf}\left(d\sqrt{\frac{\gamma}{2}}\,s\right)\right)^2$
$\Phi_{\Lambda,6\|d,\theta,\gamma}(s)$	$\exp\left(d^2\gamma\left(s^2-s\right)\right)\left(1+\operatorname{erf}\left(\sin\left(\frac{\theta}{2}\right)d\sqrt{\gamma}\,s\right)\right)$

Nonfading Channel

First we consider the nonfading case, i.e., $m \to \infty$, for which $\gamma = \bar{\gamma}$. We denote the Laplace transform for this case by $\Phi_{\Lambda|\gamma}(s)$. Starting from (2.19) and (2.20), $\Phi_{\Lambda|\gamma}(s)$ is obtained as

$$\Phi_{\Lambda|\gamma}(s) = \frac{2}{rM}\sum_{k=1}^{5}\sum_{l=1}^{q_{\max}} n_{k,l}\,\Phi_{\Lambda,k|d_l,\gamma}(s)\,, \quad d_l = l\,d_{\min}\,, \tag{2.21}$$

for a general M-ary QAM constellation and as

$$\begin{aligned}\Phi_{\Lambda|\gamma}(s) =& \frac{2}{rM}\sum_{l=1}^{\frac{M}{2}}\left[n_{1,l}\,\Phi_{\Lambda,1|d_l,\gamma}(s) + n_{6,l}\,\Phi_{\Lambda,6|d_l,\theta_l,\gamma}(s)\right]\,,\\ &\begin{cases} d_l &= \frac{\sin\left(\frac{\pi l}{M}\right)}{\sin\left(\frac{\pi}{M}\right)}d_{\min},\\ \theta_l &= \pi-\frac{2\pi l}{M},\end{cases}\end{aligned} \tag{2.22}$$

for PSK constellations, respectively. $\Phi_{\Lambda,k|\cdot,\gamma}(s)$ is the Laplace transform of $f_{\Lambda,k|\cdot,\gamma}(\lambda)$, $1 \le k \le 6$. Using the expressions for $f_{\Lambda,k|\cdot,\gamma}(\lambda)$ from Table 2.1,

Table 2.4: Laplace transform of the probability density function of LLRs when transmitting over Nakagami-m fading channels $\Phi_{\Lambda,k|\cdot,\bar{\gamma},m}(s)$ for the six different sets of competitive signal points $\mathcal{A}_{j,x}$ shown in Figure 2.2.

$\Phi_{\Lambda,1\|d,\bar{\gamma},m}(s)$	$\left(\frac{m}{m-d^2\bar{\gamma}(s^2-s)}\right)^m$
$\Phi_{\Lambda,2\|d,\bar{\gamma},m}(s)$	$\left(\frac{m}{m-d^2\bar{\gamma}(s^2-s)}\right)^m + I_{3\|d^2,d/\sqrt{2}}(s)$
$\Phi_{\Lambda,3\|d,\bar{\gamma},m}(s)$	$\left(\frac{m}{m-d^2\bar{\gamma}(s^2-s)}\right)^m + I_{3\|d^2,d}(s)$
$\Phi_{\Lambda,4\|d,\bar{\gamma},m}(s)$	$\left(\frac{m}{m-d^2\bar{\gamma}(s^2-s)}\right)^m + \frac{1}{2}I_{3\|d^2,d}(s) + I_{3\|d^2,d/\sqrt{2}}(s) + \frac{1}{2}I_{4\|d^2,d/\sqrt{2}}(s)$
$\Phi_{\Lambda,5\|d,\bar{\gamma},m}(s)$	$\left(\frac{m}{m-d^2\bar{\gamma}(s^2-s)}\right)^m + 2I_{3\|d^2,d/\sqrt{2}}(s) + I_{4\|d^2,d/\sqrt{2}}(s)$
$\Phi_{\Lambda,6\|d,\theta,\bar{\gamma},m}(s)$	$\left(\frac{m}{m-d^2\bar{\gamma}(s^2-s)}\right)^m + I_{3\|d^2,\sin(\theta/2)d}(s)$

the $\Phi_{\Lambda,k|\cdot,\gamma}(s)$ can be written as weighted sum of the following integrals:

$$I_{1|\mu}(s) = \int_{-\infty}^{\infty} \mathcal{N}_{\mu,2\mu}(x)\mathrm{erf}\left(\frac{x-\mu}{2\sqrt{\mu}}\right) u(\mu - x)\exp(-sx)\,\mathrm{d}x\,, \quad (2.23)$$

$$I_{2|\mu,\nu}(s) = \int_{-\infty}^{\infty} \mathcal{N}_{\mu,2\mu}(x)\,\mathrm{erf}\left(\nu\frac{x-\mu}{\sqrt{\mu}}\right)\exp(-sx)\,\mathrm{d}x\,, \quad (2.24)$$

where $\mu = d^2\gamma$ and $\nu = \tan(\theta/2)$. Closed-form expressions for these integrals assuming $s \in \mathbb{R}^+$ are derived in the appendix, and the resulting expressions for $\Phi_{\Lambda,k|\cdot,\gamma}(s)$ are summarized in Table 2.3.

Nakagami-m Fading Channel

We now consider the faded AWGN channel. Due to the linearity property of Laplace transform, we have

$$\Phi_{\Lambda|\bar{\gamma},m}(s) = \int_0^{\infty} f_{\gamma|\bar{\gamma},m}(\gamma)\Phi_{\Lambda|\gamma}(s)\,\mathrm{d}\gamma\,. \quad (2.25)$$

Substituting (2.21) and (2.22) for $\Phi_{\Lambda|\gamma}(s)$ in (2.25), we can write $\Phi_{\Lambda|\bar{\gamma},m}(s)$ as linear superposition of

$$\Phi_{\Lambda,k|\cdot,\bar{\gamma},m}(s) = \int_0^\infty f_{\gamma|\bar{\gamma},m}(\gamma)\Phi_{\Lambda,k|\cdot,\gamma}(s)\,\mathrm{d}\gamma\,, \tag{2.26}$$

for which expressions are given in Table 2.4 in terms of the integrals

$$I_{3|\mu,\nu}(s) = \int_0^\infty f_{\gamma|\bar{\gamma},m}(\gamma)\exp\left(-\mu(s-s^2)\gamma\right)\mathrm{erf}\,(\nu\, s\sqrt{\gamma})\,\mathrm{d}\gamma\,, \tag{2.27}$$

$$I_{4|\mu,\nu}(s) = \int_0^\infty f_{\gamma|\bar{\gamma},m}(\gamma)\exp\left(-\mu(s-s^2)\gamma\right)\left(\mathrm{erf}\,(\nu\, s\sqrt{\gamma})\right)^2\mathrm{d}\gamma\,. \tag{2.28}$$

Here, $\mu = d^2$, and $\nu \in \{d/\sqrt{2}, d, d\sin(\theta/2)\}$. In the appendix, we provide closed-form expressions for these integrals for $s \in \mathbb{R}^+$ and general m in terms of Appell's double Hypergeometric function and Gauss' Hypergeometric function [17] [18] together with simplified approximations in terms of elementary functions. Furthermore, for integer values of m exact closed-form expressions are given using only elementary functions. For example, for the important case of Rayleigh fading ($m = 1$) the integrals in (2.27) and (2.28) are obtained as

$$I_{3|\mu,\nu}(s) = \frac{\nu s}{[1+\bar{\gamma}\,\mu(s-s^2)]\sqrt{(\nu\, s)^2+\mu(s-s^2)+\frac{1}{\bar{\gamma}}}}\,,$$

$$I_{4|\mu,\nu}(s) = \frac{4}{\pi\,[1+\bar{\gamma}\,\mu(s-s^2)]}\tan^{-1}\left(\frac{\nu\, s}{\sqrt{(\nu\, s)^2+\mu(s-s^2)+\frac{1}{\bar{\gamma}}}}\right)\,.$$

Table 2.5: Asymptotic values of Probability Density Function of LLRs $f^a_{\Lambda,k|d,\gamma}(\lambda)$ for transmission over nonfading AWGN channel, its Laplace transform $\Phi^a_{\Lambda,k|d,\gamma}(s)$, and the Laplace transform of the PDF of LLRs when transmitting over Nakagami-m fading channels $\Phi^a_{\Lambda,k|d,\bar{\gamma},m}(s)$ for the six different sets of competitive signal points $\mathcal{A}_{j,x}$ shown in Figure 2.2.

Case 1	$f^a_{\Lambda,1\|d,\gamma}(\lambda)$	$\mathcal{N}_{d^2\gamma,2d^2\gamma}(\lambda)$
	$\Phi^a_{\Lambda,1\|d,\gamma}(s)$	$\exp\left(d^2\gamma\left(s^2-s\right)\right)$
	$\Phi^a_{\Lambda,1\|d,\bar{\gamma},m}(s)$	$\left(\frac{m}{m-d^2\bar{\gamma}(s^2-s)}\right)^m$
Case 2	$f^a_{\Lambda,2\|d,\gamma}(\lambda)$	$2\mathcal{N}_{d^2\gamma,2d^2\gamma}(\lambda)$
	$\Phi^a_{\Lambda,2\|d,\gamma}(s)$	$2\exp\left(d^2\gamma\left(s^2-s\right)\right)$
	$\Phi^a_{\Lambda,2\|d,\bar{\gamma},m}(s)$	$2\left(\frac{m}{m-d^2\bar{\gamma}(s^2-s)}\right)^m$
Case 3	$f^a_{\Lambda,3\|d,\gamma}(\lambda)$	$2\mathcal{N}_{d^2\gamma,2d^2\gamma}(\lambda)$
	$\Phi^a_{\Lambda,3\|d,\gamma}(s)$	$2\exp\left(d^2\gamma\left(s^2-s\right)\right)$
	$\Phi^a_{\Lambda,3\|d,\bar{\gamma},m}(s)$	$2\left(\frac{m}{m-d^2\bar{\gamma}(s^2-s)}\right)^m$
Case 4	$f^a_{\Lambda,4\|d,\gamma}(\lambda)$	$3\mathcal{N}_{d^2\gamma,2d^2\gamma}(\lambda)$
	$\Phi^a_{\Lambda,4\|d,\gamma}(s)$	$3\exp\left(d^2\gamma\left(s^2-s\right)\right)$
	$\Phi^a_{\Lambda,4\|d,\bar{\gamma},m}(s)$	$3\left(\frac{m}{m-d^2\bar{\gamma}(s^2-s)}\right)^m$
Case 5	$f^a_{\Lambda,5\|d,\gamma}(\lambda;d,\gamma)$	$4\mathcal{N}_{d^2\gamma,2d^2\gamma}(\lambda)$
	$\Phi^a_{\Lambda,5\|d,\gamma}(s)$	$4\exp\left(d^2\gamma\left(s^2-s\right)\right)$
	$\Phi^a_{\Lambda,5\|d,\bar{\gamma},m}(s)$	$4\left(\frac{m}{m-d^2\bar{\gamma}(s^2-s)}\right)^m$
Case 6	$f^a_{\Lambda,6\|d,\gamma}(\lambda)$	$2\mathcal{N}_{d^2\gamma,2d^2\gamma}(\lambda)$
	$\Phi^a_{\Lambda,6\|d,\gamma}(s)$	$2\exp\left(d^2\gamma\left(s^2-s\right)\right)$
	$\Phi^a_{\Lambda,6\|d,\bar{\gamma},m}(s)$	$2\left(\frac{m}{m-d^2\bar{\gamma}(s^2-s)}\right)^m$

2.4 Asymptotic Analysis for High SNRs

In this section, we consider the case of asymptotically high SNR to further simplify the expressions for the PDF of LLRs and its Laplace transform. We then provide the saddlepoint approximation (2.8) and the direct derivation of the PEP without saddlepoint approximation for the asymptotic case. From this analysis we immediately obtain important performance indicators for BICM transmission over Nakagami-m fading channels.

2.4.1 PDF of LLRs and Its Laplace Transform

The expressions for the PDF of LLRs and its Laplace transform for transmission over the nonfading AWGN channel shown in Table 2.1 and Table 2.3 can be simplified for high SNRs by replacing the error function with its asymptotic values, i.e., $\mathrm{erf}(x) \approx 1$ (-1) for $x \gg 0$ $(x \ll 0)$, which corresponds to high SNRs γ. The Laplace transform expressions for transmission over fading channels are then obtained from averaging using (2.26). Table 2.5 summarizes the closed-form asymptotic results $f^a_{\Lambda,k|d,\gamma}(\lambda)$, $\Phi^a_{\Lambda,k|d,\gamma}(s)$, and $\Phi^a_{\Lambda,k|d,\bar{\gamma},m}(s)$ for $1 \le k \le 6$. Using the expressions from Table 2.5 in (2.19)-(2.22), the following simplified expressions are obtained:

$$f^a_{\Lambda|c=1,\gamma}(\lambda) = \sum_{l=1}^{l_{\max}} N_l \mathcal{N}_{d_l^2\gamma, 2d_l^2\gamma}(\lambda) , \tag{2.29}$$

$$\Phi^a_{\Lambda|\gamma}(s) = \sum_{l=1}^{l_{\max}} N_l \exp\left(d_l^2 \gamma \left(s^2 - s\right)\right) , \tag{2.30}$$

$$\Phi^a_{\Lambda|\bar{\gamma},m}(s) = \sum_{l=1}^{l_{\max}} N_l \left(\frac{m}{m - d_l^2 \bar{\gamma} \left(s^2 - s\right)}\right)^m , \tag{2.31}$$

where

$$l_{\max} \triangleq \begin{cases} q_{\max}\,, & \text{for QAM,} \\ M/2\,, & \text{for PSK,} \end{cases} \tag{2.32}$$

$$N_l \triangleq \begin{cases} \frac{2}{rM}\left(n_{1,l} + 2n_{2,l} + 2n_{3,l} + 3n_{4,l} + 4n_{5,l}\right)\,, & \text{for QAM,} \\ \frac{2}{rM}\left(n_{1,l} + 2n_{6,l}\right)\,, & \text{for PSK.} \end{cases} \tag{2.33}$$

2.4.2 Saddlepoint Approximation

We now apply the saddlepoint approximation (2.8) and the asymptotic Laplace transform expressions from (2.30) and (2.31) to obtain asymptotic BER expressions. We note from the expressions for $\Phi^{a}_{\Lambda|\cdot}(s)$ in Table 2.5 that the saddlepoint $\hat{\alpha} = 1/2$ (cf. (2.9)).

Nonfading Channel

In the nonfading channel case ($m \to \infty$, $\gamma = \bar{\gamma}$), substituting the Laplace transform expression given in (2.30) into (2.8) and considering only the asymptotically dominant term, we arrive at

$$\mathrm{PEP}\left(d_{\mathrm{H}}|\gamma\right) = \frac{N_1^{d_{\mathrm{H}}}}{d_1\sqrt{\pi\, d_{\mathrm{H}}\,\gamma}} \exp\left(-\frac{1}{4} d_{\mathrm{H}}\, d_1^2\, \gamma\right)\,. \tag{2.34}$$

Finally, substituting (2.34) into (2.5) and only considering the PEP with minimum Hamming distance gives asymptotic BER for transmission over the nonfading channel.

Nakagami-m Fading Channel

The substitution of (2.31) into (2.8) results in

$$\mathrm{PEP}(d_{\mathrm{H}}|\bar{\gamma}, m) = \frac{1}{2\sqrt{\pi\, d_{\mathrm{H}}\, m}} \left[\sum_{l=1}^{l_{\max}} \left(\frac{N_l}{d_l^{2m}}\right)\right]^{d_{\mathrm{H}}} \left(\frac{4m}{\bar{\gamma}}\right)^{m d_{\mathrm{H}}} . \tag{2.35}$$

Substituting (2.35) into (2.5) we can identify the diversity order as

$$G_d = m\, d_{\text{free}} , \tag{2.36}$$

i.e., the product of the free distance of the convolutional code and the Nakagami-m fading parameter. The horizontal offset of the log-error-rate curve, and thus the coding gain, depends on modulation, labeling, and fading parameter m. In particular, the coefficient

$$d_{h|m}^2 \triangleq \left[\sum_{l=1}^{l_{\max}} \left(\frac{N_l}{d_l^{2m}}\right)\right]^{-1/m} . \tag{2.37}$$

can be considered as a direct generalization of the harmonic mean d_h^2 obtained in [2, Eq. (63)] for Gray labeling and transmission over Rayleigh fading channels ($m = 1$) to arbitrary labeling rules and fading factors m.

2.4.3 Direct Analysis

The simplified expression (2.30) also allows direct evaluation of the PEP without saddlepoint approximation.

Nonfading Channel

For transmission over the nonfading AWGN channel we use (2.30) to define

$$\Phi_{\Delta_{d_{\mathrm{H}}}|\gamma}(s) \triangleq \left[\Phi^{a}_{\Lambda|\gamma}(s)\right]^{d_{\mathrm{H}}} = \left[\sum_{l=1}^{l_{\max}} N_l \exp\left(d_l^2 \gamma \left(s^2 - s\right)\right)\right]^{d_{\mathrm{H}}} . \tag{2.38}$$

Using the multinomial-series representation (cf. [17, p. 823]), this can be written as

$$\begin{aligned}\Phi_{\Delta_{d_{\mathrm{H}}}|\gamma}(s) = \sum_{\substack{i_1, i_2, \ldots, i_{l_{\max}} \\ i_1+i_2+\ldots+i_{l_{\max}}=d_{\mathrm{H}}}} &\left(\frac{d_{\mathrm{H}}!}{\prod_{l=1}^{l_{\max}} i_l!}\right) \\ &\left(\prod_{l=1}^{l_{\max}} N_l^{i_l}\right) \exp\left[\left(\sum_{l=1}^{l_{\max}} i_l d_l^2\right) \left(s^2 - s\right) \gamma\right] .\end{aligned} \tag{2.39}$$

Since (2.39) is the Laplace transform of a linear superposition of Gaussian PDFs, the PEP is obtained in closed form as

$$\mathrm{PEP}(d_{\mathrm{H}}|\gamma) = \sum_{\substack{i_1, i_2, \ldots, i_{l_{\max}} \\ i_1+i_2+\ldots+i_{l_{\max}}=d_{\mathrm{H}}}} \left(\frac{d_{\mathrm{H}}!}{\prod_{l=1}^{l_{\max}} i_l!}\right) \left(\prod_{l=1}^{l_{\max}} N_l^{i_l}\right) Q\left[\sqrt{\frac{\gamma}{2}\left(\sum_{l=1}^{l_{\max}} i_l d_l^2\right)}\right] . \tag{2.40}$$

Considering only the asymptotically dominant term gives the approximation

$$\mathrm{PEP}(d_{\mathrm{H}}|\gamma) = N_1^{d_{\mathrm{H}}} Q\left(\sqrt{d_{\mathrm{H}} d_1^2 \frac{\gamma}{2}}\right) . \tag{2.41}$$

Hence, the asymptotic PEP is expressed as the PEP for binary (i.e., BPSK) transmission with an equivalent SNR of $d_{\mathrm{H}}\, d_1^2\, \gamma$, scaled by a constant which is a function of the minimum Hamming distance of the code and the mapping rule. From the convergence of lower and upper bounds for the Q-function for large arguments [19], we obtain for $\gamma \to \infty$

$$\mathrm{PEP}(d_{\mathrm{H}}|\gamma) = \frac{N_1^{d_{\mathrm{H}}}}{d_1\sqrt{\pi d_{\mathrm{H}}\gamma}} \exp\left(-\frac{1}{4}d_{\mathrm{H}}d_1^2\gamma\right) , \tag{2.42}$$

which coincides with the result (2.34) from the saddlepoint approximation.

Nakagami-m Fading Channel

Instead of directly using (2.31) we found it easier (i) first to determine the PEP conditioned on the vector $\gamma \triangleq [\gamma_1, \dots, \gamma_{d_{\mathrm{H}}}]$ of instantaneous SNRs experienced by the d_{H} bits involved in an error event and 9ii) then to average with respect to the PDF $f_{\gamma|\bar{\gamma},m}(\gamma)$ of the SNR vector. Hence, starting again from (2.30) we write the Laplace transform conditioned on γ

$$\Phi_{\Delta_{d_{\mathrm{H}}}|\gamma}(s) \triangleq \prod_{i=1}^{d_{\mathrm{H}}} \Phi^a_{\Lambda|\gamma_i}(s) = \sum_{\substack{\{l_1,\dots,l_{d_{\mathrm{H}}}\} \\ \in\{1,\dots,l_{\max}\}^{d_{\mathrm{H}}}}} \left(\prod_{j=1}^{d_{\mathrm{H}}} N_{l_j}\right) \exp\left(\sum_{j=1}^{d_{\mathrm{H}}} d_{l_j}^2\gamma_j(s^2 - s)\right) , \tag{2.43}$$

from which we obtain the conditioned PEP as

$$\mathrm{PEP}(d_{\mathrm{H}}|\gamma) = \sum_{\substack{\{l_1,\dots,l_{d_{\mathrm{H}}}\} \\ \in\{1,\dots,l_{\max}\}^{d_{\mathrm{H}}}}} \left(\prod_{j=1}^{d_{\mathrm{H}}} N_{l_j}\right) Q\left(\sqrt{\frac{1}{2}\sum_{j=1}^{d_{\mathrm{H}}} d_{l_j}^2\gamma_j}\right) . \tag{2.44}$$

Applying the alternative representation of the Q-function (cf. [9, p. 85]) and averaging with respect to the SNR vector leads to

$$\mathrm{PEP}(d_{\mathrm{H}}|\bar{\gamma}, m) = \frac{1}{\pi} \sum_{\substack{\{l_1,\ldots,l_{d_{\mathrm{H}}}\} \\ \in\{1,\ldots,l_{\max}\}^{d_{\mathrm{H}}}}} \left(\prod_{j=1}^{d_{\mathrm{H}}} N_{l_j}\right) \int_0^{\pi/2} \prod_{j=1}^{d_{\mathrm{H}}} \left(1 + \frac{d_{l_j}^2 \bar{\gamma}}{4m\sin^2(\phi)}\right)^{-m} \mathrm{d}\phi \,. \tag{2.45}$$

Making the high SNR assumption $1 \ll \frac{d_{l_j}^2 \bar{\gamma}}{4m\sin^2(\phi)}$, we obtain

$$\mathrm{PEP}(d_{\mathrm{H}}|\bar{\gamma}, m) = \left(\sum_{l=1}^{l_{\max}} \frac{N_l}{d_l^{2m}}\right)^{d_{\mathrm{H}}} \left(\frac{4m}{\bar{\gamma}}\right)^{md_{\mathrm{H}}} \frac{1}{\pi} \int_0^{\pi/2} (\sin\phi)^{2md_{\mathrm{H}}} \, \mathrm{d}\phi \,, \tag{2.46}$$

which finally can be solved to [20, Eq. 3.621]

$$\mathrm{PEP}(d_{\mathrm{H}}|\bar{\gamma}, m) = \frac{\Gamma(md_{\mathrm{H}}+1/2)}{2\sqrt{\pi}\Gamma(md_{\mathrm{H}}+1)} \left(\sum_{l=1}^{l_{\max}} \frac{N_l}{d_l^{2m}}\right)^{d_{\mathrm{H}}} \left(\frac{4m}{\bar{\gamma}}\right)^{md_{\mathrm{H}}} . \tag{2.47}$$

We note that the PEP in (2.47) has the same form as the PEP (2.35) obtained with the saddlepoint approximation. In particular, the diversity order G_d (2.36) and the generalized harmonic mean $d_{h|m}^2$ (2.37) are confirmed as important parameters for code and channel diversity and coding gain. Furthermore, recalling the asymptotic series

$$\frac{\Gamma(x+1/2)}{\Gamma(x+1)} = x^{-1/2}\left[1 + O(x^{-1})\right], \quad x \to \infty \,, \tag{2.48}$$

we note that (2.47) and (2.35) become identical for $md_{\mathrm{H}} \gg 1$. The discrepancy for small values of md_{H} indicates the insufficiency of the second-order approximation of the cumulant transform $\log\left(\Phi_{\Lambda|\bar{\gamma},m}(-s)\right)$ used in (2.8) for extreme cases of fading (i.e., $m \ll 1$).

2.5 Numerical Results and Discussions

In this section, we present a number of exemplary numerical results to illustrate the accuracy of cutoff rate and BER approximations based on the new closed-form expressions. For the BER results we assume BICM with the popular, quasi-standard 64-state rate-1/2 convolutional code with generator polynomials $(171, 133)_8$.

Cutoff-Rate Results

First, we consider the cutoff rate (2.12) using the closed-form approximations for the Laplace transform derived in Section 2.3.2. We found that $\alpha = 1/2$ yields practically the same results as when using the exact saddlepoint $\hat{\alpha}$ (cf. Eq. (2.9)), which is consistent with the results reported in [10] and the fact that $\hat{\alpha} \to 1/2$ with increasing SNR (cf. Section 2.4.2). We therefore adopted $\alpha = 1/2$ in all cases.

Figure 2.4 shows R_0-curves for QAM and PSK constellations with different mapping rules and channel types. In addition to popular Gray labeling (GL), two non-Gray labeling, namely, mixed labeling (ML) and set partitioning labeling (SPL) (cf. [2, 15]) are also included. The markers represent R_0-values obtained with Monte Carlo simulation, and the lines represent results from the evaluation of the closed form expression. We observe that there is an excellent agreement between analytical and simulation results for a wide range of SNR, and in particular for all R_0 values of practical inter-

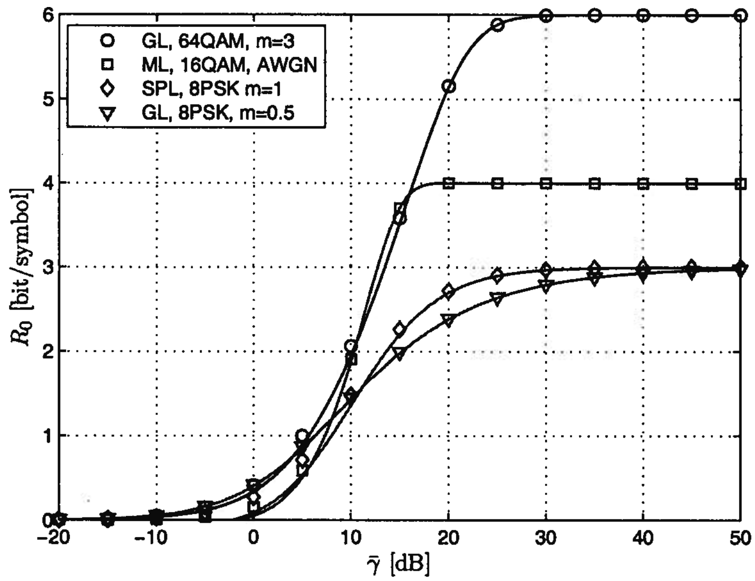

Figure 2.4: Cutoff Rate R_0 for BICM channel with different constellations, labeling rules, and channels. Lines are obtained from evaluation of (2.12) using the approximation for the Laplace transform derived in Section 2.3.2, while markers are obtained from Monte Carlo simulation.

est. The discrepancies between analytical and simulated cutoff-rate curves for non-GL and low SNRs in Figure 2.4 are expected, since the underlying approximation of the PDF of LLRs (cf. Section 2.3) is not accurate in this SNR range.

Bit-Error Rate Results

Next, we compare simulated and analytical BER results. In case of the BER union bound (2.5), only the 15 first terms of the distance spectrum of the convolutional code were taken into account, and thus, strictly speaking, the

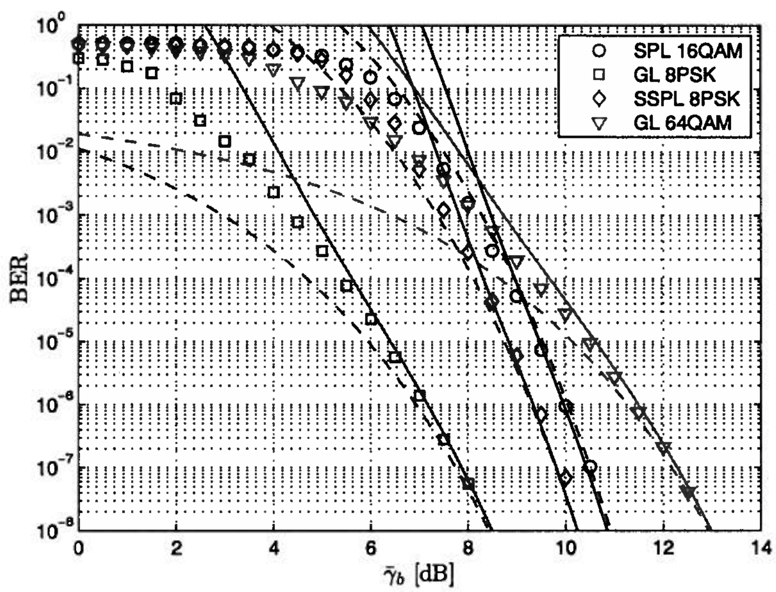

Figure 2.5: BER of BICM transmission over nonfading AWGN channel for a 64-state convolutional code of rate 1/2. Solid lines: BER union bound. Dashed lines: Asymptotic analysis with (2.41). Markers: Simulation results

BER union bound is a BER approximation.

Figure 2.5 shows the analytical (lines) and simulated (markers) BER results for different constellations and labeling for transmission over the nonfading AWGN channel. Solid lines represent the BER union bound, while dashed lines represent the asymptotic approximation (2.41) for $d_{\mathrm{H}} = d_{\mathrm{free}}$, i.e., only the asymptotically dominating error event is considered. We observe that the BER union bound is fairly tight for all modulation schemes and BERs below about 10^{-4}. Likewise, the proposed simple expression (2.41) accurately predicts the asymptotic error-rate performance at high SNR. Similar results are obtained with the expression (2.34) derived from

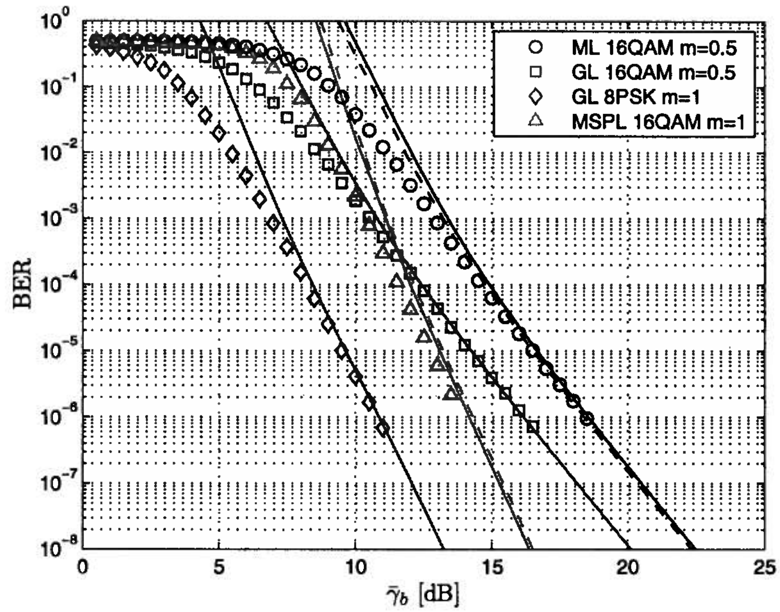

Figure 2.6: BER of BICM transmission over Nakagami-m fading channel for a 64-state convolutional code of rate 1/2. Solid lines: BER union bound using the exact closed-form solutions for integrals (2.27), (2.28). Dashed lines: BER union bound using the approximations (2.61), (2.66). Markers: Simulation results

the saddlepoint approximation, which is apparent from the equivalence of (2.41) and (2.34) for high SNR (cf. Section 2.4.3).

We now compare analytical and simulated BER results for BICM transmission over fading channels with different constellations and labeling rules. To this end, Figure 2.6 shows BER curves obtained from the BER union bound and the exact closed-form solutions for integrals (2.27), (2.28) (solid lines) and their approximations (2.61), (2.66) (dashed lines) derived in the appendix. Again, we observe an excellent match between results from analy-

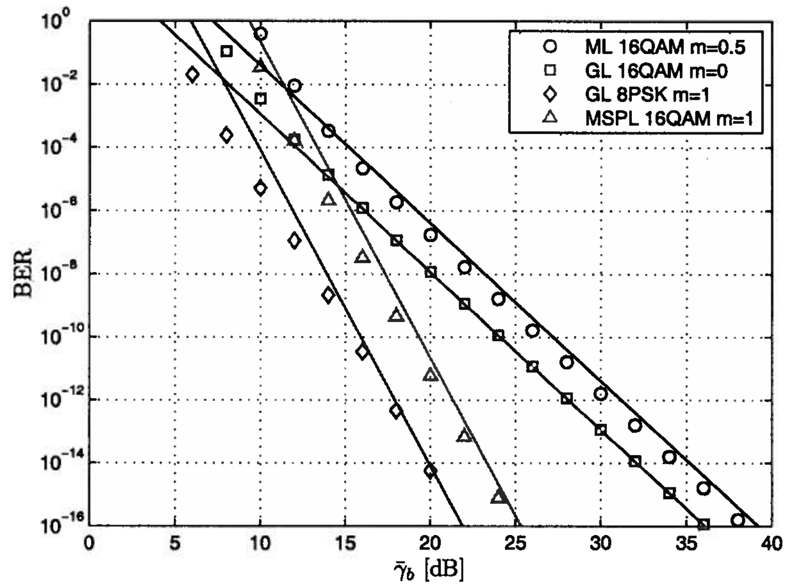

Figure 2.7: BER of BICM transmission over Nakagami-m fading channel for a 64-state convolutional code of rate 1/2. Solid lines: Asymptotic analysis with (2.47). Markers: BER union bound.

sis and simulations, which confirms the validity of the approximations made for the derivation of the closed-form BER expressions. Since this is also true for the expressions using the exponential approximations of the error function, i.e., (2.61) and (2.66), we have provided tight BER approximations in terms of elementary functions.

Finally, in Figure 2.7 the asymptotic BER results from (2.47) and $d_{\mathrm{H}} = d_{\mathrm{free}}$ (solid lines) are plotted together with the BER union bound (markers) for the same transmission scenarios as in Figure 2.6. It can be seen that the asymptotic results correctly predict coding and fading gain of the BICM scheme. Similar results are obtained when evaluating (2.35), since the term on the left-hand side of (2.48) is well approximated by $(md_{\mathrm{H}})^{-1/2}$ for $md_{\mathrm{H}} = md_{\mathrm{free}} = 10m \geq 5$ for $m \in \{0.5, 1\}$ in Figure 2.7. Hence, we conclude that the simple expressions (2.35) and (2.47) are very valuable to quickly determine the asymptotic performance of BICM transmission over fading channels.

2.6 Conclusion

In this chapter we have presented a new method for analyzing the performance of BICM transmission. Its key element is a new approximation of the PDF of the bitwise reliability metrics, which is a valuable contribution in its own right. This approximation has led us to closed-form expressions for the Laplace transform of the PDF, in terms of which BER and cutoff rate of BICM can be expressed. Notably, our results are valid for BICM with arbitrary QAM and PSK constellations and mapping rules, and transmission over Nakagami-m fading channels for arbitrary m. Furthermore, we have developed an asymptotic analysis which provides valuable insights into the performance of BICM over fading channels, namely expressions for diversity order and asymptotic coding gain. We have presented selected numerical results, which confirmed the accuracy of the proposed analytical results for SNR regions of interest for moderately complex coding schemes, such as convolutional coded BICM.

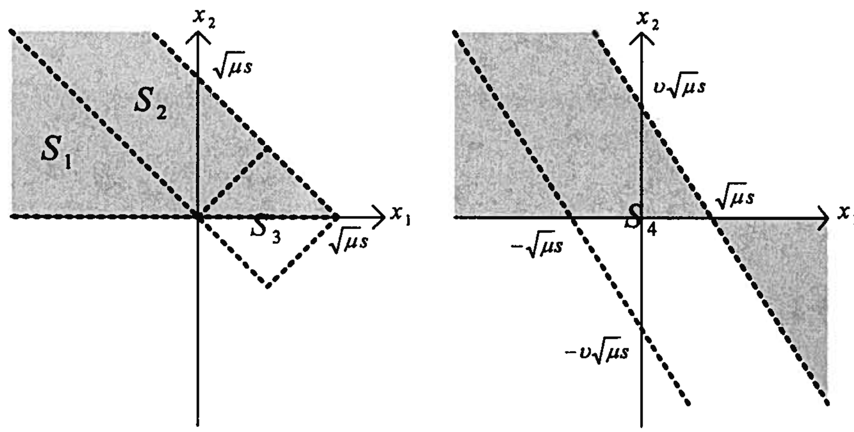

Figure 2.8: The graphical representation of integrals (2.50) (left) and (2.53) (right). Shaded areas are integration supports, and dashed lines indicate decomposition into support areas for which the integrals can be solved.

2.7 Appendix

In this appendix we present the solutions for the four integrals $I_{k|\cdot}(s)$ that appear in Section 2.3.2.

2.7.1 Closed-form Expression for $I_{1|\mu}(s)$ in (2.23) for $s \in \mathbb{R}^+$

Using the integral form of the error function, $I_{1|\mu}(s)$ from (2.23) is written as

$$I_{1|\mu}(s) = \frac{1}{\pi\sqrt{\mu}} \int_{-\infty}^{\mu} \int_{0}^{\frac{x-\mu}{2\sqrt{\mu}}} \exp\left(\frac{(x-\mu)^2}{4\mu}\right) \exp\left(-x_2^2\right) \exp\left(-sx\right) dx_2 \, \mathrm{d}x \, . \tag{2.49}$$

Applying the change of variables $x_1 \triangleq \frac{x+\mu(2s-1)}{2\sqrt{\mu}}$ leads to

$$I_{1|\mu}(s) = -\frac{2}{\pi}\exp\left(\mu\left(s^2 - s\right)\right)\int\limits_{-\infty}^{\sqrt{\mu}s}\int\limits_{0}^{\sqrt{\mu}s-x_1}\exp\left(-\left(x_1^2 + x_2^2\right)\right)dx_2\,dx_1\,. \tag{2.50}$$

The support of this integral is illustrated in Figure 2.8 (shaded area in the left sub-figure), from which we can express it as

$$I_{1|\mu}(s) = -\frac{2}{\pi}\exp\left(\mu\left(s^2 - s\right)\right)\left(S_1 + S_2 + \frac{S_3}{2}\right)\,, \tag{2.51}$$

where S_1, S_2, and S_3 denote the corresponding areas indicated in the Figure 2.8 (left sub-figure). Using the rotational invariance of the integrand in (2.50), the areas are easily determined and from (2.51) the integral is finally obtained as

$$I_{1|\mu}(s) = -\frac{1}{4}\left(1 + \operatorname{erf}\left(\sqrt{\frac{\mu}{2}}s\right)\right)^2\,. \tag{2.52}$$

2.7.2 Closed-form Expression for $I_{2|\mu,\nu}(s)$ in (2.24) for $s \in \mathbb{R}^+$

Starting from (2.24) and performing the same transformations as above, we obtain

$$I_{2|\mu,\nu}(s) = -\frac{2}{\pi}\exp\left(\mu\left(s^2 - s\right)\right)\int\limits_{-\infty}^{\infty}\int\limits_{0}^{2\nu(\sqrt{\mu}s-x_1)}\exp\left(-\left(x_1^2 + x_2^2\right)\right)dx_2\,dx_1\,. \tag{2.53}$$

The support of this integral is illustrated in Figure 2.8 (shaded area in the right sub-figure). Exploiting again the fact that integrand in (2.50) is rotational invariant, we can write

$$I_{2|\mu,\nu}(s) = -\frac{2}{\pi}\exp\left(\mu\left(s^2 - s\right)\right)\left(\frac{S_4}{2}\right) , \tag{2.54}$$

where S_4 is illustrated in Figure 2.8 (right sub-figure). Finally, we arrive at the closed-form expression

$$I_{2|\mu,\nu}(s) = -\exp\left(\mu\left(s^2 - s\right)\right)\operatorname{erf}\left(\frac{2\nu}{1+(2\nu)^2}\sqrt{\mu s}\right) . \tag{2.55}$$

2.7.3 Computation of $I_{3|\mu,\nu}(s)$ in (2.27) for $s \in \mathbb{R}^+$

Exact Solution

Applying the alternative representation of the Q-function (cf. [9, p. 85]), the integral (2.27) can be written as

$$I_{3|\mu,\nu}(s) = \left(\frac{m}{m + \bar{\gamma}\mu(s - s^2)}\right)^m [1 - 2P_1] , \tag{2.56}$$

where

$$P_1 \triangleq \frac{1}{\pi}\int_0^{\frac{\pi}{2}}\left(1 + \frac{c}{\sin^2(\varphi)}\right)^{-m} d\varphi , \quad c \triangleq \frac{(\nu s)^2}{\frac{m}{\bar{\gamma}} + \mu(s - s^2)} . \tag{2.57}$$

The integral P_1 has been solved in [9, p. 127] as

$$\mathcal{P}_1 = \frac{1}{2\sqrt{\pi}}\frac{\sqrt{c}}{(1+c)^{(m+0.5)}}\frac{\Gamma\left(m+\frac{1}{2}\right)}{\Gamma(m+1)}\ {}_2F_1\left(1, m+\frac{1}{2}; m+1; \frac{1}{1+c}\right) . \tag{2.58}$$

for general values of m in terms of the Gauss Hypergeometric function ${}_2F_1(\cdot,\cdot;\cdot;\cdot)$, which simplifies to

$$P_1 = \frac{1}{2}\left[1 - p(c)\sum_{k=0}^{m-1}\binom{2k}{k}\left(\frac{1-[p(c)]^2}{4}\right)^k\right], \quad p(c) \triangleq \sqrt{\frac{c}{1+c}}, \tag{2.59}$$

for positive integer m. Substituting (2.58) or (2.59) into (2.56) gives the desired closed form.

Approximation

For non-integer m an approximation of $I_{3|\mu,\nu}(s)$ in terms of elementary functions may be desirable. This is possible through the use of the exponential approximations of erf (x). For example, using the tight approximation [21]

$$\text{erf}\,(x) \approx 1 - \frac{1}{6}\exp\left(-x^2\right) - \frac{1}{2}\exp\left(\frac{-4x^2}{3}\right), \tag{2.60}$$

the integral (2.27) can be approximated as

$$I_{3|\mu,\nu}(s) \approx \sum_{i=1}^{3} a_i \left(\frac{m}{m + [\mu(s-s^2) + b_i(\nu s)^2]\,\bar{\gamma}}\right)^m, \tag{2.61}$$

where $[a_1, a_2, a_3] = \left[1, -\frac{1}{6}, -\frac{1}{2}\right]$ and $[b_1, b_2, b_3] = \left[0, 1, \frac{4}{3}\right]$.

2.7.4 Computation of $I_{4|\mu,\nu}(s)$ in (2.28) for $s \in \mathbb{R}^+$

Exact Solution

Using again the alternative representation of the Q-function (cf. [9, p. 85]), we can rewrite the integral (2.28) as

$$I_{4|\mu,\nu}(s) = \left(\frac{m}{m + \bar{\gamma}\mu(s - s^2)}\right)^m [1 - 4P_1 + 4P_2] \ , \tag{2.62}$$

where P_1 and c are defined in (2.57), and

$$P_2 \triangleq \frac{1}{\pi} \int_0^{\frac{\pi}{4}} \left(1 + \frac{c}{\sin^2(\varphi)}\right)^{-m} d\varphi \, . \tag{2.63}$$

The integral P_2 has been computed in [22, p.538] for general m in terms of Appell's double Hypergeometric function $F_1(\cdot;\cdot,\cdot;\cdot;\cdot,\cdot)$:

$$P_2 = \frac{1}{2\pi\,(2m+1)} \left(\frac{1}{1+2c}\right) F_1\left(1; m, 1; m + \frac{3}{2}; \frac{1+c}{1+2c}, \frac{1}{2}\right) , \tag{2.64}$$

In case of positive integer m, a closed-form expression in terms of elementary functions can be obtained [9, p. 130]:

$$\begin{aligned} P_2 = &\frac{1}{4} - \frac{1}{\pi}\, p(c) \left\{ \left(\frac{\pi}{2} - \tan^{-1}(p(c))\right) \sum_{k=0}^{m-1} \left[\binom{2k}{k} \frac{1}{(4\,(1+c))^k} \right] \right. \\ &\left. - \sin\left(\tan^{-1}(p(c))\right) \sum_{k=1}^{m-1} \sum_{i=1}^{k} \left[\frac{T_{ik}}{(1+c)^k} \left[\cos\left(\tan^{-1}(p(c))\right)\right]^{2(k-i)+1} \right] \right\} , \end{aligned} \tag{2.65}$$

where $T_{ik} \triangleq \frac{\binom{2k}{k}}{\binom{2(k-i)}{k-i} 4^i [2(k-i)+1]}$.

Approximation

Exponential approximations of erf (x) allow us to express $I_{4|\mu,\nu}(s)$ in terms of elementary functions also for non-integer m. For example, applying again approximation (2.60), we obtain

$$I_{4|\mu,\nu}(s) \approx \sum_{i=1}^{6} a_i \left(\frac{m}{m + [\mu(s - s^2) + b_i(\nu s)^2]\,\bar{\gamma}} \right)^m , \tag{2.66}$$

where $[a_1, a_2, a_3, a_4, a_5, a_6] = \left[1, -\frac{1}{3}, -1, \frac{1}{36}, \frac{1}{6}, \frac{1}{4}\right]$ and $[b_1, b_2, b_3, b_4, b_5, b_6] = \left[0, 1, \frac{4}{3}, 2, \frac{7}{3}, \frac{8}{3}\right]$.

Bibliography

[1] E. Zehavi, "8-PSK trellis codes for a Rayleigh channel," *IEEE Trans. Commun.*, vol. 40, no. 5, pp. 873–884, May 1992.

[2] G. Caire, G. Taricco, and E. Biglieri, "Bit-interleaved coded modulation," *IEEE Trans. Inform. Theory*, vol. 44, no. 3, pp. 927–946, May 1998.

[3] G. Ungerboeck, "Channel coding with multilevel/phase signals," *IEEE Trans. Inform. Theory*, vol. 28, pp. 55–67, Jan. 1982.

[4] P.-C. Yeh, S. Zummo, and W. Stark, "Error probability of bit-interleaved coded modulation in wireless environments," *IEEE Trans. Veh. Technol.*, vol. 55, no. 2, pp. 722–728, March 2006.

[5] V. Sethuraman and B. Hajek, "Comments on "Bit-interleaved coded modulation"," *IEEE Trans. Inform. Theory*, vol. 52, no. 4, pp. 1795–1797, Apr. 2006.

[6] A. Martinez, A. Guillen i Fabregas, and G. Caire, "Error probability analysis of bit-interleaved coded modulation," *IEEE Trans. Inform. Theory*, vol. 52, no. 1, pp. 262–271, Jan. 2006.

[7] C. Goutis and G. Casella, "Explaining the saddlepoint approximation," *The American Statistician*, vol. 53, no. 3, pp. 216–224, Aug. 1999.

[8] L. Szczecinski, R. Bettancourt, and R. Feick, "Probability density function of reliability metrics in BICM with arbitrary modulation: Closed-

form through algorithmic approach," *IEEE Trans. Commun.*, vol. 56, no. 5, pp. 736–742, May 2008.

[9] M. K. Simon and M. S. Alouini, *Digital Communication Over Fading Channels.* New York: Wiley-Interscience, 2000.

[10] L. Szczecinski, A. Alvarado, and R. Feick, "Closed-form approximation of coded BER in QAM-based BICM faded transmission," *IEEE Sarnoff Symposium*, pp. 1–5, Apr. 2008.

[11] A. J. Viterbi and J. K. Omura, *Principles of Digital Communication and Coding.* New York: McGraw-Hill, Inc., 1979.

[12] E. Biglieri, G. Caire, G. Taricco, and J. Ventura-Traveset, "Computing error probabilities over fading channels: A unified approach," *Eur. Trans. Telecommun.*, vol. 9, no. 1, pp. 15–25, Jan./Feb. 1998.

[13] C. Schlegel and D. Costello, Jr., "Bandwidth efficient coding for fading channels: Code construction and performance analysis," *IEEE J. Select. Areas Commun.*, vol. 7, no. 9, pp. 1356–1368, Dec. 1989.

[14] C. Stierstorfer and R. Fischer, "(gray) mappings for bit-interleaved coded modulation," in *IEEE 65th Vehicular Technology Conference*, April 2007, pp. 1703–1707.

[15] A. Chindapol and J. Ritcey, "Design, analysis, and performance evaluation for BICM-ID with square QAM constellations in Rayleigh fading channels," *"IEEE J. Select. Areas Commun."*, vol. 19, no. 5, pp. 944–957, May 2001.

[16] X. Li, A. Chindapol, and J. Ritcey, "Bit-interleaved coded modulation with iterative decoding and 8PSK signaling," *IEEE Trans. Commun.*, vol. 50, no. 8, pp. 1250–1257, Aug 2002.

[17] M. Abramowitz and I. Stegun, *Handbook of Mathematical Functions.* New York: Dover Publications, 1972.

[18] R. Askey, "Multiple hypergeometric functions and applications (harold exton)," *SIAM Review*, vol. 20, no. 4, pp. 874–875, 1978. [Online]. Available: http://link.aip.org/link/?SIR/20/874/1

[19] T. Philips and A. Sahraoui, "A sequence of upper and lower bounds for the Q function," *IEEE Trans. Inform. Theory*, vol. 30, no. 6, pp. 877–878, Nov. 1984.

[20] I. Gradshteyn and I. Ryzhik, *Table of Integrals, Series, and Products*, 7th ed. Academic Press, 2007.

[21] M. Chiani, D. Dardari, and M. Simon, "New exponential bounds and approximations for the computation of error probability in fading channels," *IEEE Trans. Wireless Commun.*, vol. 2, no. 4, pp. 840–845, July 2003.

[22] H. Shin and J. H. Lee, "On the error probability of binary and M-ary signals in Nakagami-m fading channels," *IEEE Trans. Commun.*, vol. 52, no. 4, pp. 536–539, April 2004.

Chapter 3

Performance Analysis for BICM Transmission over Gaussian Mixture Noise Fading Channels[5]

3.1 Introduction

While bit-interleaved coded modulation (BICM) has been thoroughly investigated for the additive white Gaussian noise (AWGN) case, the analysis of BICM transmission impaired by non-Gaussian noise has received relatively little attention, cf. e.g. [1, 2]. In general, the study of communication in non-Gaussian environments has become very popular due to its practical relevance. In many practical cases such as indoor radio communication, partial-time jamming, ultrawideband communication, and power line communication, this interference is well modeled as a Gaussian mixture noise (GMN) [3–9]. It is therefore of immediate interest to extend BICM performance analysis as those mentioned above to the case of GMN. To this

[5]A version of this chapter has been submitted for publication. A. Kenarsari Anhari and L. Lampe, "Performance Analysis for BICM Transmission over Gaussian Mixture Noise Fading Channels," *submitted for publication*, June 2009

end, the authors of [2] present a framework that modifies the BICM expurgated bound (BICM-EB) from [10] to encompass non-Gaussian noise. Since the analysis relies on the expurgated bound, it is limited to the case of Gray labeling and does not result in closed-form expressions for bit-error rate (BER). Furthermore, the asymptotic performance analysis in [2] is valid only when the diversity order of the system is an integer.

In this chapter, we present a novel approach for performance evaluation of BICM transmission over general frequency-flat fading channels impaired by GMN. As in [2] it is assumed that the system employs the standard Euclidean-distance decoder. Our analysis mainly builds upon (i) the saddlepoint approximation proposed for BICM in [11] and (ii) the approximation of the PDF of bitwise reliability metrics from Chapter 2. The main contributions of this chapter can be summarized as follows.

- A closed-form approximation for the PDF of bit-wise reliability metrics when transmitting over nonfading GMN channels and using Euclidean-distance based decoding is derived. The resulting PDF expression is valid for arbitrary signal constellations and labeling rules.
- Based on this new expression, we derive the Laplace transform of the PDF of reliability metrics for general fading GMN channels. Using this result together with the saddlepoint approximation [11], the PEP between codewords can be obtained. For the general GMN case, the saddlepoint needs to be found numerically, which however can be done very efficiently due to the convexity of the Laplace transform [12]. The BER for BICM with linear codes is then readily approximated in terms of these PEP expressions.
- For the special case of fading AWGN channels, for which the Euclidean-distance based metric is maximum likelihood, the PEP is given in closed form. This is a valuable result in its own right, as previous

studies have been limited to Nakagami-m fading channels [13–15].

- We simplify the saddlepoint-based approximation for the high signal-to-noise ratio (SNR) regime, which results in closed-form expressions for asymptotically high SNR. It is shown that the diversity order of the system is the product of the fading diversity order and the minimum Hamming distance of the BICM code. The asymptotic coding gain consists of two terms, one of which is a function of the GMN parameters and the other is a generalization of the harmonic distance obtained in [10, 14].
- In the case of nonfading GMN, where the noise component with the largest power dominates the asymptotic BER, the convergence of the asymptotic BER approximation occurs only at very low BERs for typical GMN scenarios. We therefore also derive a novel closed-form expression for the PEP in nonfading GMN, which takes all mixture-noise components into account and is confirmed to be tight in BER ranges typically of interest.

We present a number of selected numerical results for convolutional coded BICM and different constellations, labeling rules, and fading and noise scenarios, which clearly illustrate the usefulness of the proposed approximations and asymptotic results to predict the BER performance.

The remainder of this chapter is organized as follows. In Section 3.2, the BICM transmission model is introduced. The new expressions to analyze the BICM error rate are derived in Section 3.3. In Section 3.4 we provide the simplifications applicable in the high SNR regime. Numerical results obtained from the proposed analytical approximations and simulations are compared and discussed in Section 3.5. Section 3.6 concludes this chapter.

3.2 System Model

The block diagram of the equivalent baseband discrete-time BICM transmission system is shown in Figure 3.1. At the transmitter, the output of a binary encoder $\boldsymbol{c} = [c_1, c_2, ..., c_B]$ is first interleaved into $\boldsymbol{c}^{\pi} = [c_1^{\pi}, c_2^{\pi}, ..., c_B^{\pi}]$ and then input to a mapper $\mu : \{0,1\}^r \to \mathcal{X}$ to obtain the transmitted symbol $x_i = \mu\left[c^{\pi}_{(i-1)r+1}, c^{\pi}_{(i-1)r+2}, ..., c^{\pi}_{ir}\right]$ at symbol time i. The transmitted symbols x_i are taken from a general complex-valued constellation $\mathcal{X}$ of size 2^r.

The channel considered in this work is flat fading with additive non-Gaussian noise. Assuming coherent reception, the equivalent discrete-time transmission model can be written as

$$y_i = \sqrt{\bar{\gamma}}\, h_i\, x_i + z_i \, , \tag{3.1}$$

where $y_i \in \mathbb{C}$, $h_i \in \mathbb{R}^+$, and $z_i \in \mathbb{C}$ are the ith received sample, channel gain, and noise sample, respectively. Taking into account the effect of interleaving, the fading gains h_i are modeled as i.i.d. random variables with unit power $\mathbb{E}\left\{h_i^2\right\} = 1$. Similarly, the noise samples are also i.i.d. and distributed according to the zero-mean Gaussian mixture distribution

$$f_Z(z) = \sum_{n=1}^{N} \frac{\epsilon_n}{2\pi\sigma_n^2} \exp\left(-\frac{\|z\|^2}{2\sigma_n^2}\right) \, , \tag{3.2}$$

where

$$\sum_{n=1}^{N} \epsilon_n = 1 \, , \tag{3.3}$$

$$\sum_{n=1}^{N} \epsilon_n \sigma_n^2 = \frac{1}{2} \, , \tag{3.4}$$

and thus $\mathbb{E}\left\{\|z_i\|^2\right\} = 1$. Also, without loss of generality, we assume that

$$\sigma_i < \sigma_j \,, \quad \forall (i,j)\; i > j \,. \tag{3.5}$$

The finite-order GMN PDF (3.2) can well approximate many continuous probability density functions (PDFs) and is often used to represent the combined effect of Gaussian background noise and man-made or impulsive noise [2–9]. We will repeatedly consider the special case of AWGN, for which $N = 1$ in (3.2).

Considering the fading and noise power normalization, $\bar{\gamma}$ in (3.1) represents the average SNR at the receiver. We define the instantaneous SNR as

$$\gamma_i \triangleq \bar{\gamma}\, h_i^2 \,. \tag{3.6}$$

At the receiver, the demapper outputs r bitwise reliability metrics per symbol according to

$$\lambda^{\pi}_{(i-1)r+j} = -\min_{a\in\mathcal{X}_{j,1}} \left(\|y_i - \sqrt{\bar{\gamma}}\, h_i\, a\|^2\right) + \min_{a\in\mathcal{X}_{j,0}} \left(\|y_i - \sqrt{\bar{\gamma}}\, h_i\, a\|^2\right) , \tag{3.7}$$

where $\mathcal{X}_{j,b}$ is the set of symbols in the constellation with the jth bit in the binary label fixed to b. Even though (3.7) is not the true log-likelihood ratio (LLR) in the presence of GMN, optimum maximum-likelihood decoding would require the knowledge of noise PDF or the active mixture component (i.e., the noise state n) and its variance. Since this knowledge is usually not available at the receiver, the use of the conventional Euclidean distance metric (3.7) is often considered, e.g. [2]. The "max-log" approximation applied in (3.7) is appealing from an implementation point of view and has been shown to be effective in Gaussian noise environments [10, 16]. The metrics λ^{π}_j are deinterleaved into λ_j, which are then input to the decoder for the binary code in order to retrieve the binary transmitted data.

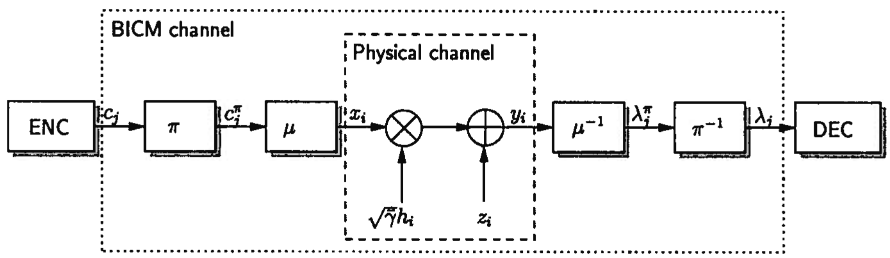

Figure 3.1: Block diagram of BICM transmission over a fading channel impaired by Gaussian mixture noise. Also indicated is the binary-input continuous-output equivalent BICM channel. π and π^{-1} denote interleaving and deinterleaving, respectively. μ and μ^{-1} denote bit-to-symbol mapping and demapping (i.e., bit-metric computation), respectively.

We make the common approximation of perfect (i.e., infinite-depth) interleaving, so that the transmission channel between encoder output c_j and decoder input λ_j can be modeled as an equivalent binary-input output-symmetric (BIOS) channel, which is known as equivalent BICM channel [17] (refer to Figure 3.1).

3.3 Error Rate Analysis

In this section, we derive expressions to approximate the BICM BER for fading GMN channels. To this end, we first briefly review the saddlepoint approximation for the PEP [11] (Section 3.3.1) and the approximation of the PDF of reliability metrics developed in Chapter 2 (Section 2.3). The latter is then extended to the case of GMN (Section 3.3.3), and its Laplace transform for fading GMN channels, which is required for the PEP saddlepoint approximation, is derived (Section 3.3.4).

3.3.1 BER Estimation

We consider the popular union bound BER estimation [18], which relies on the code's distance spectrum and expressions for the PEP between two codewords. Assuming a linear code and the BIOS channel with perfect interleaving, the PEP only depends on the Hamming weight d_{H} of the corresponding error event and can be expressed as the tail probability of the random variable

$$\Delta_{d_{\mathrm{H}}} \triangleq \sum_{j=1}^{d_{\mathrm{H}}} \Lambda_j \,, \tag{3.8}$$

generated by adding d_{H} i.i.d. random variables Λ_j which have the same distribution as the reliability metrics (3.7) when transmitting $c = 1$.[6] That is,

$$\mathrm{PEP}(d_{\mathrm{H}}) = \Pr\left(\Delta_{d_{\mathrm{H}}} < 0\right) \,. \tag{3.9}$$

For a closed-form estimation of (3.9), the saddlepoint approximation

$$\Pr\left(\Delta_{d_{\mathrm{H}}} < 0\right) \approx \frac{1}{\hat{s}\sqrt{2\pi\, d_{\mathrm{H}}\, \Phi''_{\Lambda|f_\gamma}(\hat{s})}} \left(\Phi_{\Lambda|f_\gamma}(\hat{s})\right)^{d_{\mathrm{H}}+1/2} \,, \tag{3.10}$$

has become very popular, e.g. [11, 13, 17]. In (3.10), $\Phi_{\Lambda|f_\gamma}(s)$ denotes the Laplace transform of the PDF of reliability metrics when transmitting $c = 1$ over a fading channel with PDF $f_\gamma(\gamma)$ for the instantaneous SNR[7] γ defined in (3.6), $\Phi''_{\Lambda|f_\gamma}(s)$ is the second derivative of $\Phi_{\Lambda|f_\gamma}(s)$, and $\hat{s} \in (0, s_{\max})$ is known as the saddlepoint, where $s_{\max} \in \mathbb{R}^+$ denotes the leftmost pole of $\Phi_{\Lambda|f_\gamma}(s)$. The saddlepoint $\hat{s}$ is defined as

$$\left.\frac{\mathrm{d}\Phi_{\Lambda|f_\gamma}(s)}{\mathrm{d}s}\right|_{s=\hat{s}} = 0 \,. \tag{3.11}$$

[6]The choice of $c = 1$ is without loss of generality.
[7]We drop the time index since variables are i.i.d.

Table 3.1: Probability density function of reliability metrics, $f_{\Lambda,k|\gamma,d}(\lambda)$ and $f_{\Lambda,k|\gamma,d,\theta}(\lambda)$, for transmission over nonfading AWGN channel, used in (3.12) and (3.13).

$k=1$	$\mathcal{N}_{d^2\gamma,2d^2\gamma}(\lambda)$
$k=2$	$\mathcal{N}_{d^2\gamma,2d^2\gamma}(\lambda)\left[1-\mathrm{erf}\left(\frac{\lambda-d^2\gamma}{2d\sqrt{\gamma}}\right)\right]$
$k=3$	$2\mathcal{N}_{d^2\gamma,2d^2\gamma}(\lambda)u\left(d^2\gamma-\lambda\right)$
$k=4$	$\mathcal{N}_{d^2\gamma,2d^2\gamma}(\lambda)\left[1-2\mathrm{erf}\left(\frac{\lambda-d^2\gamma}{2d\sqrt{\gamma}}\right)\right)u\left(d^2\gamma-\lambda\right]$
$k=5$	$-4\mathcal{N}_{d^2\gamma,2d^2\gamma}(\lambda)\mathrm{erf}\left(\frac{\lambda-d^2\gamma}{2d\sqrt{\gamma}}\right)u\left(d^2\gamma-\lambda\right)$
$k=6$	$\mathcal{N}_{d^2\gamma,2d^2\gamma}(\lambda)\left[1-\mathrm{erf}\left(\tan\left(\frac{\theta}{2}\right)\frac{\lambda-d^2\gamma}{2d\sqrt{\gamma}}\right)\right]$

For BIOS channels with maximum likelihood demapping it is known that $\hat{s}=1/2$, which is also a close approximation for the max-log metric (3.7) in the case of AWGN [13]. However, for general GMN the saddlepoint deviates significantly from 1/2. In this case, since $\Phi_{\Lambda|f_\gamma}(s)$ is a convex function [12], $\hat{s}$ can be determined by fast search methods [19, Ch. 9, 10].

3.3.2 Previous Result

The following derivations build on the fundamental result from Chapter 2 that the PDF of reliability metrics for transmission of $c=1$ over the nonfading AWGN channel are well approximated by[8]

$$f_{\Lambda|\gamma}^{\mathrm{QAM}}(\lambda)=\frac{1}{r\,2^{r-1}}\sum_{k=1}^{5}\sum_{l=1}^{2^{r-1}-1}n_{k,l}\,f_{\Lambda,k|\gamma,d_l}(\lambda)\;,\quad d_l=l d_{\min}\;,\qquad(3.12)$$

[8]The notation "$\cdot|\gamma$" means that the expression is conditioned on the instantaneous SNR γ, while "$\cdot|f_\gamma$" denotes an expression for given SNR distribution f_γ. In the nonfading case, we have $\gamma=\bar{\gamma}$ and thus the expression conditioned on γ is the final result.

for regular quadrature amplitude modulation (QAM) constellations and

$$
\begin{aligned}
f_{\Lambda|\gamma}^{\mathrm{PSK}}(\lambda) = & \frac{1}{r\,2^{r-1}} \sum_{l=1}^{2^{r-1}} \left[n_{1,l}\, f_{\Lambda,1|\gamma,d_l}(\lambda) + n_{6,l}\, f_{\Lambda,6|\gamma,d_l,\theta_l}(\lambda) \right] , \\
& \begin{cases} d_l &= \left[\sin\left(\frac{\pi l}{2^r}\right) \Big/ \sin\left(\frac{\pi}{2^r}\right) \right] d_{\min}, \\ \theta_l &= \pi - \frac{2\pi l}{2^r}. \end{cases}
\end{aligned}
\tag{3.13}
$$

for phase-shift keying (PSK) constellations with minimum Euclidean distance $d_{\min}$. In (3.12) and (3.13), $f_{\Lambda,k|\gamma,d_l,(\theta_l)}(\lambda)$ is the PDF of the reliability metric given $c = 1$ was transmitted considering a subset of "competitive" signal points representing $c = 0$ at distance d_l. There are six non-equivalent types of subsets for QAM and PSK constellations and, for convenience, the closed-form expressions for $f_{\Lambda,k|\gamma,d_l}(\lambda)$ are given in Table 3.1, where $\mathcal{N}_{\mu,\sigma^2}(x)$ denotes the real-valued Gaussian PDF with mean μ and variance σ^2, $\operatorname{erf}(x)$ is the Gauss error function, and $u(x)$ is the unit step function. The coefficient $n_{k,l}$ denotes the number of subsets of type k at Euclidean distance d_l. Table 2.2 provides numerical values for $n_{k,l}$ for a number of popular constellations and labeling rules.

3.3.3 Extension of PDF Result to Nonfading GMN

We note that the PDF approximation developed in Chapter 2 is applicable to arbitrary signal constellations, including, for example, PSK with non-uniformly spaced signal points and amplitude phase-shift keying (APSK) [20] constellations. The resulting PDF expressions have the same form as those in (3.12) and (3.13), with appropriately modified numerical values for $n_{k,l}$, d_l, and θ_l. In the following, we therefore use the general expression

$$
f_{\Lambda|\gamma}(\lambda) = \frac{1}{r2^{r-1}} \sum_{k\in\mathcal{K}} \sum_{l=1}^{M} n_{k,l} f_{\Lambda,k|\gamma,\eta_l}(\lambda) , \tag{3.14}
$$

Table 3.2: Expressions for the PDF of reliability metrics, $f_{\Lambda,k|\gamma,n,\eta}(\lambda)$, for transmission over nonfading GMN channel, used in (3.17). $\eta = d$ for $k = 1, \ldots, 5$, and $\eta = [d, \theta]$ for $k = 6$.

	PDF $f_{\Lambda,k\|\gamma,n,\eta}(\lambda)$
$k=1$	$\mathcal{N}_{d^2\gamma, 4\sigma_n^2 d^2\gamma}(\lambda)$
$k=2$	$\mathcal{N}_{d^2\gamma, 4\sigma_n^2 d^2\gamma}(\lambda)\left[1 - \mathrm{erf}\left(\frac{\lambda - d^2\gamma}{2\sqrt{2}\sigma_n d\sqrt{\gamma}}\right)\right]$
$k=3$	$2\,\mathcal{N}_{d^2\gamma, 4\sigma_n^2 d^2\gamma}(\lambda)\, u\left(d^2\gamma - \lambda\right)$
$k=4$	$\mathcal{N}_{d^2\gamma, 4\sigma_n^2 d^2\gamma}(\lambda)\left[1 - 2\mathrm{erf}\left(\frac{\lambda - d^2\gamma}{2\sqrt{2}\sigma_n d\sqrt{\gamma}}\right)\right] u\left(d^2\gamma - \lambda\right)$
$k=5$	$-4\,\mathcal{N}_{d^2\gamma, 4\sigma_n^2 d^2\gamma}(\lambda)\,\mathrm{erf}\left(\frac{\lambda - d^2\gamma}{2\sqrt{2}\sigma_n d\sqrt{\gamma}}\right) u\left(d^2\gamma - \lambda\right)$
$k=6$	$\mathcal{N}_{d^2\gamma, 4\sigma_n^2 d^2\gamma}(\lambda)\left[1 - \mathrm{erf}\left(\tan\left(\frac{\theta}{2}\right) \frac{\lambda - d^2\gamma}{2\sqrt{2}\sigma_n d\sqrt{\gamma}}\right)\right]$

where $\mathcal{K}$ is the set of non-equivalent types, M is the maximal number of non-zero coefficients $n_{k,l}$, and η_l denotes the constellation parameters. For example, $\mathcal{K} = \{1, \ldots, 5\}$, $M = 2^{r-1} - 1$, and $\eta_l = d_l$ for QAM, and $\mathcal{K} = \{1, 6\}$, $M = 2^{r-1}$, and $\eta_l = [d_l, \theta_l]$ for PSK.

In order to extend (3.14) to the case of GMN, we introduce the auxiliary random variable ξ_i which identifies to which component n of the PDF (3.2) z_i belongs. The "noise-state" variable ξ_i is i.i.d. with distribution $\Pr\{\xi_i = n\} = \epsilon_n$.

Instead of directly using the PDF of GMN for performance analysis, we use ξ_i to define the component-noise random variable Z^{ξ_i} with

$$p_{Z^n}(z) = \frac{1}{2\pi\sigma_n^2} \exp\left(-\frac{\|z\|^2}{2\sigma_n^2}\right) . \tag{3.15}$$

Then, the PDF of reliability metrics can be considered as a weighted sum of PDFs $f_{\Lambda|\gamma,n}(\lambda)$ conditioned on the state of GMN $\xi_i = n$,

$$f_{\Lambda|\gamma}(\lambda) = \sum_{n=1}^{N} \epsilon_n \, f_{\Lambda|\gamma,n}(\lambda) \,, \tag{3.16}$$

where $f_{\Lambda|\gamma,n}(\lambda)$ is expressed analogous to (3.14) as

$$f_{\Lambda|\gamma,n}(\lambda) = \frac{1}{r2^{r-1}} \sum_{k\in\mathcal{K}} \sum_{l=1}^{M} n_{k,l} f_{\Lambda,k|\gamma,n,\eta_l}(\lambda) \,. \tag{3.17}$$

Since $f_{\Lambda,k|\gamma,n,\eta_l}(\lambda)$ is conditioned on $\xi_i = n$, one may be inclined to obtain its PDF by replacing the instantaneous SNR γ with $\gamma/(2\sigma_n^2)$ in the expressions for $f_{\Lambda,k|\gamma,\eta_l}(\lambda)$ in Table 3.1 (recall the normalization $\sum\limits_{n=1}^{N} \epsilon_n \sigma_n^2 = 1/2$). This would indeed be correct, if the receiver had knowledge about the instantaneous noise state ξ_i, which however is not the case for the conventional demapper (3.7) considered here. A proper derivation of $f_{\Lambda,k|\gamma,n,\eta_l}(\lambda)$ following the steps in Chapter 2 leads to the closed-form expressions presented in Table 3.2.

We observe that the resulting PDF expression (3.16) using (3.17) and the results in Table 3.2 is very easy to evaluate, and its computation does not require any numerical integration.

3.3.4 Laplace Transform of the PDF of Reliability Metrics for Fading GMN

Using the PDF expression (3.16), we now proceed to derive expressions for the Laplace transform $\Phi_{\Lambda|f_\gamma}(s)$, which is required for the PEP saddlepoint approximation (3.10). We will assume $s \in \mathbb{R}^+$, which is sufficient for evaluation of (3.10).

Using the fact that PDF of reliability metrics for fading channels can be

Table 3.3: Expressions for the Laplace transform of the PDF of LLRs for transmission over unfaded channel $\Phi_{\Lambda,k|\gamma,n,\eta}(s)$ used in (3.23). $s \in \mathbb{R}^+$, $\eta = d$ for $k = 1, \ldots, 5$, and $\eta = [d, \theta]$ for $k = 6$.

	Laplace transform $\Phi_{\Lambda,k|\gamma,n,\eta}(s)$
$k=1$	$\exp\left(d^2\gamma\left(2\sigma_n^2 s^2 - s\right)\right)$
$k=2$	$\exp\left(d^2\gamma\left(2\sigma_n^2 s^2 - s\right)\right)\left(1+\operatorname{erf}\left(\sigma_n d\sqrt{\gamma}s\right)\right)$
$k=3$	$\exp\left(d^2\gamma\left(2\sigma_n^2 s^2 - s\right)\right)\left(1+\operatorname{erf}\left(\sqrt{2}\sigma_n d\sqrt{\gamma}s\right)\right)$
$k=4$	$\frac{1}{2}\exp\left(d^2\gamma\left(2\sigma_n^2 s^2 - s\right)\right)\times$ $\left(1+\operatorname{erf}\left(\sqrt{2}\sigma_n d\sqrt{\gamma}s\right)+\left(1+\operatorname{erf}\left(\sigma_n d\sqrt{\gamma}s\right)\right)^2\right)$
$k=5$	$\exp\left(d^2\gamma\left(2\sigma_n^2 s^2 - s\right)\right)\left(1+\operatorname{erf}\left(\sigma_n d\sqrt{\gamma}s\right)\right)^2$
$k=6$	$\exp\left(d^2\gamma\left(2\sigma_n^2 s^2 - s\right)\right)\left(1+\operatorname{erf}\left(\sin\left(\frac{\theta}{2}\right)\sqrt{2}\sigma_n d\sqrt{\gamma}s\right)\right)$

expressed as

$$f_{\Lambda|f_\gamma}(\lambda) = \int_0^\infty f_\gamma(\gamma)\, f_{\Lambda|\gamma}(\lambda)\, \mathrm{d}\gamma\,, \tag{3.18}$$

we write the Laplace transform

$$\begin{aligned}
\Phi_{\Lambda|f_\gamma}(s) &= \int_{-\infty}^{\infty} f_{\Lambda|f_\gamma}(\lambda) \exp(-s\lambda)\, \mathrm{d}\lambda & (3.19)\\
&= \int_0^\infty f_\gamma(\gamma) \left[\int_{-\infty}^{\infty} f_{\Lambda|\gamma}(\lambda)\, \exp(-s\lambda)\, \mathrm{d}\lambda\right] \mathrm{d}\gamma & (3.20)\\
&\triangleq \int_0^\infty f_\gamma(\gamma)\, \Phi_{\Lambda|\gamma}(s)\, \mathrm{d}\gamma\,, & (3.21)
\end{aligned}$$

where we changed the order of integration (assuming s is such that $\Phi_{\Lambda|f_\gamma}(s)$ exists) and defined $\Phi_{\Lambda|\gamma}(s)$ as the Laplace transform of $f_{\Lambda|\gamma}(\lambda)$. From (3.16), (3.17), and the linearity property of the Laplace transform we have

$$\Phi_{\Lambda|\gamma}(s) = \sum_{n=1}^{N} \epsilon_n \Phi_{\Lambda|\gamma,n}(s) , \tag{3.22}$$

where

$$\Phi_{\Lambda|\gamma,n}(s) = \frac{1}{r2^{r-1}} \sum_{k \in \mathcal{K}} \sum_{l=1}^{M} n_{k,l} \, \Phi_{\Lambda,k|\gamma,n,\eta_l}(s) \tag{3.23}$$

and $\Phi_{\Lambda,k|\gamma,n,\eta_l}(s)$ is the Laplace transform of $f_{\Lambda,k|\gamma,n,\eta_l}(\lambda)$. Considering the expressions for $f_{\Lambda,k|\gamma,n,\eta_l}(\lambda)$ in Table 3.2 and using the integration technique presented in Chapter 2 (Section 2.7.1 and Section 2.7.2), closed-form expressions for $\Phi_{\Lambda,k|\gamma,n,\eta_l}(s)$ are obtained, which are summarized in Table 3.3. These results together with (3.23) and (3.22) give us closed-form expressions for $\Phi_{\Lambda|\gamma}(s)$, which allows us to evaluate the saddlepoint approximation (3.10) for nonfading GMN channels.

For fading GMN channels we define

$$\Phi_{\Lambda,k|f_\gamma,n,\eta_l}(s) \triangleq \int_0^\infty f_\gamma(\gamma) \, \Phi_{\Lambda,k|\gamma,n,\eta_l}(s) \, \mathrm{d}\gamma , \tag{3.24}$$

and it follows from (3.21), (3.22), and (3.23) that

$$\Phi_{\Lambda|f_\gamma}(s) = \frac{1}{r2^{r-1}} \sum_{n=1}^{N} \epsilon_n \sum_{k \in \mathcal{K}} \sum_{l=1}^{M} n_{k,l} \, \Phi_{\Lambda,k|f_\gamma,n,\eta_l}(s) . \tag{3.25}$$

Applying the methods from Chapter 2 (Section 2.7.3 and Section 2.7.4), the integral in (3.24) can be solved in closed form with elementary function for Nakagami-m fading channels with integer parameter m, and in terms of hypergeometric functions for non-integer m. However, no closed-form solution exists for other popular fading distributions like Nakagami-n or

Nakagami-q. Therefore, we propose the use of the approximations

$$\operatorname{erf}(x) \approx P(x) \triangleq \sum_{i=1}^{K} a_i \exp\left(b_i x^2\right), \tag{3.26}$$

$$(\operatorname{erf}(x))^2 \approx \bar{P}(x) \triangleq \sum_{i=1}^{\bar{K}} \bar{a}_i \exp\left(\bar{b}_i x^2\right), \tag{3.27}$$

with coefficients a_i, b_i, $\bar{a}_i$, $\bar{b}_i$ and number of terms K, $\bar{K}$ chosen according to the particular approximation method and required accuracy. Such approximations for the error function can be obtained using the alternative representation of the Gaussian Q-function and approximation of the integral using a Riemann sum, cf. [21]. Equipped with (3.26), (3.27), and defining the moment generating function (MGF) of the instantaneous SNR γ

$$M_{f_\gamma}(s) \triangleq \int_0^\infty f_\gamma(t) \exp(s\,t)\,\mathrm{d}t, \tag{3.28}$$

as well as the finite series

$$S_1(s;\omega,\nu,\rho) \triangleq \sum_{i=1}^{K} a_i\, M_{f_\gamma}\left(-\nu s + \left(\omega + b_i\rho^2\right)s^2\right), \tag{3.29}$$

$$S_2(s;\omega,\nu,\rho) \triangleq \sum_{i=1}^{K'} a'_i\, M_{f_\gamma}\left(-\nu s + \left(\omega + b'_i\rho^2\right)s^2\right), \tag{3.30}$$

the resulting expressions for $\Phi_{\Lambda,k|f_\gamma,n,\eta_l}(s)$ are presented in Table 3.4.

Hence a simple closed-form approximation of $\Phi_{\Lambda|f_\gamma}(s)$ for fading GMN channels is obtained as long as the MGF of the SNR is available in closed form, which is the case for almost all the practical fading distributions [22]. Table 3.5 (second column) summarizes the formulas for $M_{f_\gamma}(s)$ for the most popular fading models.

Table 3.4: Expressions for the Laplace transform $\Phi_{\Lambda,k|f_\gamma,n,\eta}(s)$ for fading GMN channels as function of MGF $M_{f_\gamma}(s)$ (3.28) and the finite-series expressions $S_1(s;\omega,\nu,\rho)$ (3.29) and $S_2(s;\omega,\nu,\rho)$ (3.30). $s \in \mathbb{R}^+$, $\eta = d$ for $k = 1,\ldots,5$, and $\eta = [d,\theta]$ for $k = 6$.

	Laplace transform $\Phi_{\Lambda,k\|f_\gamma,n,\eta}(s)$
$k=1$	$M_{f_\gamma}\left(d^2\left(2\sigma_n^2 s^2 - s\right)\right)$
$k=2$	$M_{f_\gamma}\left(d^2\left(2\sigma_n^2 s^2 - s\right)\right) + S_1\left(s; 2\sigma_n^2 d^2, d^2, \sigma_n d\right)$
$k=3$	$M_{f_\gamma}\left(d^2\left(2\sigma_n^2 s^2 - s\right)\right) + S_1\left(s; 2\sigma_n^2 d^2, d^2, \sqrt{2}\sigma_n d\right)$
$k=4$	$M_{f_\gamma}\left(d^2\left(2\sigma_n^2 s^2 - s\right)\right) + \frac{1}{2}S_1\left(s; 2\sigma_n^2 d^2, d^2, \sqrt{2}\sigma_n d\right) +$ $S_1\left(s; 2\sigma_n^2 d^2, d^2, \sigma_n d\right) + \frac{1}{2}S_2\left(s; 2\sigma_n^2 d^2, d^2, \sigma_n d\right)$
$k=5$	$M_{f_\gamma}\left(d^2\left(2\sigma_n^2 s^2 - s\right)\right) + 2S_1\left(s; 2\sigma_n^2 d^2, d^2, \sigma_n d\right) +$ $S_2\left(s; 2\sigma_n^2 d^2, d^2, \sigma_n d\right)$
$k=6$	$M_{f_\gamma}\left(d^2\left(2\sigma_n^2 s^2 - s\right)\right) + S_1\left(s; 2\sigma_n^2 d^2, d^2, \sqrt{2}\sin\left(\frac{\theta}{2}\right)\sigma_n d\right)$

Table 3.5: The MGF of SNR $M_{f_\gamma}(s)$ and its asymptotic form $M^{\mathrm{a}}_{f_\gamma}(s)$ for a number of popular fading distributions.

Fading model	$M_{f_\gamma}(s)$	$M^{\mathrm{a}}_{f_\gamma}(s)$
Rayleigh	$(1 - s\,\bar{\gamma})^{-1}$	$-\frac{1/s}{\bar{\gamma}}$
Nakagami-m	$\left(1 - \frac{s\,\bar{\gamma}}{m}\right)^{-m}$	$\frac{m^m/(-s)^m}{\bar{\gamma}^m}$
Nakagami-n	$\frac{(1+n^2)}{(1+n^2) - s\,\bar{\gamma}} \times$ $\exp\left(\frac{n2\,s\,\bar{\gamma}}{(1+n^2)-s\,\bar{\gamma}}\right)$	$-\frac{(1+n^2)\exp\left(-n^2\right)/s}{\bar{\gamma}}$
Nakagami-q	$\left(1 - 2s\bar{\gamma} + \frac{(2s\bar{\gamma})^2 q^2}{(1+q^2)^2}\right)^{-0.5}$	$-\frac{\frac{1+q^2}{2q}/s}{\bar{\gamma}}$

3.4 Analysis in the High-SNR Regime

In this section, we consider the high-SNR regime to obtain further simplified expressions for the PEP. We first consider the nonfading GMN channel (where $\bar{\gamma} = \gamma$) and derive the PEP saddlepoint approximation for high SNR. Since the saddlepoint analysis does not result in a fully analytical solution (the numerical search for the saddlepoint remains), we also derive an alternative BER expression, which does not rely on the saddlepoint approximation. For general fading channels, we consider the PEP saddlepoint approximation for the case of asymptotically high SNR, which leads us to expressions for the coding and diversity gain for BICM transmission.

3.4.1 Simplified Expression for PDF of Reliability Metric and Its Laplace Transform

In the case of high SNR, the PDF expressions in Tables 3.2, 3.3, and 3.4 can be well approximated by

$$f^{\mathrm{a}}_{\Lambda,k|\gamma,n,d_l}(\lambda) = c_k \mathcal{N}_{d_l^2\gamma, 4\sigma_n^2 d_l^2\gamma}(\lambda) \; , \tag{3.31}$$

where $[c_1, c_2, c_3, c_4, c_5, c_6] = [1, 2, 2, 3, 4, 2]$, and thus the PDF expression given in (3.16) simplifies to

$$f^{\mathrm{a}}_{\Lambda|\gamma}(\lambda) = \sum_{n=1}^{N} \epsilon_n \left[\sum_{l=1}^{M} N_l \mathcal{N}_{d_l^2\gamma, 4\sigma_n^2 d_l^2\gamma}(\lambda) \right] \; , \tag{3.32}$$

where $N_l = \frac{1}{r2^{r-1}} \sum\limits_{k\in\mathcal{K}} c_k n_{k,l}$ can be interpreted as the average number of competitive signal points at distance d_l. The Laplace transform of $f^{\mathrm{a}}_{\Lambda|\gamma}(\lambda)$ is given by

$$\Phi^{\mathrm{a}}_{\Lambda|\gamma}(s) = \sum_{n=1}^{N} \epsilon_n \left[\sum_{l=1}^{M} N_l \exp\left(d_l^2 \gamma \left(2\sigma_n^2 s^2 - s \right) \right) \right] \; , \tag{3.33}$$

and its average with respect to the instantaneous SNR for fading channels is obtained as

$$\Phi^{\mathrm{a}}_{\Lambda|f_\gamma}(s) = \sum_{n=1}^{N} \epsilon_n \left[\sum_{l=1}^{M} N_l \, M_{f_\gamma}\left(d_l^2 \left(2\sigma_n^2 s^2 - s \right) \right) \right] . \tag{3.34}$$

3.4.2 Nonfading GMN Channel

Saddlepoint Analysis

From the Laplace transform expression in (3.33) we find the saddlepoint $\hat{s}$ as the (unique) solution of (see (3.11))

$$\frac{\mathrm{d}}{\mathrm{d}s}\Phi^{\mathrm{a}}_{\Lambda|\gamma}(s) = \sum_{n=1}^{N} \epsilon_n \left[\sum_{l=1}^{M} N_l \left(d_l^2 \gamma \left(4\sigma_n^2 s - 1 \right) \right) \exp\left(d_l^2 \gamma \left(2\sigma_n^2 s^2 - s \right) \right) \right] = 0 \, , \tag{3.35}$$

from which we infer that $1/\sigma_1^2 < 4\hat{s} < 1/\sigma_N^2$. Hence, a numerical search for $\hat{s}$ in $(1/(4\sigma_1^2), 1/(4\sigma_N^2))$ is required.

In asymptotically high SNR $\gamma \to \infty$, all terms $(2\sigma_n^2 s^2 - s)$ need to be negative and thus the term for $n = 1$ and $l = 1$ dominates the sum in (3.35), since $d_1^2(2\sigma_1^2 s^2 - s) = \max_{l,n}\{d_l^2(2\sigma_n^2 s^2 - s)\}$. Hence, the saddlepoint approaches the solution

$$\lim_{\gamma\to\infty} \hat{s} = \frac{1}{4\sigma_1^2} \tag{3.36}$$

and the PEP asymptotic approximation

$$\mathrm{PEP}^{\mathrm{a}}(d_{\mathrm{H}}) = \frac{(\epsilon_1 N_1)^{d_{\mathrm{H}}}}{d_1\sigma_1\sqrt{2\pi\, d_{\mathrm{H}}\,\gamma}} \exp\left(-\frac{d_{\mathrm{H}}\, d_1^2}{8\sigma_1^2}\,\gamma \right) \tag{3.37}$$

is obtained from (3.10). We observe that the asymptotic PEP is the same as the PEP for binary transmission with an equivalent SNR of $(d_{\mathrm{H}}\, d_1^2\,\gamma)/\,(2\sigma_1^2)$, scaled by a constant which is a function of the Hamming distance, mapping rule, and GMN parameter ϵ_1 associated with the component with the largest variance. Due to the multiplicative term $\epsilon_1^{d_{\mathrm{H}}}$, we expect (3.37) to be relevant only for very low BERs in most practical cases, since the probability of the impulsive components is typically relatively low, cf. e.g. [2–9]. Therefore, next we present a different expression for the PEP in high SNRs which includes all mixture noise components.

Direct Analysis

We again start from the expression for Laplace transform of reliability metrics given in (3.32), and compute the Laplace transform of the PDF of $\Delta_{d_{\mathrm{H}}}$ defined in (3.8). Due to the perfect interleaving assumption we obtain

$$
\begin{aligned}
&\Phi^{\mathrm{a}}_{\Delta_{d_{\mathrm{H}}}|\gamma}(s) \\
=\ & \left[\Phi^{\mathrm{a}}_{\Lambda|\gamma}(s)\right]^{d_{\mathrm{H}}} && (3.38)\\
\overset{(a)}{=}\ & \sum_{\substack{n_1,\ldots,n_N \\ n_1+\ldots+n_N=d_{\mathrm{H}}}} \frac{d_{\mathrm{H}}!}{\left[\prod\limits_{i=1}^{N}(n_i!/\epsilon_i^{n_i})\right]} \prod_{i=1}^{N}\left[\sum_{l=1}^{M} N_l \exp\left(d_l^2\gamma(2\sigma_i^2 s^2 - s)\right)\right]^{n_i} && (3.39)\\
\overset{(b)}{=}\ & \sum_{\substack{n_1,\ldots,n_N \\ n_1+\ldots+n_N=d_{\mathrm{H}}}} \frac{d_{\mathrm{H}}!}{\left[\prod\limits_{i=1}^{N}(n_i!/\epsilon_i^{n_i})\right]} \times \\
& \prod_{i=1}^{N}\left[\sum_{\substack{l_1,\ldots,l_M \\ l_1+\ldots+l_M=n_i}} \frac{n_i!}{\left[\prod\limits_{j=1}^{M}(l_j!/N_j^{l_j})\right]} \exp\left(\sum_{j=1}^{M} l_j d_j^2\gamma(2\sigma_i^2 s^2 - s)\right)\right] && (3.40)\\
=\ & \sum_{\substack{n_1,\ldots,n_N \\ n_1+\ldots+n_N=d_{\mathrm{H}}}} \frac{d_{\mathrm{H}}!}{\left[\prod\limits_{i=1}^{N}(n_i!/\epsilon_i^{n_i})\right]} \sum_{\substack{l_{1,1},\ldots,l_{1,M} \\ l_{1,1}+\ldots+l_{1,M}=n_1}} \cdots \sum_{\substack{l_{N,1}\ldots,l_{N,M} \\ l_{N,1}+\ldots+l_{N,M}=n_N}} \\
& \left[\prod_{i=1}^{N}\prod_{j=1}^{M}\frac{n_i! N_j^{l_{i,j}}}{l_{i,j}!}\right] \exp\left(\sum_{i=1}^{N}\sum_{j=1}^{M} l_{i,j} d_j^2\gamma(2\sigma_i^2 s^2 - s)\right), && (3.41)
\end{aligned}
$$

where we applied the multinomial series expansion in (a) and (b). From (3.41) we observe that the PDF of $\Delta_{d_{\mathrm{H}}}$ is a superposition of Gaussian PDFs and thus we can directly evaluate (3.9) as

$$\begin{aligned}\mathrm{PEP}\,(d_{\mathrm{H}}) \;=\; & \sum_{\substack{n_1,\ldots,n_N\\ n_1+\ldots+n_N=d_{\mathrm{H}}}} \frac{d_{\mathrm{H}}!}{\left[\prod\limits_{i=1}^{N}(n_i!/\epsilon_i^{n_i})\right]} \sum_{\substack{l_{1,1},\ldots,l_{1,M}\\ l_{1,1}+\ldots+l_{1,M}=n_1}} \cdots \sum_{\substack{l_{N,1}\ldots,l_{N,M}\\ l_{N,1}+\ldots+l_{N,M}=n_N}} \\ & \left[\prod_{i=1}^{N}\prod_{j=1}^{M}\frac{n_i!N_j^{l_{i,j}}}{l_{i,j}!}\right] Q\left(\frac{\sqrt{\gamma}\sum\limits_{i=1}^{N}\sum\limits_{j=1}^{M} l_{i,j}d_j^2}{2\sqrt{\sum\limits_{i=1}^{N}\sum\limits_{j=1}^{M} l_{i,j}d_j^2\sigma_i^2}}\right) . \end{aligned} \tag{3.42}$$

This is a closed-form result for the PEP for transmission over nonfading GMN channels with high SNR. We note that for the asymptotic case $\gamma \to \infty$, where the term with the largest argument of the Q-function dominates the sum, it can be shown that (3.42) converges to (3.37). However, as noted above, this asymptotic result is of interest only for very low BERs.

3.4.3 Fading GMN Channels

In the case of fading channels, we consider the case of asymptotically high SNR $\bar{\gamma}$ and assume that the MGF of the instantaneous SNR $M_{f_\gamma}(s)$ can be expressed as

$$M_{f_\gamma}^{\mathrm{a}}(s) = \frac{\alpha}{(-s)^g\,\bar{\gamma}^g}\,, \tag{3.43}$$

where $\alpha > 0$ and the diversity order $g > 0$ depend on the fading distribution, cf. [23, AS3)]. For integer g, (3.43) can be considered as the first term of the Maclaurin series expansion of $M_{f_\gamma}(s)$ in $1/\bar{\gamma}$. Table 3.5 (third column) presents the respective expressions for $M_{f_\gamma}^{\mathrm{a}}(s)$ for a number of popular fading distributions. Substituting (3.43) into (3.34) we have

$$\Phi^{\mathrm{a}}_{\Lambda|f_\gamma}(s) = \sum_{n=1}^{N} \epsilon_n \left[\sum_{l=1}^{M} N_l \frac{\alpha}{(d_l^2\,(s - 2\sigma_n^2 s^2))^g\, \bar{\gamma}^g}\right] \tag{3.44}$$

$$= \left[\sum_{l=1}^{M} \frac{\alpha\, N_l}{d_l^{2g}}\right] \left[\sum_{n=1}^{N} \frac{\epsilon_n}{(s - 2\sigma_n^2 s^2)^g}\right] \frac{1}{\bar{\gamma}^g}\,. \tag{3.45}$$

Therefore, the asymptotic saddlepoint is the (unique) solution of

$$\sum_{i=1}^{N} \frac{\epsilon_n\,(4\sigma_n^2 s - 1)}{(1 - 2\sigma_n^2 s)^{g+1}} = 0\,, \tag{3.46}$$

which cannot be given in closed form. However, we note that the saddlepoint only depends on the GMN parameters and diversity order g of the fading process. We can further limit the numerical search interval considering that $s_{\max} = 1/(2\sigma_1^2)$ is the leftmost pole of the Laplace transform (3.45) and that (3.46) is negative for $s \le 1/(4\sigma_1^2)$. Hence, we get the lower and upper limit

$$\frac{1}{4\sigma_1^2} < \hat{s} < \frac{1}{2\sigma_1^2}\,. \tag{3.47}$$

In order to arrive at a closed-form approximation, we may consider the midpoint of the above interval,

$$\hat{s}_{\mathrm{e}} = \frac{3}{8\sigma_1^2}\,, \tag{3.48}$$

as an estimate for the asymptotic saddlepoint.

Given the saddlepoint $\hat{s}$, defining

$$\zeta(s) \triangleq \sum_{n=1}^{N} \frac{\epsilon_n}{(4\,[s - 2\sigma_n^2 s^2])^g}\,, \tag{3.49}$$

and substituting (3.45) into (3.10), we obtain after some simplifications the asymptotic PEP expression

$$\mathrm{PEP}(d_{\mathrm{H}}) = \frac{(\zeta(\hat{s}))^{d_{\mathrm{H}}+1/2}}{\hat{s}\sqrt{2\pi\, d_{\mathrm{H}}\, \zeta''(\hat{s})}} \left[\sum_{l=1}^{M} \frac{\alpha N_l}{\left(\frac{d_l^2}{4}\right)^g}\right]^{d_{\mathrm{H}}} \frac{1}{\bar{\gamma}^{d_{\mathrm{H}} g}} . \tag{3.50}$$

We observe that the diversity gain for BICM transmission over fading GMN channels is given by the product $d_{\mathrm{H}}g$. The coding gain consists of two terms, where the first one depends on the GMN parameters through $\zeta(s)$ (3.49). The second term

$$\left[\sum_{l=1}^{M} \frac{\alpha N_l}{\left(\frac{d_l^2}{4}\right)^g}\right] , \tag{3.51}$$

depends on the signal constellation and labeling, and can be considered as a generalization of the harmonic distance for BICM with Gray labeling obtained in [10] and [14] for Rayleigh and Nakagami-m fading, respectively.

In the special case of fading AWGN channels, for which $\hat{s} = 1/2$, (3.50) simplifies to

$$\mathrm{PEP}\,(d_{\mathrm{H}}) = \frac{1}{2\sqrt{\pi\, d_{\mathrm{H}}\, g}} \left[\sum_{l=1}^{M} \frac{\alpha\, N_l}{\left(\frac{d_l^2}{4}\right)^g}\right]^{d_{\mathrm{H}}} \frac{1}{\bar{\gamma}^{d_{\mathrm{H}}\, g}} , \tag{3.52}$$

which is a generalization of the asymptotic result in Chapter 2 for Nakagami-m fading channels.

3.5 Numerical Results and Discussion

In this section, we present and discuss a number of exemplary numerical results to illustrate the accuracy of the proposed PDF and PEP approximations (cf. Sections 3.3.3, 3.3.4, and 3.4). For this purpose, we use the

PEP expressions in the BER union bound for a convolutional code of rate $R_c = k_c/n_c$, which is given by [18]

$$P_b \leq \frac{1}{k_c} \sum_{d_H = d_{free}}^{\infty} w_{d_H} \, \mathrm{PEP}(d_H) \,, \tag{3.53}$$

where d_{free} denotes the free distance of the convolutional code and w_{d_H} denotes the total input weight of error events at Hamming distance d_H.

3.5.1 Parameters

For the BER results we assume BICM with the popular 64-state rate-1/2 convolutional code with generator polynomials $(171, 133)_8$ and $d_{free} = 10$. The union bound (3.53) is truncated to $d_H \leq 25$. To evaluate the series terms $S_1(s;\cdot)$ (3.29) and $S_2(s;\cdot)$ (3.30) needed in Table 3.4, we use the error-function approximation (cf. (3.26) and (3.27)) [21]

$$P(x) = 1 - \frac{1}{6}\exp\left(-x^2\right) - \frac{1}{2}\exp\left(-\frac{4x^2}{3}\right) \,, \quad \bar{P}(x) = P^2(x) \,. \tag{3.54}$$

Furthermore, we consider the following labeling rules: Gray labeling (GL), set partitioning labeling (SPL), modified set partitioning labeling (MSPL), semi set partitioning labeling (SSPL), and mixed labeling (ML). While GL is of importance when used with non-iterative decoders [10], the other labelings are of practical and theoretical importance for the case of, e.g., BICM transmission with iterative decoding [24,25], for which our analytical results would provide an approximation of BER after the first decoding iteration and facilitate the selection of the labeling rule.

The BER results for different constellations are presented as function of the bit-wise SNR

$$\gamma_b \triangleq \gamma/(R_c r) \,, \quad \bar{\gamma}_b \triangleq \bar{\gamma}/(R_c r) \,. \tag{3.55}$$

Finally, we consider ϵ-mixture noise, which is an important instance of general GMN with two terms, e.g., [5]. The first term represents impulsive noise due to some ambient phenomenon, while the second term accounts for Gaussian background noise. The ϵ-mixture noise parameters can be expressed as

$$\begin{aligned}
\epsilon_1 &= \epsilon\,, \\
\epsilon_2 &= 1-\epsilon\,, \\
\sigma_1 &= \sqrt{\kappa}\Big/\left(\sqrt{2\,(1+\kappa\epsilon-\epsilon)}\right)\,, \\
\sigma_2 &= 1\Big/\left(\sqrt{2\,(1+\kappa\epsilon-\epsilon)}\right)\,,
\end{aligned}$$

where $\kappa = \sigma_1^2/\sigma_2^2$ is a measure for the strength of the impulsive component compared to the thermal noise. In the following, we specify the parameters of ϵ-mixture noise by (ϵ, κ).

3.5.2 Results

PDF Approximation Results

Figure 3.2 shows a comparison of PDF histograms, obtained through Monte Carlo simulation, and the approximation (3.16) for different constellations, labeling, and noise parameters. The SNR $\gamma = \bar{\gamma} = 20$ dB is adjusted for these results. We observe that the proposed approximation is very accurate in all cases. In particular, the negative tail of the PDF (i.e., $\lambda < 0$) is faithfully matched, which is critical for performance evaluation.

BER Results for Nonfading GMN Channels

Figure 3.3 shows the analytical (lines) and simulated (markers) BER results for two different constellations and labeling rules assuming transmission over

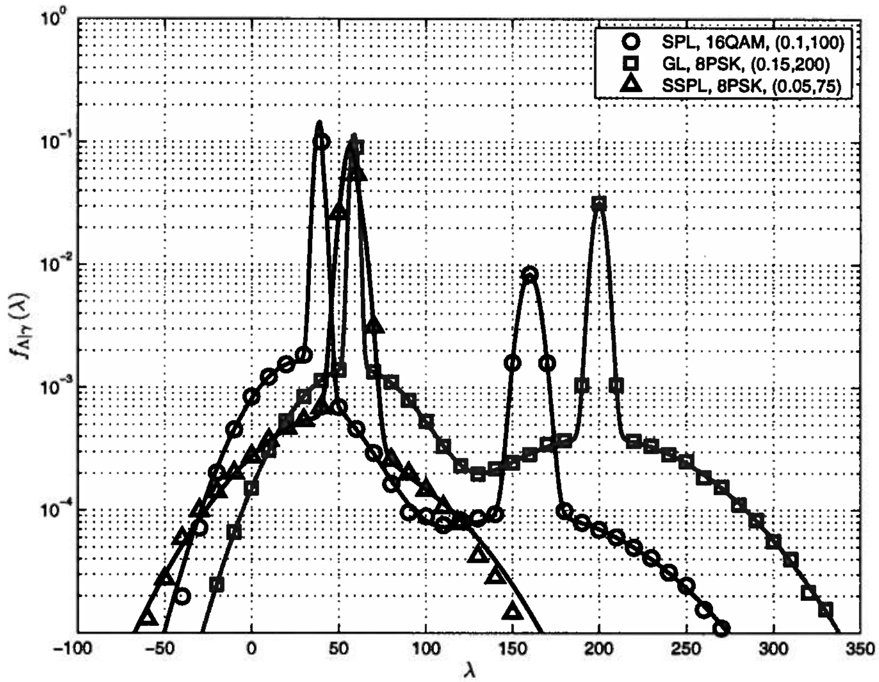

Figure 3.2: PDF of reliability metrics for BICM transmission over nonfading channel impaired by ϵ-mixture noise with parameters (ϵ, κ) for different constellations, labeling, and noise parameters. Solid lines represent the PDF approximation given in (3.16), while markers represent the simulated histograms.

the nonfading channel impaired by ϵ-mixture noise. The figure includes (i) the BER union bound (3.53) with the saddlepoint approximation (3.10) using the saddlepoint found numerically for each SNR (solid lines), (ii) the the BER union bound (3.53) using the PEP expression for high SNR in (3.42) (dashed lines), and (iii) the PEP expression in (3.42) for $d_{\mathrm{H}} = d_{\mathrm{free}}$ (dash-dotted lines). It can be seen that the BER union bound is fairly tight for both BICM examples. Likewise, the closed-form expression (3.42) provides very good BER approximations and the curves converge to those

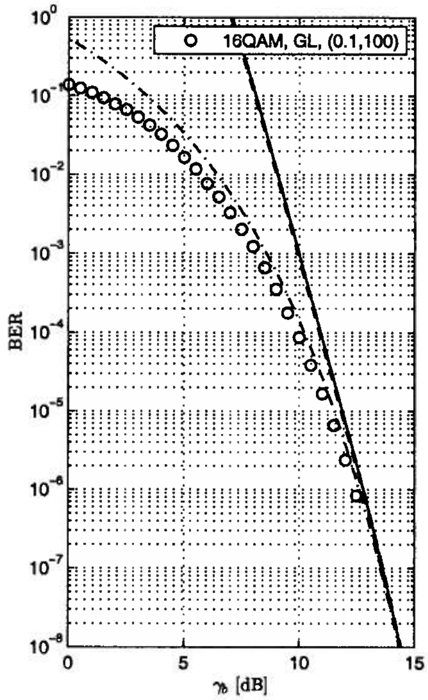

Figure 3.3: BER of BICM transmission over a nonfading channel impaired by ϵ-mixture noise with parameters (ϵ, κ) for a 64-state convolutional code of rate 1/2. Solid lines: BER union bound using the saddlepoint approximation (3.10). The saddlepoint is found numerically for each SNR. Dashed lines: BER union bound using the PEP expression for high SNR in (3.42). Dash-dotted lines: BER using only the PEP expression in (3.42) for $d_{\mathrm{H}} = d_{\mathrm{free}}$. Markers are simulation results.

from the non-asymptotic saddlepoint analysis. Considering only the PEP from (3.42) for the minimum Hamming distance term enables a quick and fairly accurate BER estimation. We note that the asymptotic saddlepoint approximation (3.37) (not shown in this figure) becomes tight only for BERs below $\epsilon^{d_{\mathrm{free}}}$, and thus it is more useful for codes with lower d_{free} and ϵ-mixture noise with high probability of impulses.

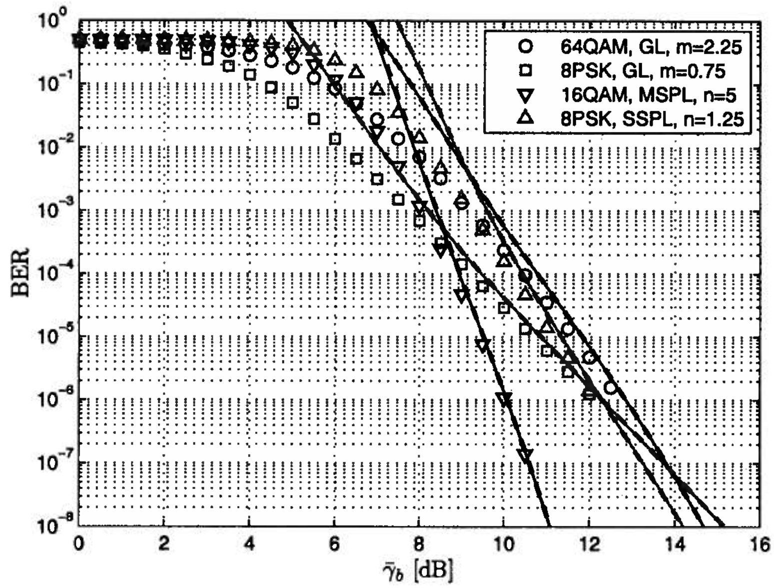

Figure 3.4: BER of BICM transmission over fading AWGN channels for a 64-state convolutional code of rate 1/2. Nakagami-m and Nakagami-n fading with different parameters m and n. Solid lines: BER union bound using the saddlepoint approximation, $\hat{s} = 1/2$ is assumed. Dashed lines: BER union bound using saddlepoint approximation, saddlepoint has been found numerically. (Note that solid and dashed lines overlap almost perfectly.) Markers are simulation results.

BER Results for Fading AWGN Channels

Next we consider BER results for BICM transmission over fading AWGN channels (i.e., $\epsilon = 1$) with different constellations and labeling rules. Specifically, Nakagami-m and Nakagami-n fading distributions are applied. Figure 3.4 shows BER curves obtained from the BER union bound using the saddlepoint approximation (lines) together with simulation results (markers). For the former, both the actual saddlepoint, which has been determined numerically (dashed lines), and the approximation $\hat{s} = 1/2$ (solid lines) has been used. We observe a very good match between results from analysis and simulations. In particular, since for AWGN the applied decoding metric is almost the maximum-likelihood metric (note that the max-log approximation is used in (3.7)), the difference between the results using the true saddlepoint $\hat{s}$ and $\hat{s} = 1/2$ is negligible (the dashed and solid lines overlap almost completely). We note that, considering the expressions for $\Phi_{\Lambda,k|f_\gamma,n,\eta}(s)$ in Table 3.4 with $S_1(s;\cdot)$ and $S_2(s;\cdot)$ given in (3.29) and (3.30) using the exponential approximations of the error function (3.54), we have provided tight BER approximations in terms of elementary functions.

BER Results for Fading GMN Channels

We now consider the case of both fading and GMN, and present selected BER results for different fading parameters, ϵ-mixture noise parameters, and BICM constellations and labeling rules. Figure 3.5 compares the BER curves obtained from the BER union bound using the saddlepoint approximation (lines) and simulations (markers). For the saddlepoint approximation three cases are included: (i) the exact saddlepoint $\hat{s}$ is determined for each SNR (solid lines), (ii) the asymptotic saddlepoint is determined from (3.46) and used for all SNRs (dashed lines), and (iii) the asymptotic saddlepoint approximation given in (3.48) is used (dash-dotted lines). Therefore the dash-dotted lines are obtained from a truly closed-form expression for approximating the BER. Also, solving (3.46) only once and over the small interval (3.47) requires little computational effort. The BER results confirm the usefulness of the proposed BER approximations for fading GMN. Clearly, the convergence of the union bound depends on the fading rate and mixture noise parameters. As can be seen from Figure 3.5, using asymptotic saddlepoint approximations gives relatively close union-bound approximations, with more noticeable gaps for the cases where the asymptotic analysis

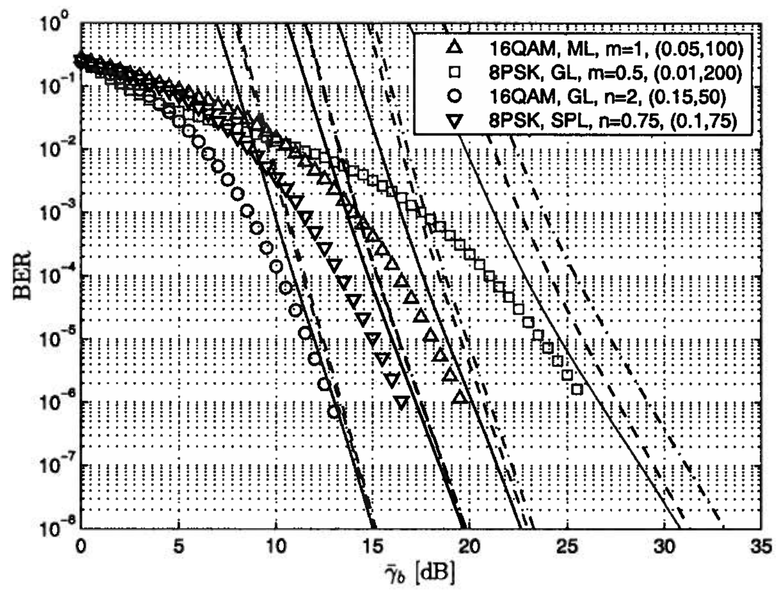

Figure 3.5: BER of BICM transmission over fading channels impaired by ϵ-mixture noise with parameters (ϵ, κ) for a 64-state convolutional code of rate 1/2. Nakagami-m and Nakagami-n fading with different parameters m and n. Solid lines: BER union bound using saddlepoint approximation, saddlepoint has been found numerically. Dashed lines: BER union bound using saddlepoint approximation, the asymptotic saddlepoint from (3.46) is used. Dash-dotted lines: BER union bound using saddlepoint approximation, the asymptotic saddlepoint approximation given in (3.48) is used. Markers are simulation results.

converges at lower BERs.

In Figure 3.6 the asymptotic BER results (lines) using the PEP expression (3.50) and only $d_{\mathrm{H}} = d_{\mathrm{free}}$ are plotted together with the BER union bound (markers). In this figure, Nakagami-m, Nakagami-n, and Nakagami-q fading distributions are used. For the evaluation of the asymptotic expressions the numerically found saddlepoint (solid lines) and the saddlepoint approximation $\hat{s}_{\mathrm{e}}$ from (3.48) (dashed lines) is applied. It can be seen that the

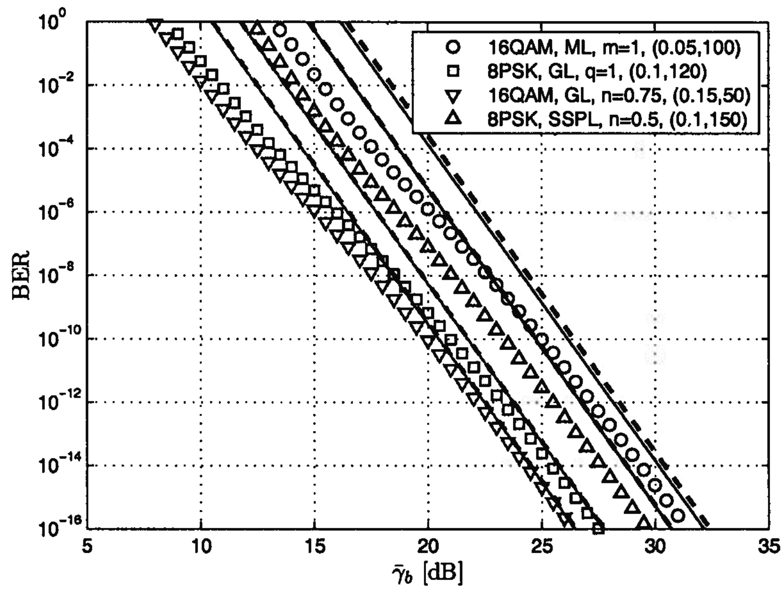

Figure 3.6: BER of BICM transmission over fading channels impaired by ϵ-mixture noise with parameters (ϵ, κ) for a 64-state convolutional code of rate 1/2. Nakagami-m, Nakagami-n, and Nakagami-q fading with different parameters m, n, and q. Solid lines: Asymptotic BER from PEP (3.50) for $d_{\mathrm{H}} = d_{\mathrm{free}}$ and numerically found saddlepoint. Dashed lines: Asymptotic BER from PEP (3.50) for $d_{\mathrm{H}} = d_{\mathrm{free}}$ and the saddlepoint approximation $\hat{s}_{\mathrm{e}}$ from (3.48). Markers: BER union bound.

asymptotic results correctly predict the diversity gain and the asymptotic coding gain of the BICM scheme. Furthermore, the closed-form saddlepoint approximation (3.48) leads to negligible shifts in the asymptotic BER results. Hence, using (3.50) with $\hat{s}_{\mathrm{e}}$ from (3.48) allows us to approximate the asymptotic performance of BICM from a closed-form expression.

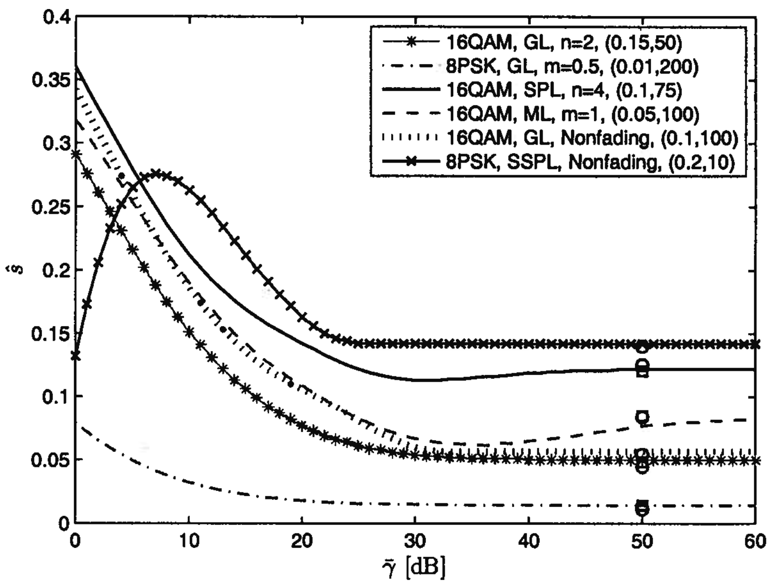

Figure 3.7: Evolution of saddlepoint $\hat{s}$ as a function of $\bar{\gamma}$ for different constellations, labeling, and noise parameters. The circles indicate the asymptotic values of saddlepoint given in (3.36) for nonfading channels and in (3.48) for fading channels. The squares denote the exact asymptotic saddlepoint for fading channels given in (3.46)

Saddlepoint

Finally, in Figure 3.7 we take a look at the evolution of the saddlepoint $\hat{s}$ as function of the SNR $\bar{\gamma}$ for the GMN cases studied in Figures 3.3 and 3.5. Also included are the asymptotic values for the saddlepoint (3.36) for nonfading and (3.46) for fading channels, and the asymptotic saddlepoint approximation (3.48) for fading channels, respectively. We observe that the saddlepoint strongly deviates from 1/2, the solution for the AWGN case, and eventually converges to the value obtained through the asymptotic analysis developed in Section 3.4. The simple estimation given in (3.48) is shown to be reasonably accurate for these exemplarily cases. The range for $\hat{s}$ strongly depends on the mapping rule, while its value at high SNR solely depends on the channel parameters as seen from (3.36) and (3.46).

3.6 Conclusions

BICM is a very popular spectrally and power efficient coded modulation scheme, whose BER analysis has received a lot of attention in the recent past. In this chapter, we have extended and generalized previous approaches considering BICM transmission over general fading channels and additive GMN. We have derived closed-form approximations for the PDF of reliability metrics for the nonfading GMN channel, and its Laplace transform for fading GMN channels. Using the latter together with the saddlepoint approximation for PEP, we have provided a method for quick BER performance approximation. Since in the GMN case the saddlepoint needs to be computed numerically, we have also derived approximations for the (asymptotically) high SNR regime, which involve a single saddlepoint computation (for all SNR values) or are given in closed form. This analysis has also established expressions for the diversity and coding gain of BICM transmission over fading GMN channels. The presented numerical results have confirmed the relative accuracy of the analytical BER approximations for convolutionally coded BICM.

Bibliography

[1] T. Li, W. Mow, and M. Siu, "Bit-interleaved coded modulation in the presence of unknown impulsive noise," in *IEEE International Conference on Communications (ICC)*, Istanbul, Turkey, June 2006, pp. 3014 – 3019.

[2] A. Nasri and R. Schober, "Performance of BICM-SC and BICM-OFDM systems with diversity reception in non-Gaussian noise and interference," *to appear in the IEEE Trans. Commun., available online at www.ece.ubc.ca/˜amirn/TCOM-08-0180.pdf.*

[3] D. Middleton, "Statistical-physical models of man-made radio noise-parts I and II," *U.S. Dept. Commerece Office Telecommun.*, April 1974 and 1976.

[4] D. Stein, "Detection of Random Signals in Gaussian Mixture Noise," *IEEE Trans. Inform. Theory*, vol. 41, no. 6, pp. 1788–1801, Nov. 1995.

[5] X. Wang and V. Poor, "Robust Multiuser Detection in Non-Gaussian Channels," *IEEE Trans. Signal Processing*, vol. 47, no. 2, pp. 289–305, Feb. 1999.

[6] J.-W. Moon, T. Wong, and J. Shea, "Pilot-assisted and Blind Joint Data Detection and Channel Estimation in Partial-time Jamming," *IEEE Trans. Commun.*, vol. 54, no. 11, pp. 2092–2102, Nov. 2006.

[7] M. Flury and J.-Y. Le Boudec, "Interference Mitigation by Statistical Interference Modeling in an Impulse Radio UWB Receiver," in *IEEE Intl. Conf. on Ultra-Wideband (ICUWB)*, Waltham, MA, Sept. 2006, pp. 393–398.

[8] M. Zimmermann and K. Dostert, "Analysis and Modeling of Impulsive Noise in Broadband Powerline Communications," *IEEE Trans. Electromagn. Compat.*, vol. 44, no. 1, pp. 249–258, Feb. 2002.

[9] J. Häring and A. Vinck, "Performance Bounds for Optimum and Suboptimum Reception under Class-A Impulsive Noise," *IEEE Trans. Commun.*, vol. 50, no. 7, pp. 1130–1136, July 2002.

[10] G. Caire, G. Taricco, and E. Biglieri, "Bit-interleaved coded modulation," *IEEE Trans. Inform. Theory*, vol. 44, no. 3, pp. 927–946, May 1998.

[11] A. Martinez, A. Guillén i Fàbregas, and G. Caire, "New simple evaluation of the error probability of bit-interleaved coded modulation using the saddlepoint approximation," in *ISITA 2004 International Symposium on Information Theory and Applications, October 10-13, 2004, Parma, Italy*, Oct 2004.

[12] E. Biglieri, G. Caire, G. Taricco, and J. Ventura-Traveset, "Computing error probabilities over fading channels: A unified approach," *Eur. Trans. Telecommun.*, vol. 9, no. 1, pp. 15–25, Jan./Feb. 1998.

[13] L. Szczecinski, A. Alvarado, and R. Feick, "Distribution of max-log metrics for QAM-based BICM in fading channels," *to appear in the IEEE Trans. Commun., available online at http://externe.emt.inrs.ca/users/leszek/Publications.html.*

[14] A. Martinez and A. Guillén i Fàbregas, "Large-SNR error probability analysis of BICM with uniform interleaving in fading channels," *IEEE Trans. Wireless Commun.*, vol. 8, no. 1, pp. 38–44, Jan. 2009.

[15] A. Kenarsari-Anhari and L. Lampe, "An analytical approach for performance evaluation of BICM transmission over Nakagami-m fading channels," *submitted to IEEE Trans. Commun.*, May 2009.

[16] B. Classon, K. Blankenship, and V. Desai, "Channel codng for 4g systems with adaptive modulation and codng," *Wireless Communications, IEEE*, vol. 9, no. 2, pp. 8–13, April 2002.

[17] A. Martinez, A. Guillen i Fabregas, and G. Caire, "Error probability analysis of bit-interleaved coded modulation," *IEEE Trans. Inform. Theory*, vol. 52, no. 1, pp. 262–271, Jan. 2006.

[18] A. J. Viterbi and J. K. Omura, *Principles of Digital Communication and Coding.* New York: McGraw-Hill, Inc., 1979.

[19] W. Press, S. Teukolsky, W. Vetterling, and B. Flannery, *Numerical Receipes in C++*, 2nd ed. New York: Cambridge University Press, 2002.

[20] C. Chan, "Combined Digital Phase and Amplitude Modulation Communication Systems," *IRE Trans. Commun. Systems*, vol. 8, pp. 150–155, Sept. 1960.

[21] M. Chiani, D. Dardari, and M. Simon, "New exponential bounds and approximations for the computation of error probability in fading channels," *IEEE Trans. Wireless Commun.*, vol. 2, no. 4, pp. 840–845, July 2003.

[22] M. K. Simon and M. S. Alouini, *Digital Communication Over Fading Channels.* New York: Wiley-Interscience, 2000.

[23] Z. Wang and G. Giannakis, "A simple and general parameterizaation quantifying performance in fading channels," *IEEE Trans. Commun.*, vol. 51, no. 8, pp. 1389–1398, Aug. 2003.

[24] A. Chindapol and J. Ritcey, "Design, analysis, and performance evaluation for BICM-ID with square QAM constellations in Rayleigh fading channels," *"IEEE J. Select. Areas Commun."*, vol. 19, no. 5, pp. 944–957, May 2001.

[25] X. Li, A. Chindapol, and J. Ritcey, "Bit-interleaved coded modulation with iterative decoding and 8PSK signaling," *IEEE Trans. Commun.*, vol. 50, no. 8, pp. 1250–1257, Aug 2002.

Chapter 4

Power Allocation for Coded OFDM via Linear Programming[9]

4.1 Introduction

Bit-interleaved coded modulation (BICM) [1] has gained immense popularity for coded multilevel transmission. In combination with orthogonal frequency-division multiplexing (OFDM), i.e., BIC-OFDM, it is a powerful technique for transmission over frequency selective channels [2], which has been adopted in a number of recent standards.

OFDM enables transmitter side adaptation according to the present channel conditions, assuming that the channel remains unchanged over a sufficiently long interval. In particular, numerous algorithms for bit-loading and power allocation per OFDM sub-carrier have been developed, cf. e.g. [3–5]. Recently, [6] has studied the problem of power allocation for BIC-OFDM

[9]A version of this chapter has been submitted for publication. A. Kenarsari Anhari and L. Lampe, "Power Allocation for Coded OFDM via Linear Programming," *submitted for publication*, July 2009.

aiming at the minimization of bit-error rate (BER) under a power budget constraint, i.e.,

$$\begin{aligned} \min_{\underline{p}} \quad & P_{\mathrm{BER}} \\ \text{s.t.} \quad & \sum_{i=1}^{L} p_i \leq P_{\mathrm{T}} , \\ & p_i \geq 0 \quad \forall i \in \{1, \ldots, L\} , \end{aligned} \tag{4.1}$$

where $\underline{p} \triangleq [p_1, \ldots, p_L]$ denotes the vector of powers allocated to each OFDM sub-carrier, P_{BER} denotes the BER, P_{T} is the maximal transmit power, and L is the number of OFDM sub-carriers. Using the union bound approach to approximate P_{BER}, it was shown [6] that (4.1) is a convex optimization problem. However, the solution presented in [6] is limited to (complex) binary transmission, i.e., binary and quadrature phase-shift keying (BPSK and QPSK), since linearity of coding and modulation was required.

Motivated by the approach in [6], we revisit the problem of power allocation for BIC-OFDM in this chapter. We stipulate an approximative binary channel model for BIC-OFDM and make use of the derived expression for BICM error event probability from Chapter 2 to arrive at a simplified objective function. This allows us to translate the optimization problem into a linear program (LP). Solving this LP using standard numerical methods is much faster than solving the general convex optimization problem obtained in [6] (cf. e.g. [7]). Numerical results show that the LP-based power allocation achieves a performance very close to that from convex programming of [6] for QPSK. Furthermore, the proposed method is applicable to arbitrary signal constellations and thus overcomes the restriction of BPSK and QPSK signaling needed in [6].

The rest of this chapter is organized as follows. Section 4.2 introduces the system model for BIC-OFDM transmission. In Section 4.3, a method for performance evaluation of BIC-OFDM is presented, based on which the power allocation optimization problem is formulated as an LP. Selected simulation results are shown in Section 4.4 to illustrate the performance of the proposed method. Section 4.5 concludes the chapter.

4.2 System Model

We consider a BIC-OFDM system with L sub-carriers. At the transmitter, the codeword $\underline{c} = [c_1, c_2, \cdots, c_N]$ generated from a linear binary encoder is bit-wise interleaved into $\underline{c}^{\pi} = [c_1^{\pi}, c_2^{\pi}, \cdots, c_N^{\pi}]$. The interleaved codeword is partitioned into blocks of r binary symbols, which are input to a subsequent mapper $\mu \{0,1\}^r \to \mathcal{X}$ such that $x_i = \mu\left(c^{\pi}_{(i-1)r+1}, \cdots, c^{\pi}_{ir}\right)$ is the signal point transmitted over the ith sub-carrier. The signal constellation $\mathcal{X}$ can be arbitrary, but most commonly PSK or quadrature amplitude modulation (QAM) constellations are considered. Furthermore, binary-reflected Gray mapping is applied.

Assuming a sufficiently long cyclic prefix and coherent reception, the equivalent baseband channel model is given by

$$y_i = \sqrt{\gamma p_i}\, h_i x_i + z_i \,, \quad i = 1, \cdots, L \,, \tag{4.2}$$

where y_i, h_i, p_i, and z_i are the received symbol, the frequency-domain channel gain, the allocated power, and the additive white Gaussian noise

(AWGN) sample for the ith sub-carrier, respectively. For (4.2) we assumed that $L = N/r$ is an integer. Without loss of generality, we apply the normalizations

$$P_{\mathrm{T}} = L \,, \tag{4.3}$$

and $\mathbb{E}\{|z_i|^2\} = 1$. Since the power constrain in (4.1) is always met with equality, i.e., $\sum_{i=1}^{L} p_i = P_{\mathrm{T}}$, these normalizations ensure that $\bar{\gamma}$ in (4.2) is the average signal-to-noise ratio (SNR) at the receiver.

At the receiver, the demapper outputs bit-wise reliability metrics

$$\lambda_{i,j} = -\min_{a \in \mathcal{X}_{j,1}} \left\| y_i - \sqrt{\bar{\gamma} p_i} h_i a \right\|^2 + \min_{a \in \mathcal{X}_{j,0}} \left\| y_i - \sqrt{\bar{\gamma} p_i} h_i a \right\|^2 , \tag{4.4}$$

$j = 1, \ldots, r$, for the r coded bits transmitted over the ith sub-carrier. $\mathcal{X}_{j,b}$ denotes the set of symbols in $\mathcal{X}$ with the jth bit in the binary label fixed to b. Finally, the metrics are deinterleaved and input to the maximum-likelihood decoder of the binary code in order to retrieve the information bits.

4.3 Power Allocation Method

In this section, we present the new power allocation method. To this end, we first derive an expression for the probability of decoding errors, which relies on a simplified BIC-OFDM channel model and the result from Chapter 2. We then show that this expression allows us to formulate the power allocation problem for BIC-OFDM with arbitrary constellations as an LP.

4.3.1 Error Event Probability

For a given vector of frequency-domain channel gains $\underline{h} \triangleq [h_1, \ldots, h_L]$ we model the effective channel between encoder output at the transmitter and decoder input at the receiver as a memoryless binary-input output symmetric (MBIOS) channel. This model is only an approximation for BIC-OFDM, as it neglects the dependencies between binary symbols c_k mapped to the same transmitted symbol x_i. However, their effect on the overall error probability of BIC-OFDM is negligible as long as interleaving distributes these c_k across dominant error events.

Let us identify an error event by the tuple (d_{H}, j), where d_{H} denotes its Hamming weight and j its index within the group of events with distance d_{H}. Under the MBIOS channel model, the probability for this error event can be written as

$$P_{\mathrm{e}}(d_{\mathrm{H}}, j, \underline{h}) = \Pr(\Delta \leq 0) , \tag{4.5}$$

where

$$\Delta \triangleq \sum_{k=1}^{d_{\mathrm{H}}} \lambda_{s_k, b_k} , \tag{4.6}$$

is the accumulated metric difference, and s_k and b_k denote the sub-carrier index and label position of the kth non-zero bit for the event, i.e., s_k and b_k are functions of (d_{H}, j). The bit metrics in (4.6) are mutually independent for the MBIOS model, and thus we can apply the PDF approximation for

$\lambda_{i,j}$ developed in Chapter 2 (Section 2.3.1) to arrive at

$$P_e(d_H, j, \underline{h}) = \sum_{l_1=1}^{n} \cdots \sum_{l_{d_H}=1}^{n} \left[\prod_{k=1}^{d_H} \beta_{b_k, l_k} \right] Q \left(\sqrt{ \left[\sum_{k=1}^{d_H} p_{s_k} h_{s_k}^2 \, (l_k d_{\min})^2 \right] \frac{\bar{\gamma}}{2} } \right) , \tag{4.7}$$

where $d_{\min}$ is the minimum Euclidean distance between signal points of $\mathcal{X}$, and n and $\beta_{j,l}$ are parameters solely defined by $\mathcal{X}$ (cf. Section 2.3.1 for details).

4.3.2 Linear Program Power Allocation

The error event probability can be used as a lower bound for the BIC-OFDM BER:

$$P_{\mathrm{BER}} \geq \max_{d_H, j} \left[c(d_H, j) P_e(d_H, j, \underline{h}) \right] , \tag{4.8}$$

where the factor $c(d_H, j)$ accounts for the number of errors caused by an error event. Considering the expression (4.7), the lower bound (4.8) will be asymptotically dominated by the component with the minimum effective squared Euclidean distance

$$d_{\mathrm{E}}^2(d_H, j) \triangleq \sum_{k=1}^{d_H} p_{s_k} h_{s_k}^2 d_{\min}^2 . \tag{4.9}$$

Thus, we suggest to apply power allocation such that the minimum of $d_{\mathrm{E}}^2(d_H, j)$ is maximized. That is, the power allocation problem (4.1) can be reformulated as

$$\begin{aligned} \max_{\underline{p}} \quad & \min_{d_{\mathrm{H}},j} d_{\mathrm{E}}^2(d_{\mathrm{H}},j) \\ \text{s.t.} \quad & \sum_{i=1}^{L} p_i \leq P_{\mathrm{T}} , \\ & p_i \geq 0 \quad \forall i \in \{1,\dots,L\} . \end{aligned} \tag{4.10}$$

Considering (4.9), this problem can be re-written as (recall that the index s_k is a function of (d_{H}, j))

$$\begin{aligned} \max_{\underline{p}} \quad & t \\ \text{s.t.} \quad & t \leq \sum_{k=1}^{d_{\mathrm{H}}} p_{s_k} h_{s_k}^2 \quad \forall (d_{\mathrm{H}},j) \\ & \sum_{i=1}^{L} p_i \leq P_{\mathrm{T}} , \\ & p_i \geq 0 \quad \forall i \in \{1,\dots,L\} , \end{aligned} \tag{4.11}$$

which is an LP. The number of inequality constraints in (4.11) needs to be limited by considering only significant error events with $d_{\mathrm{H}} \leq d_{\mathrm{H,max}}$, as has been done in [6]. Different from the convex program in [6], the LP is independent of the SNR. Using `CVX`, a package for specifying and solving convex programs [8], we have observed that the LP is solved ten times faster than the convex program from [6] (for a given SNR).

4.4 Numerical Results

In this section, we present selected simulation results for the proposed power allocation method. We have used the WLAN IEEE 802.11a OFDM system with 48 active sub-carriers and the quasi-standard memory-6 convolutional code with generator polynomials $[133, 171]_8$ and rate $R_c = 1/2$. All error events with Hamming weight $10 \leq d_H \leq 14$ have been considered in (4.11). The channel realization $\underline{h}$ is randomly generated according to an exponentially decaying power delay profile.

Figure 4.1 compares the BER performances for (i) uniform power allocation (UPA), (ii) minimum BER allocation for uncoded transmission according to [5], (iii) power allocation (PA) for BIC-OFDM according to [6], and (iv) the proposed PA from (4.11) as function of the bit-wise SNR $\bar{\gamma}_b = \bar{\gamma}/(rR_c)$. QPSK and 16QAM are considered for all methods but the method from [6], which is only applicable to QPSK. We observe that the proposed method clearly outperforms UPA and PA designed for uncoded transmission. More importantly, its performance closely approaches that achieved with the considerably more complex method from [6] for the case of QPSK.

The difference between the PA solutions obtained from [6] and from the LP (4.11) is plotted in Figure 4.2. It can be seen that the LP solution converges to the PA from convex programming as SNR grows. This is due to the increasing dominance of the minimum distance error event for the overall error rate with increasing SNR.

Finally, Figure 4.3 illustrates the effect of LP-based PA on the distance profile of BIC-OFDM. For this purpose, the empirical cumulative density function (CDF) of d_E^2 defined in (4.9) is shown for UPA and the proposed PA. We observe that by maximizing the minimum distance, the LP effectively shifts the profile towards larger distances. This in turn reduces the overall

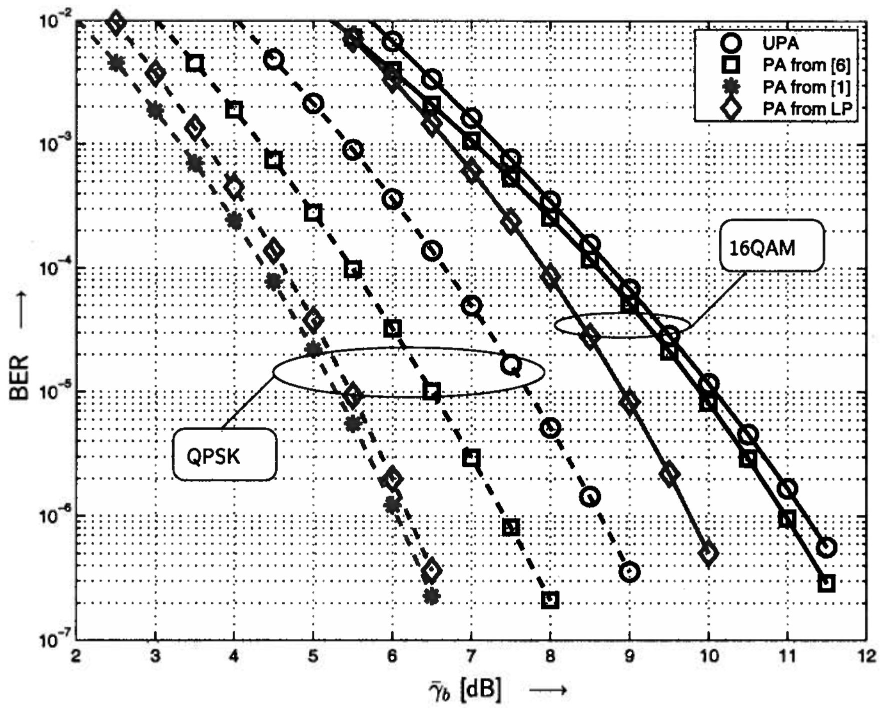

Figure 4.1: BER of BIC-OFDM transmission systems with QPSK and 16QAM. Uniform power allocation (UPA), optimal power allocation (PA) for uncoded transmission, PA according to convex optimization, and PA using the proposed LP (4.11) are compared.

error rate as has been seen in Figure 4.1.

4.5 Conclusions

We have developed a new power allocation policy for BIC-OFDM transmission. It is based on maximizing the minimum effective Euclidean distance of error events, which is equivalent to BER minimization in the high SNR regime. Different from the BER union-bound based method developed in [6],

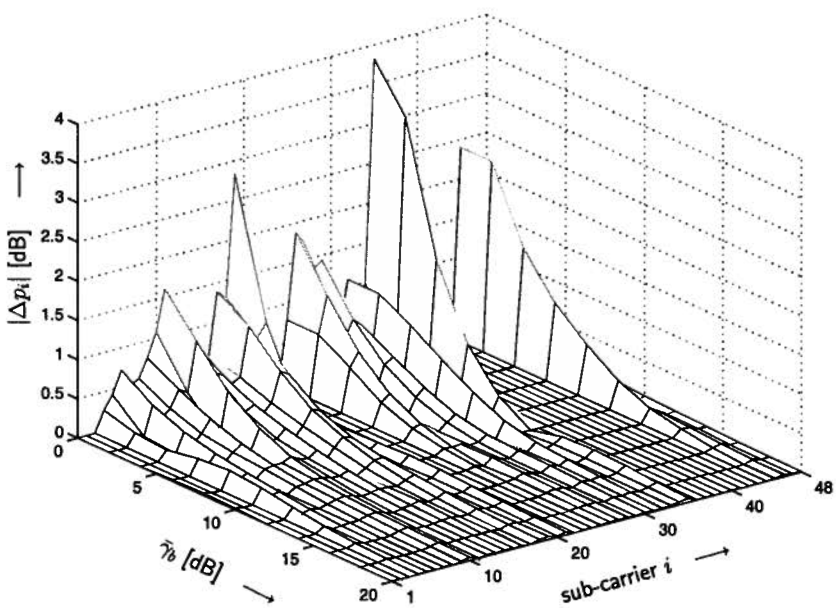

Figure 4.2: Absolute difference $|\Delta p_i|$ between the power allocation solutions obtained from convex optimization and the LP (4.11) (for QPSK).

the proposed method is not limited to binary modulations. Furthermore, the power allocation problem has been formulated as an LP, which can be solved faster than the convex optimization needed in [6].

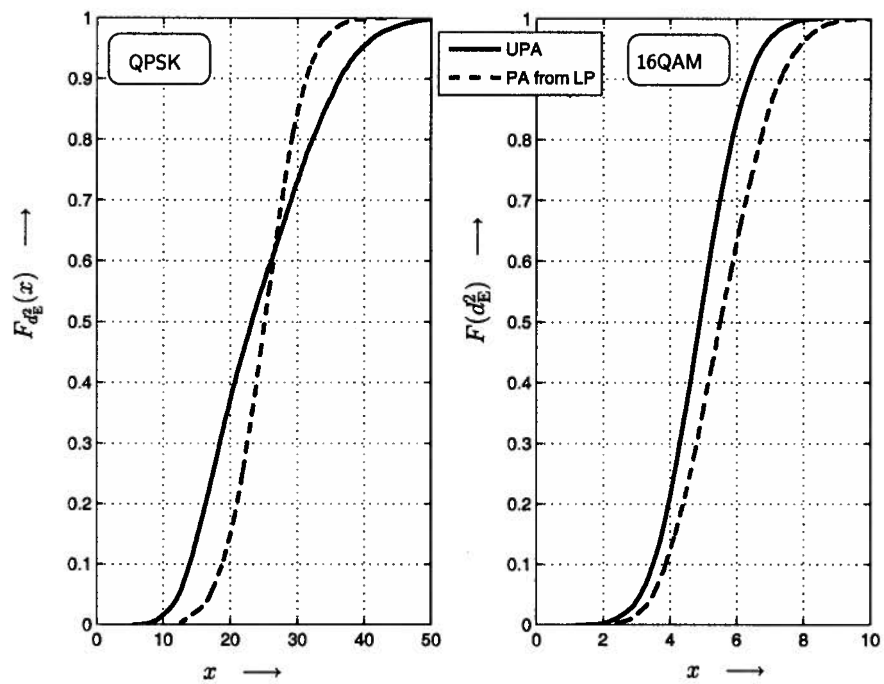

Figure 4.3: CDF of d_E^2 from (4.9) for uniform power allocation (UPA) and PA with the proposed LP (4.11).

Bibliography

[1] A. Guillén i Fàbregas, A. Martinez, and G. Caire, "Bit-interleaved coded modulation," *Foundations and Trends in Communications and Information Theory*, vol. 5, no. 1-2, pp. 1–153, 2008.

[2] B. Le Floch, M. Alard, and C. Berrou, "Coded orthogonal frequency division multiplex," *Proc. IEEE*, vol. 83, no. 6, pp. 982 – 996, June 1995.

[3] P. Chow, J. Cioffi, and J. Bingham, "A practical discrete multitone transceiver loading algorithm for data transmission over spectrally shaped channels," *IEEE Trans. Commun.*, vol. 43, no. 234, pp. 773–775, Feb/Mar/Apr 1995.

[4] R. Fischer and J. Huber, "A new loading algorithm for discrete multitone transmission," vol. 1, Nov 1996, pp. 724–728 vol.1.

[5] L. Goldfeld, V. Lyandres, and D. Wulich, "Minimum BER power loading for OFDM in fading channel," *IEEE Trans. Commun.*, vol. 50, no. 11, pp. 1729 – 1733, 2002.

[6] H. Moon and D. Cox, "Efficient power allocation for coded OFDM systems," *IEEE Trans. Commun.*, vol. 57, no. 4, pp. 943–947, April 2009.

[7] S. Boyd and L. Vandenberghe, *Convex Optimization.* Cambridge, UK: Cambridge University Press, 2005.

[8] M. Grant and S. Boyd. (2009, June) CVX: Matlab software for disciplined convex programming (web page and software). [Online]. Available: http://stanford.edu/ boyd/cvx

Chapter 5

New Designs for Bit-Interleaved Coded Modulation with Hard-Decision Feedback Iterative Decoding[10]

5.1 Introduction

The bit-interleaved coded modulation (BICM) structure can also be looked at as a concatenated coding system, with the forward error correction (FEC) encoder and the multilevel modulator as outer and inner encoder, respectively. The inner encoder is made "stronger", if non-Gray labeling is applied, cf. e.g. [1–3]. Interestingly, this BICM with non-Gray labeling can achieve excellent error-rate performance with relatively simple outer binary codes,

[10]A version of this chapter has been submitted for publication. A. Kenarsari Anhari and L. Lampe, "New Designs for Bit-Interleaved Coded Modulation with Hard-Decision Feedback Iterative Decoding," *submitted for publication*, July 2009.

such as for example convolutional codes. BICM considered as concatenated code is commonly decoded in an iterative fashion, in which the demapper and a soft-input soft-output (SISO) channel decoder for the outer FEC code exchange extrinsic information. We will refer to this structure as BICM with soft-feedback iterative decoding (BICM-SID). An alternative decoder proposed in [4] uses a soft-input hard-output (SIHO) outer decoder, like the Viterbi decoder for convolutional codes. This BICM with hard-decision feedback iterative decoding (BICM-HID) has two complexity advantages over BICM-SID. First, the outer SIHO decoder is less complex than its SISO counterpart, and second, the demapper using hard-decision feedback needs to consider only two instead of all constellation points for each labeling bit [1]. On the downside, BICM-HID is considerably outperformed by BICM-SID due to the effect of erroneous feedback.

In this chapter, we propose two novel demapper designs for BICM-HID which mitigate the effect of feedback errors and thus improve the overall error-rate performance of BICM-HID. We focus on convolutionally coded transmission, for which SIHO FEC decoding, i.e., Viterbi decoding is commonly applied. The first key idea is that the demapper makes use of the error rate of the hard-decision feedback after iteration i, which we denote by P_i. As we will show, this essentially provides the demapper with reliability information and penalizes unreliable feedback. The corresponding demapper is similar to that proposed in [5]. However, different from the scheme in [5], which relies on a SISO outer decoder, our approach retains the outer Viterbi decoder and makes use of the analytical result, developed in Chapter 2, for the error rate performance of coded BICM to estimate P_i.

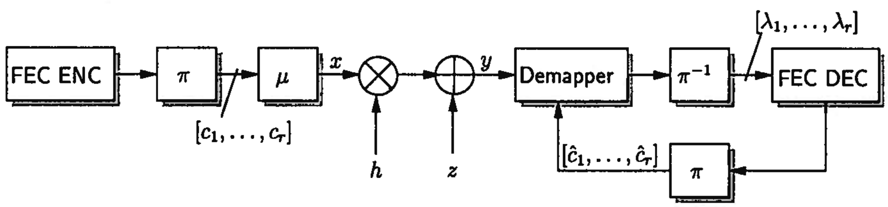

Figure 5.1: Block diagram of BICM transmission over a fading channel and iterative decoding. π and π^{-1} denote interleaving and deinterleaving, respectively. r coded binary symbols $[c_1, \ldots, c_r]$ are mapped to one transmitted symbol x. The feedback from the FEC decoder (FEC DEC) to the demapper is shown the form of decoded code symbols $[\hat{c}_1, \ldots, c_r]$, i.e., hard-decision feedback.

Furthermore, parameter tuning as in [5, Eq.(10)] is unnecessary. The second key idea is the interpretation of the effect of feedback errors as additive impulsive noise, and its statistical approximation through a two-term Gaussian mixture probability density function (PDF). This leads us to the second proposed demapper, whose complexity is practically the same as that of the demapper used in conventional BICM-HID. We provide simulative evidence that BICM-HID with the proposed designs effectively bridges the error-rate gap between conventional BICM-HID and BICM-SID.

The remainder of this chapter is organized as follows. In Section 5.2, BICM with iterative decoding and demappers for conventional BICM-HID and BICM-SID are briefly reviewed. In Section 5.3, we derive the two new demapper designs. Numerical results are presented in Section 5.4. In Section 5.5, concluding remarks are offered.

5.2 Preliminaries

We consider a convolutionally coded BICM system, whose block diagram is shown in Figure 5.1. The bit-interleaved output of the FEC encoder is input to a subsequent mapper $\mu : \{0,1\}^r \to \mathcal{X}$ assigning r coded bits $[c_1, \ldots, c_r]$ to a signal point $x \in \mathcal{X}$. The signal x is transmitted over a flat fading AWGN channel, and assuming a coherent receiver the corresponding received sample $y \in \mathbb{C}$ is given by

$$y = h\,x + z\,, \tag{5.1}$$

where $h \in \mathbb{R}^+$ denotes the channel gain and $z \in \mathbb{C}$ is the AWGN sample. Without loss of generality, we assume $\mathbf{E}\{|x|^2\} = 1$, $\mathbf{E}\{h^2\} = \gamma$, and $\mathbf{E}\{|z|^2\} = 1$, and thus γ is the average SNR.

The receiver applies a concatenated demapper-decoder structure (see Figure 5.1), where the demapper generates r bit-wise decoding metrics

$$\begin{aligned}\lambda_j = &\log\left[\sum_{a\in\mathcal{X}_{j,1}} \exp\left(f(a,j) - |y - h\,a|^2\right)\right] \\ &- \log\left[\sum_{a\in\mathcal{X}_{j,0}} \exp\left(f(a,j) - |y - h\,a|^2\right)\right]\,,\end{aligned} \tag{5.2}$$

$1 \leq j \leq r$, for each transmitted symbol x. In the above expression, $\mathcal{X}_{j,b}$ denotes the set of symbols in the constellation with the jth binary label fixed to b, and $f(a,j)$ represents a-priori information or a *bias* provided by the FEC decoder. Of course, $f(a,j) = 0$ for the first iteration, in which no feedback from the decoder is available.

In the case of a BICM-SID with soft feedback $\Pr(c_j = b)$, $1 \leq j \leq r$, we can write the bias-term as

$$f(a,j) = \sum_{\substack{\ell=1 \\ \ell \neq j}}^{r} \log\left(\Pr(c_\ell = b_\ell)\right) \ , \tag{5.3}$$

where $[b_1, \ldots, b_r] = \mu^{-1}(a)$. For BICM-HID with hard-decision feedback $\hat{c}_j \in \{0,1\}$, $1 \leq j \leq r$, we have

$$f(a,j) = \begin{cases} 0, & \text{if } b_\ell = \hat{c}_\ell, \forall \ell \in \{1, \ldots, r\}, \ell \neq j, \\ -\infty, & \text{otherwise} \end{cases} \ . \tag{5.4}$$

We observe that BICM-HID has two complexity advantages over BICM-SID. First, a SIHO decoder, typically the Viterbi decoder, can be used instead of a more complex SISO decoder. Second, the summation in (5.2) and thus the 2^r-times evaluation of the Euclidean distance can be omitted and the computation of the bias term $f(a,j)$ is greatly simplified.

5.3 New BICM-HID Scheme

We now present two new demapper designs for BICM-HID. The additional information that is used by the proposed demappers is an estimate of the average bit-error rate (BER) for the coded bits c_j after the ith iteration, P_i. The first proposed demapper has the same computational complexity as the demapper proposed in [5], but does not require outer SISO decoding and parameter tuning. The second demapper design enjoys a very similar complexity advantage over BICM-SID as the conventional BICM-HID, but achieves a greatly improved error-rate performance.

For the moment, let us assume that P_i is known perfectly at the demapper.

5.3.1 Demapper Design I

Given P_i and $\hat{c}_j$, the best estimate for $\Pr(c_j = b_\ell)$ is given by $P_i^{d_j}(1-P_i)^{1-d_j}$, where $d_j = d_{\mathrm{H}}(\hat{c}_j, b_j)$ and $d_{\mathrm{H}}(\cdot,\cdot)$ returns the Hamming distance between its arguments. Hence, the bias $f(a,j)$ from (5.3) is replaced by

$$\begin{aligned} f(a,j) &= \alpha_i + \sum_{\substack{\ell=1 \\ \ell\neq j}}^{r} \log\left(P_i^{d_\ell}(1-P_i)^{1-d_\ell}\right) \\ &= \beta_i \sum_{\substack{\ell=1 \\ \ell\neq j}}^{r} d_\ell \\ &= \beta_i d_{\mathrm{H}}\left(\hat{\mathbf{c}}_{j,b}, \mu^{-1}(a)\right), \end{aligned} \tag{5.5}$$

where we added the constant term

$$\alpha_i \triangleq -(r-1)\log(1-P_i) \tag{5.6}$$

for convenience and defined

$$\beta_i \triangleq \log\left(\frac{P_i}{1-P_i}\right), \quad \hat{\mathbf{c}}_{j,b} \triangleq [\hat{c}_1, \ldots, \hat{c}_{j-1}, b, \hat{c}_{j+1}, \ldots, \hat{c}_r]. \tag{5.7}$$

Substituting the bias from (5.5) in the metric (5.2) leads to

$$\begin{aligned} \lambda_j = &\log\left[\sum_{a\in\mathcal{X}_{j,1}} \exp\left(\beta_i d_{\mathrm{H}}\left(\hat{\mathbf{c}}_{j,1}, \mu^{-1}(a)\right) - |y - h\,a|^2\right)\right] \\ &-\log\left[\sum_{a\in\mathcal{X}_{j,0}} \exp\left(\beta_i d_{\mathrm{H}}\left(\hat{\mathbf{c}}_{j,0}, \mu^{-1}(a)\right) - |y - h\,a|^2\right)\right], \end{aligned} \tag{5.8}$$

which is our first new demapper design and referred to as "design I".

In passing, we remark that an efficient implementation of the log-sum of exponentials or the max-log approximation [6] can equally be applied to (5.2) and (5.8), if the exp-operation is to be avoided.

5.3.2 Demapper Design II

To derive the second demapper design ("design II"), we first provide an interpretation of feedback errors $\hat{c}_j \neq c_j$ as impulsive noise.

Gaussian Mixture Noise Interpretation

The new metric (5.8) allows the interpretation of BICM-HID as transmission over a channel affected by additive Gaussian mixture noise [7]. More specifically, the bit-wise metric (5.8) is also obtained when considering detection for a channel with the effective noise

$$z_\nu^{\mathrm{e}} = z + z_\nu^{\mathrm{f}} \, , \tag{5.9}$$

where z_ν^{f} is due to the hard-decision feedback and thus depends on bit position j, feedback $\hat{c}_{j,b}$, and fading gain h, which are collected in the parameter vector $\nu \triangleq [j, \hat{c}_{j,b}, h]$. The feedback noise has a probability mass function $p_{z_\nu^{\mathrm{f}}}(m)$ with mass

$$p(a, \hat{c}_{j,b}) \triangleq P_i^{d_{\mathrm{H}}(\hat{c}_{j,b}, \mu^{-1}(a))}(1 - P_i)^{[r-1-d_{\mathrm{H}}(\hat{c}_{j,b}, \mu^{-1}(a))]} \tag{5.10}$$

at location $m = h(\mu(\hat{c}_{j,b}) - a)$.

Hence, the PDF of z_v^{e} is the Gaussian mixture density

$$p_{z_v^{\mathrm{e}}}(m) = \frac{1}{\pi} \sum_{a \in \mathcal{X}_{j,b}} p(a, \hat{c}_{j,b}) \exp\left(-\left|m - [h(\mu(\hat{c}_{j,b}) - a)]\right|^2\right) . \tag{5.11}$$

Simplified Demapper

For the second, simplified demapper, we propose the approximation of (5.11) by a single two-term Gaussian mixture function for all j, $\hat{c}_{j,b}$, and h. To this end, we consider the average of the PDF (5.11) with respect to these variables, which can be shown to have zero mean and variance

$$\sigma_{\mathrm{e}}^2 = 1 + \frac{1}{2^r r} \sum_{\substack{j \in \{1,\dots r\} \\ b \in \{0,1\} \\ \hat{c}_{j,b} \in \{0,1\}^{(r-1)}}} \left[\gamma \sum_{a \in \mathcal{X}_{j,b}} p(a, \hat{c}_{j,b}) |\mu(\hat{c}_{j,b}) - a|^2\right] . \tag{5.12}$$

The two-term approximation is then given by

$$\tilde{p}_{z^{\mathrm{e}}}(m) = \frac{(1-P_i)^{r-1}}{\pi} \exp\left(-|m|^2\right) + \frac{1-(1-P_i)^{r-1}}{\pi\sigma^2} \exp\left(-\frac{|m|^2}{\sigma^2}\right) , \tag{5.13}$$

where $\sigma^2 = \frac{\sigma_{\mathrm{e}}^2 - (1-P_i)^{r-1}}{1-(1-P_i)^{r-1}}$ to maintain the same variance as in (5.11). Intuitively, in (5.13) the first term indicates the noise when there is no error in the feedback from the FEC decoder, and the second term represents the equivalent noise in the presence of feedback errors. We note that σ^2 only depends on the signal constellation $\mathcal{X}$, the SNR γ, and the BER P_i, and thus it is computed once per iteration.

Using the noise PDF given in (5.13), defining

$$\delta_i \triangleq \log\left(\frac{\sigma^2}{1-(1-P_i)^{r-1}}\right) , \tag{5.14}$$

and applying the max-log approximation [6], we can re-write the bit-metric (5.2) as

$$\begin{aligned} \lambda_j \;=\; & -\min\left\{\alpha_i + |y - h\mu(\hat{\mathbf{c}}_{j,1})|^2, \delta_i + \frac{|y - h\mu(\hat{\mathbf{c}}_{j,1})|^2}{\sigma^2}\right\} \\ & +\min\left\{\alpha_i + |y - h\mu(\hat{\mathbf{c}}_{j,0})|^2, \delta_i + \frac{|y - h\mu(\hat{\mathbf{c}}_{j,0})|^2}{\sigma^2}\right\} . \end{aligned} \tag{5.15}$$

We observe that (5.15) requires only two additional comparisons relative to conventional BICM-HID using (5.4).

5.3.3 Low-Complexity Estimation of P_i

We now consider the estimation of P_i, which is required for the new demapper designs (5.8) and (5.15). It should be noted that the overall error-rate performance is relatively robust with respect to the estimation accuracy, and thus we are content with a simple method that provides a coarse estimate for P_i.

For the error rate P_1 after the first iteration, we consider the dominant error events of the Viterbi decoder and thus use the estimate

$$\tilde{P}_1 = \frac{1}{n_c} w_{d_{\text{free}}} \mathrm{PEP}(d_{\text{free}}) , \tag{5.16}$$

where $\mathrm{PEP}(d_{\text{free}})$ is the pairwise error probability between two codewords with Hamming distance d_{free}, d_{free} denotes the free distance of the convolutional code of rate $R_c = k_c/n_c$, and $w_{d_{\text{free}}}$ is the total weight of *output* bits in error events with Hamming weight d_{free}. Using the saddlepoint approximation [8, Eq.(12)], closed-form expressions/approximations for this PEP have been provided in Chapter 2 and Chapter 3 for arbitrary AWGN fading channels, and thus (5.16) can be easily evaluated. Next, for the BER P_n after the final iteration $i = n$, we use the perfect-feedback lower bound from [1] together with the saddlepoint approximation, which again results in a closed-form PEP expression and thus estimate $\tilde{P}_n$. Finally, we estimate the BER for iteration i using the interpolation

$$\log(\tilde{P}_i) = \frac{n-i}{n-1}\log(\tilde{P}_1) + \frac{i-1}{n-1}\log(\tilde{P}_n)\,. \qquad (5.17)$$

5.4 Simulation Results

In this section, we present selected simulation results to illustrate the performance of BICM-HID with the proposed demappers. We use the example of 16-ary quadrature amplitude modulation (QAM) BICM with modified set-partitioning labeling over a Rayleigh fading channel, cf. [1], and employ the maximum-free distance 4-state rate-1/2 convolutional code (very similar results have been obtained for codes with larger memory). BER and frame-error rate (FER) results are shown as function of the average bit-wise SNR $\gamma_b = \gamma/(R_c r) = \gamma/2$. First, we take a look at the goodness of the proposed PDF approximation (5.13). For this purpose, Figure 5.2 shows the analytical two-term PDF $\tilde{p}_{z^e}(m)$ and the empirical PDF obtained from

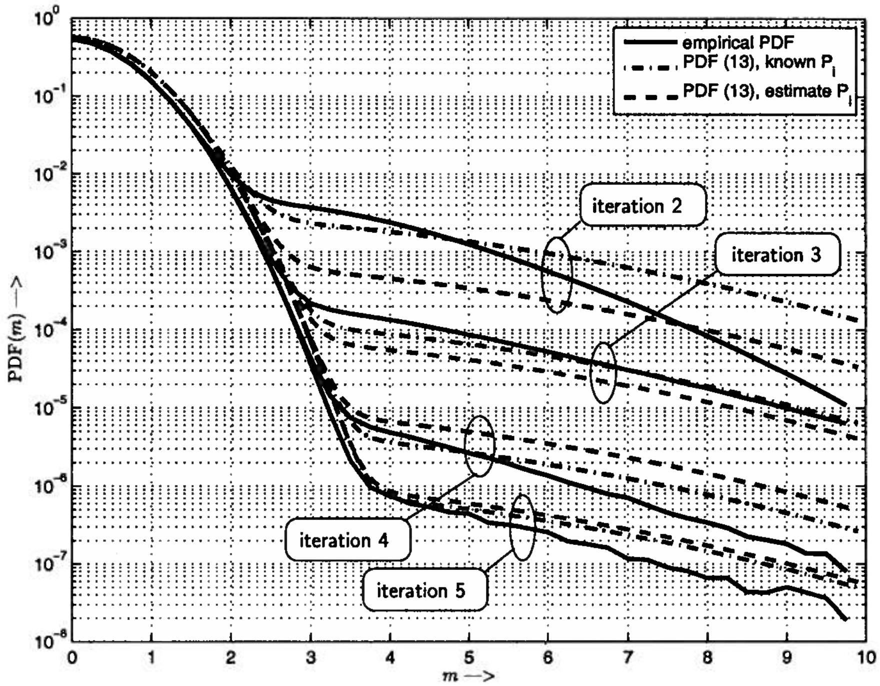

Figure 5.2: Two-term PDF approximation from (5.13) and empirical PDF from simulations during the $(i+1)$st iteration, $i = 1, .., 4$, at SNR $\gamma_b = 10$ dB. The PDF approximation is shown for the cases of known P_i and using the estimate $\tilde{P}_i$ from (5.17). A total of $n = 5$ iterations is assumed.

Monte Carlo simulation for an SNR of $\gamma_b = 10$ dB. The two-term PDF is plotted for known P_i and using the estimate $\tilde{P}_i$ from (5.17), respectively. A total of $n = 5$ iterations is assumed, so four sets of curves are plotted in Figure 5.2. The interleaver length is set to 10000 binary symbols. It can be seen that the empirical PDF displays a markedly non-Gaussian shape, which is a result of erroneous feedback and explains the relatively poor performance of conventional BICM-HID that is based on the Euclidean distance metric (see also results below). The two-term approximation seems to mimic the

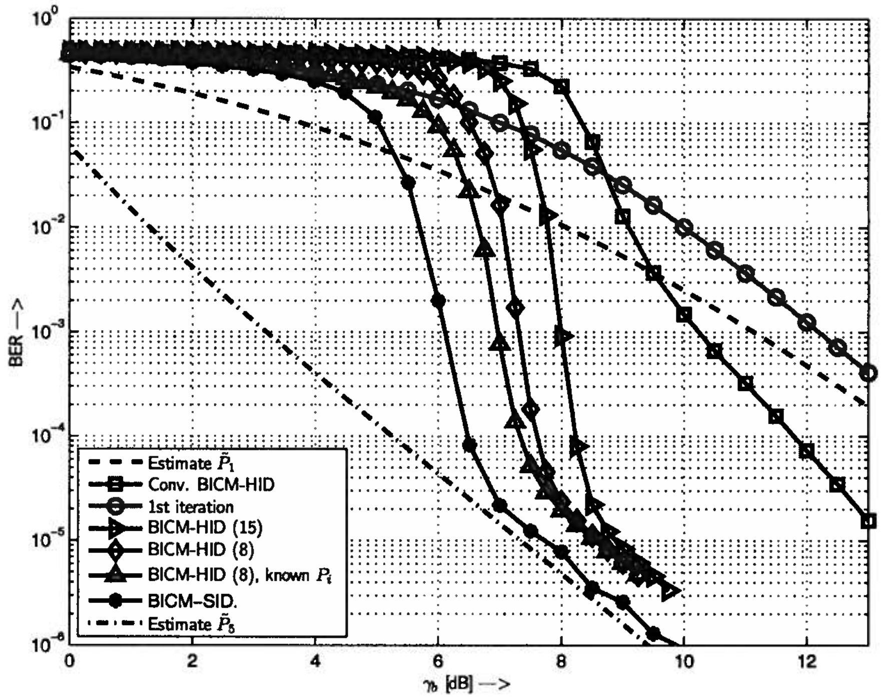

Figure 5.3: BER for BICM-HID with conventional and proposed demappers. As reference, BER for BICM-SID, and BER estimates $\tilde{P}_1$ and $\tilde{P}_5$ are also included.

non-Gaussian behaviour fairly well, which corroborates the proposed demapper design approach. The difference between P_i and its estimate $\tilde{P}_i$ reflects mainly in a vertical shift of the second term of the mixture PDF. This can be also seen from (5.13) when approximating $(1-P_i)^{r-1}$ by $(1-rP_i)$, which is valid for small P_i, for which also $\sigma^2 \approx \sigma_e^2$.

Figure 5.3 presents the simulated BER[11] after the first and fifth iteration

[11] As usual, we plot the BER for binary *information* symbols. To enable a direct comparison, the shown analytical results for $\tilde{P}_1$ and $\tilde{P}_5$ are also determined with respect to information symbols.

for BICM-HID with (a) the conventional demapper ((5.2) with bias (5.4)), (b) demapper design I (5.8), and (c) demapper design II (5.15). For design I we also include the case of perfect BER estimation, i.e., $\tilde{P}_i = P_i$. Furthermore, as a reference, the curves for BICM-SID and the estimated BERs $\tilde{P}_1$ and $\tilde{P}_n = \tilde{P}_5$ after the first and fifth iteration are shown (see Footnote 11). The total number of iterations and interleaver length are the same as for the results in Figure 5.2.

We observe that the proposed demapper designs significantly improve the BER performance relative to the conventional demapper for BICM-HID. In particular, the considerable gap between conventional BICM-HID and BICM-SID is largely closed through the modified demappers. Demapper design II achieves a performance close to that of demapper design I, which renders it the perhaps preferred choice considering its low computational complexity. It can also be seen that the feedback-BER approximation $\tilde{P}_i$ of P_i is sufficiently accurate for the purposes of BICM-HID, since the two BER curves for estimated and known P_i almost coincide. The quality of the estimate $\tilde{P}_i$ is also confirmed by the relatively good approximation of the actually BER after one and five iteration through $\tilde{P}_1$ and $\tilde{P}_5$, respectively. Figure 5.4 shows the FER for the same scenario as above, but a relatively short interleaver of length 2000. This allows a comparison with the results from [5, Fig. 3]. We observe that the proposed designs achieve a performance very close to that from [5], despite the use of a SIHO decoder (designs I and II) and a less complex demapper (design II). The small consistent gap between design I and the demapper from [5] could likely be removed through scaling of β_i in (5.8), which however requires a simulation-based tuning of

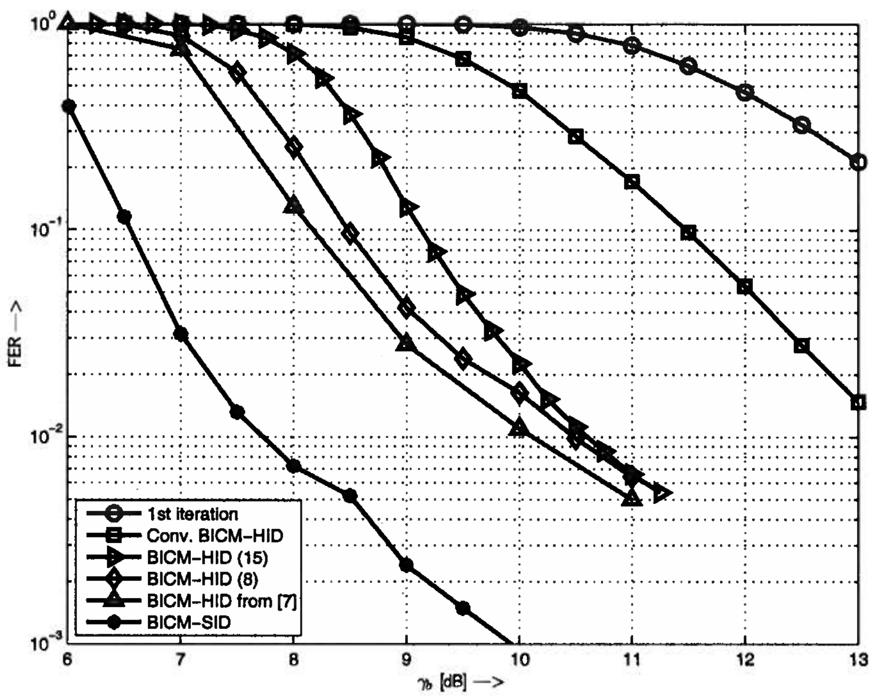

Figure 5.4: FER for BICM-HID with conventional and proposed demappers, and demapper previously proposed for improving the performance of BICM-HID. As reference, FER for BICM-SID.

the scaling parameter that was done in [5]. Since design II performs close to design I also in terms of FER and for this relatively short interleaver length, it is an attractive choice for low-complexity BICM-HID.

5.5 Conclusion

In this chapter, we have presented two novel demapper designs for BICM-HID. The key ideas are the use of an simple approximation of the feedback error-rate and the interpretation of feedback errors as additive impulsive noise. The first demapper design makes optimal use of error-rate information, while the second design is suboptimal but enjoys the low complexity of conventional BICM-HID. Our simulation results have shown that the proposed schemes significantly outperform conventional BICM-HID and approach the performance of BICM-SID, which is the ultimate performance limit for BICM with iterative decoding.

Bibliography

[1] A. Chindapol and J. Ritcey, “Design, analysis, and performance evaluation for BICM-ID with square QAM constellations in Rayleigh fading channels,” *"IEEE J. Select. Areas Commun."*, vol. 19, no. 5, pp. 944–957, May 2001.

[2] J. Tan and G. Stüber, “Analysis and design of symbol mappers for iteratively decoded BICM,” *IEEE Trans. Wireless Commun.*, vol. 4, no. 2, pp. 662–672, Mar. 2005.

[3] F. Schreckenbach, N. Görtz, J. Hagenauer, and G. Bauch, “Optimization of symbol mappings for bit-interleaved coded modulation with iterative decoding,” *IEEE Commun. Lett.*, vol. 7, no. 12, pp. 593–595, Dec. 2003.

[4] X. Li and J. Ritcey, “Bit-interleaved coded modulation with iterative decoding,” in *IEEE International Conference on Communications (ICC)*, vol. 2, Vancouver, BC, Canada, june 1999, pp. 858–863.

[5] T. Li, W. Mow, and M. Siu, “Bit-interleaved coded modulation in the presence of unknown impulsive noise,” in *IEEE International Conference on Communications (ICC)*, Istanbul, Turkey, June 2006, pp. 3014 – 3019.

[6] P. Robertson, P. Hoeher, and E. Villebrun, “Optimal and sub-optimal maximum a posteriori algorithms suitable for turbo decoding,” *European Transactions on Telecommunication*, vol. 2, no. 8, pp. 119–125, Mar./Apr. 1997.

[7] D. Stein, "Detection of Random Signals in Gaussian Mixture Noise," *IEEE Trans. Inform. Theory*, vol. 41, no. 6, pp. 1788–1801, Nov. 1995.

[8] A. Martinez, A. Guillen i Fabregas, and G. Caire, "Error probability analysis of bit-interleaved coded modulation," *IEEE Trans. Inform. Theory*, vol. 52, no. 1, pp. 262–271, Jan. 2006.

Chapter 6

Summary, Conclusions, and Future Work

6.1 Summary and Conclusions

This work delivers three major breakthroughs in the analysis and design of communication systems based on bit-interleaved coded modulation (BICM). Generally, in Chapter 2 and Chapter 3, we have presented the first main contribution which is a novel analytical framework for performance evaluation of BICM. In addition to additive white Gaussian noise (AWGN) model, the practically important case of transmission over fading channels impaired by Gaussian mixture noise (GMN) has also been studied. The proposed framework is based on the assumptions of perfect interleaving and the use of max-log simplification at the receiver which are common in almost all previously proposed methods. Different from previous approaches available in the literature, the proposed framework is applicable to arbitrary mapping rules and results in closed-form expressions disregarding the probability density function (PDF) of channel's fading process. The key idea is to approximate the PDF of reliability metrics using the so-called nearest neighbours approximation. It is shown that the error caused by using the proposed PDF approximation becomes negligible in the signal-to-noise ratio (SNR) region wherein the bit-error rate (BER) union bound converges to the real BER the system. Furthermore this approach makes use of the saddlepoint approximation [1] and the finite exponential series approximation of the Gaussian error function [2]. Additionally, Chapter 2 contains other interesting contributions such as:

- The derivation of *exact* Laplace transform of the newly found PDF expression for general Nakagami-m fading AWGN channels.
- A closed-form expression for the cutoff of BICM
- Based on the new PDF approximation, the asymptotic BER expressions as SNR goes to infinity, is derived. It is shown that for the nonfading channel the BER is closely approximated by the BER expression for an equivalent binary transmission scaled by a constant which is a function of the minimum Hamming distance d_{free} of the code and the mapping rule. For the case of Nakagami-m fading it is shown that the diversity order is the product of m and d_{free}. Furthermore, the asymptotic coding gain is shown to depend on a parameter which is a generalization of the harmonic mean presented in [3].

Furthermore, in Chapter 3 we present the following specific contributions

- Based on this new PDF expression and a finite series approximation of error function, we derive an *approximation* for the Laplace transform of the PDF of reliability metrics for general fading GMN channels.

- We simplify the saddlepoint-based approximation for the high SNR regime. It is shown that the diversity order of the system is the product of the fading diversity order and the minimum Hamming distance of the BICM code. The asymptotic coding gain consists of two terms, one of which is a function of the GMN parameters and the other is a generalization of the harmonic distance obtained in [3, 4].

- In the case of nonfading GMN, where the noise component with the largest power dominates the asymptotic BER, the convergence of the asymptotic BER approximation occurs only at very low BERs for typical GMN scenarios. We therefore also derive a novel closed-form expression for the PEP in nonfading GMN, which takes all mixture-noise components into account and is confirmed to be tight in BER ranges typically of interest.

Then, making use of the performance expressions developed in Chapter 2 and Chapter 3, two novel transmission strategies are designed. In particular, in Chapter 4, the problem of optimal power allocation aiming at BER minimization for a systems employing BICM along with orthogonal frequency division multiplexing (OFDM), also known as BIC-OFDM, is considered. A recent study of the problem, presented in [5], translates the problem into a convex optimization problem but is only applicable to (complex) binary transmission. Based on the PDF approximation developed in Chapter 2, a general algorithm applicable to arbitrary constellations has been proposed. In particular, we show that the power allocation problem can be transformed into a linear program in the high SNR regime. The use of linear programming considerably reduces the complexity of the algorithm in comparison to what has been proposed by [5]. Furthermore, our simulation results reveals that the performance loss due to employing linear program instead on convex optimization is negligible.

Finally, Chapter 5 considers the design of a practical iterative decoder for BICM transmission. The decoder employs hard decision feedback from the decoder in order to recompute the reliability metrics. It is known that the bit-errors in the feedback substantially degrades the performance of the system. It is shown that substantial gains can be achieved if the effect of this errors is considered. Since the error rate of the system is not available at the receiver we make use of error rate approximations developed in Chapter 2 and Chapter 3. Based on this, the optimal detector architecture has been derived and further simplified. We show that computational complexity of our proposed iterative decoding scheme using the simplified detector is the same as the original method while it results in considerable performance gains.

6.2 Future Work

There are quite a few open avenues for future research in the topics related to BICM transmission. In the following, two potential research topic along with proposed approaches are discussed briefly.

6.2.1 Adaptive Bit/Power Allocation and Code Selection for BIC-OFDM

While the problem of power allocation for BIC-OFDM transmission has been considered in Chapter 4, adaptive bit and code (rate) selection for BIC-OFDM is an open avenue to be explored. Notably, the fairly recent paper by Song [6] has considered a similar problem. But, the analysis developed in [6] could not be used for design purposes as in their expression for pairwise error probability (PEP) the number of terms exponentially grows with the Hamming distance of the PEP. Therefore the authors of [6] proposed to use a heuristic (sub-optimal) optimization criterion which has been previously used in [7] for uncoded transmission. Therefore, there is an interest to design optimal bit/power loading and code selection algorithms using the exact BER expression. We stipulate that the use of novel PDF approximation proposed in Chapter 2 will alleviate the problem of exponential growth of number of terms in PEP expression.

6.2.2 BICM Transmission over Block Fading Channels

It is known that the standard BER union bound is not tight for transmission over block fading channels. An intuitive explanation can be achieved by noting that this bound, in fact, is the expected value of the BER union bound over unfaded channel with regard to the PDF of instantaneous SNR. Since the BER union bound diverges for low SNRs, this average tends to not be tight in the SNR region of interest. A rather intuitive remedy has been proposed in [8] which is to limit the BER union bound by 1/2 when averaging over instantaneous SNR. While the BER bound achieved using this method is considerably tighter than the standard union bound, this method does not result in closed-form expressions and it needs multi-dimensional numerical integration.

One possible remedy to get rid of the multi-dimensional integration is the use of newly developed expressions for the PDF of LLRs. For complex binary transmission it is easy to examine that this reveals the equivalent SNR at the receiver. Furthermore, such a perspective for higher modulations can be achieved using the Gaussian approximation of the PDF of LLRs [1,9]. Finally, the area of integration for computing the PEP is a multi-dimensional sphere in the space of fading coefficients. The radius should be found numerically by equating the BER union bound for unfaded transmission to 1/2. Even if this integral does not result in closed-form expressions, using its symmetry property, it can be simplified to one dimensional integration.

Bibliography

[1] A. Martinez, A. Guillen i Fabregas, and G. Caire, "Error probability analysis of bit-interleaved coded modulation," *IEEE Trans. Inform. Theory*, vol. 52, no. 1, pp. 262–271, Jan. 2006.

[2] M. Chiani, D. Dardari, and M. Simon, "New exponential bounds and approximations for the computation of error probability in fading channels," *IEEE Trans. Wireless Commun.*, vol. 2, no. 4, pp. 840–845, July 2003.

[3] G. Caire, G. Taricco, and E. Biglieri, "Bit-interleaved coded modulation," *IEEE Trans. Inform. Theory*, vol. 44, no. 3, pp. 927–946, May 1998.

[4] A. Martinez and A. Guillén i Fàbregas, "Large-SNR error probability analysis of BICM with uniform interleaving in fading channels," *IEEE Trans. Wireless Commun.*, vol. 8, no. 1, pp. 38–44, Jan. 2009.

[5] H. Moon and D. Cox, "Efficient power allocation for coded OFDM systems," *IEEE Trans. Commun.*, vol. 57, no. 4, pp. 943–947, April 2009.

[6] K.-B. Song, A. Ekbal, S. T. Chung, and J. Cioffi, "Adaptive modulation and coding (AMC) for bit-interleaved coded OFDM (BIC-OFDM)," vol. 6, June 2004, pp. 3197–3201 Vol.6.

[7] P. Chow, J. Cioffi, and J. Bingham, "A practical discrete multitone transceiver loading algorithm for data transmission over spectrally

shaped channels," *IEEE Trans. Commun.*, vol. 43, no. 234, pp. 773–775, Feb/Mar/Apr 1995.

[8] E. Malkamaki and H. Leib, "Evaluating the performance of convolutional codes over block fading channels," *IEEE Trans. Inform. Theory*, vol. 45, no. 5, pp. 1643–1646, Jul 1999.

[9] A. Guillén i Fàbregas, A. Martinez, and G. Caire, "Error probability of bit-interleaved coded modulation using the Gaussian approximation," in *38th annual Conference on Information Sciences and Systems (CISS2004)*, Princeton University, USA, Mar. 2004.